MODEL-BASED CONTROL OF VENETIAN BLINDS

Brendan O'Neill

A Thesis

in

The Department

Of

Building, Civil and Environmental Engineering

Presented in Partial Fulfillment of the Requirements

for the Degree of Master of Applied Science (Building Engineering) at

Concordia University

Montréal, Québec, Canada

March 2008

Abstract

Model-Based Control of Venetian Blinds

Brendan O'Neill

Commercial and institutional buildings are being designed with increased transparent areas of the façade. Provision of views to the exterior is desirable, but more importantly, human health and productivity benefits may result from well day-lit interior spaces. The increased use of natural light, coupled with daylight responsive lighting systems, can reduce the peak electrical load and internal heat gains caused by artificial lighting. However, excessive transmission of solar irradiance can result in a net increase in energy consumption required for cooling, and may also affect the visual comfort of occupants. Manually operated shading devices are commonly used to deal with this problem, though their control is generally not optimal.

This thesis investigates the potential of an automated model-based control strategy for diffuse reflecting venetian blinds. Radiosity theory was used to numerically approximate the transmittance of a blind and glazing system for clear-sky conditions, and to determine the venetian slat angle required to maintain favourable transmission values based on the HVAC demand and the visual comfort of the building occupants.

Experimental measurements were carried out using a controlled motorized venetian blind installed on a clear glass window unit in a small-office space. The daylight transmission of the system was quantified and compared to the modelled prediction. A dimmable luminaire was also installed in this zone to determine the electric lighting energy savings possible in perimeter zones with the blinds continuously controlled to intercept direct sun rays.

Acknowledgements

First and foremost, I would like to thank my supervisor, Dr. Andreas K. Athienitis, for the opportunities he has given me to extend my knowledge and develop experience in the field. His support, trust, guidance and audacity were very much appreciated.

I am indebted to my colleagues, turned good friends. The ability to discuss, share and laugh together was indispensable.

For their insight, aid, and exceptional technical knowledge, I would like to especially thank José Candanedo and Dr. Athanassios Tzempelikos. The collaboration of Dr. Michael Collins of the University of Waterloo was also very much appreciated.

Special thanks to George Strickland of Somfy, and to Howard Yaphe and Man-Lok Choi of Canlyte. Learning about your products – and trying to get them to work – gave me the appreciation of those who implement complex systems on a grand scale.

The technical support of Luc Demers, for this project and for others, was very helpful.

Above all, I would like to thank my family and friends for their encouragement, and Patricia for her patience and understanding.

Financial support for this work was provided by NSERC through the Solar Buildings Research Network

Gnáthamh na hoibre an t-eólas

Table of Contents

List of Figures

List of Tables

Nomenclature

A	*surface area (m^2)*
c	*optical atmospheric extension coefficient*
d	*profile angle*
E	*illuminance (lux)*
F_{ij}	*view factor between surfaces i and j*
L	*luminance (cd/m^2)*
M_i	*luminous exitance of surface i (lux)*
m	*relative optical air mass*
n	*julian day number*
s	*separation distance between venetian slats (mm)*
w	*slat width (mm)*
α	*solar altitude angle*
β	*blind slat angle*
γ	*solar surface azimuth angle*
δ	*solar declination angle*
θ	*solar incidence angle*
ρ	*reflectance*
τ	*transmittance*
φ	*solar azimuth angle*
ψ	*surface azimuth angle*
ω	*solid angle (steradians)*

Chapter 1: Introduction

1.1 Background

The trend towards low-energy buildings has been spurred by two recent events: the international scientific community reaching the consensus that human activity is "very likely" the cause of increases in globally averaged temperatures since the mid-20th century (IPCC, 2007); and the continuing global rise of energy prices. In 2003, commercial and institutional buildings consumed 14% of Canada's secondary energy production. A significant amount of this energy consumption, 13%, was for electric lighting alone (OEE, 2006). In the province of Quebec, 17% of total energy use in 2002 was in the commercial building sector (MRNF, 2004).

The United Nations Environment Programme (UNEP) states that efficiency in the building sector has considerable potential to reduce global energy consumption and mitigate greenhouse gases. Active solutions such as lighting controls and solar-shading are identified as areas where advances could be made. This is due to the relationship between lighting and cooling: as a rule of thumb, one watt of air cooling energy savings results from every three watts of lighting energy savings (UNEP, 2007). This is especially true in hot climates, but also in cold climates. For example, the UNEP report points out that modern commercial buildings built in Sweden's cold climate require cooling even at outdoor temperatures of -10°C (UNEP, 2007).

It has been well understood for centuries, but perhaps neglected during the era of electrification and inexpensive hydrocarbons, that the radiative energy from the sun can be exploited for both the lighting and heating needs of a building. As a light source,

studies show that human health and productivity benefits can result from well day-lit interior spaces. However, the thermal energy of solar radiation is not always required, and excessive transmission through the building façade may increase overall energy consumption due to mechanical cooling.

The changing sun position throughout the year and the dynamic nature of the intensity of the solar flux means that buildings optimised to take advantage of the free heat and light cannot be designed under static conditions. The building must adapt to the energy source based on the visual and thermal needs of the controlled indoor environment, and most importantly, the comfort requirements of the occupants.

1.2 Motivation

Commercially available fenestration with low U-Values has been successfully developed through the use of multiple glazing with dense gas fills (such as argon), and low-emissivity coatings. This technology has given designers the option of having a larger transparent area on the building façade, beneficial for daylighting, without significantly decreasing the thermal performance of the building envelope. Spectrally selective coatings for glazing have also been developed to manage the risk of overheating. These coatings reduce the transmittance in the non-visible infrared and ultra-violet wavelengths of the solar spectrum. However, visible light contains about 45% of total incident solar energy (Murdoch, 2003). As a result, for the case of clear glazing with spectrally selective coatings, overheating may still occur.

The delicate balance of maximizing daylight transmittance and maintaining visual comfort is an ever present control problem. As presented in Figure 1-1, one effective

daylighting method in perimeter office zones is to reflect direct beam sunlight towards the ceiling, and allow diffuse transmittance in the lower portion of the window. Electric lighting savings can be achieved by using dimmable luminaries that are responsive to changes in the work-plane illuminance.

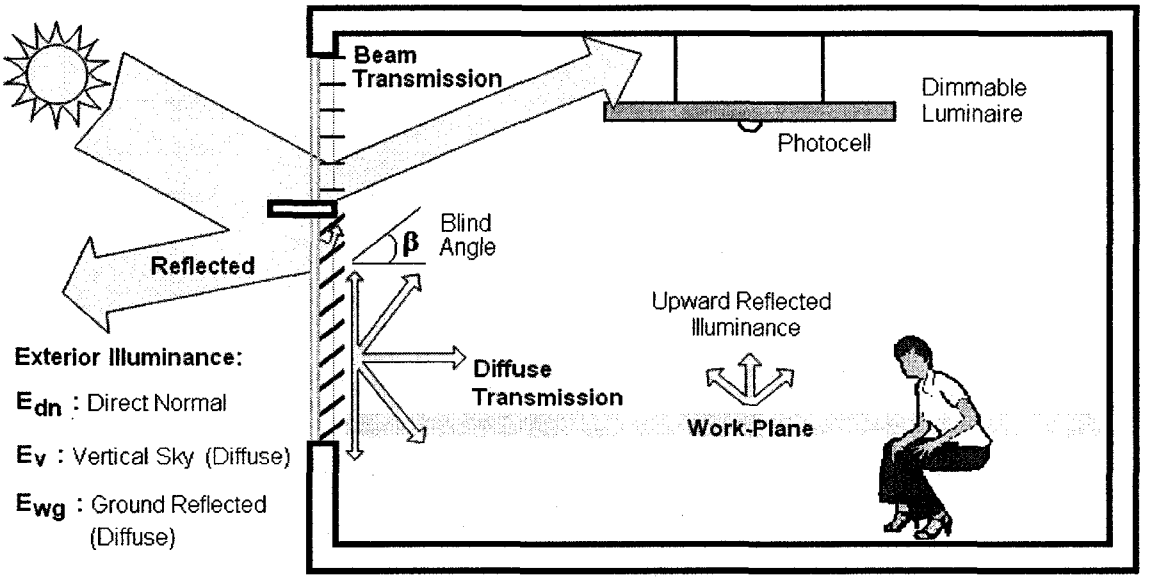

Figure 1-1: *Daylighting Schematic for a Perimeter Office*

Occupants who manually control shading devices, such as venetian and roller blinds, rarely consider energy savings associated with increasing or reducing the solar heat gains. Automated shading devices can be employed to carry out this task, and various researchers have noted the benefit.

The motivation of this work was to develop and investigate an automated method of controlling venetian type shading devices that addresses two important issues relevant to the control problem: particularly, the prohibitive cost of multiple sensors required for control, and the lack of continuous consideration of visual comfort.

1.3 Thesis Objectives

This thesis investigates the control of motorized venetian blind shading devices that protect occupants from the discomfort of glare on clear-sky days, while allowing the transmittance of a prescribed amount of daylight. A combined control of the interior electric lighting can allow for savings in energy consumption corresponding to peak usage by reducing both the electric lighting consumption as well as the related internal heat gain from the lamps. Maximizing daylight transmission during times of heating demand, and allowing the minimum transmission to meet perimeter lighting needs during the cooling season - all while considering discomfort glare - is the ultimate goal of the control strategy.

In this work, a novel control method that uses a simplified venetian blind transmittance model is developed and investigated. By using a model-based control, the need for interior sensors for blind control is eliminated. The control of this system is open-loop, with the disturbance variable being the exterior vertical illuminance, and the final control variable being the illuminance on the interior side of the venetian blind.

A numerical model of a fenestration system was created and compared to measurements from a full-scale controlled setup. A motorized venetian blind was controlled in conjunction with dimmable fluorescent luminaries in order to investigate the relationship between the two components, and define a potential for energy savings within perimeter zones.

In summary, the objectives of this thesis are as follow:

1. Develop a simplified transmittance model of a fenestration system composed of glazing, window frames, and an interior horizontal venetian blind. The venetian blind, to be placed in the 'view' portion of a window, will be modelled to continuously intercept direct solar radiation, and is to be diffuse reflecting. The numerical model will also include an exterior illuminance simulation that will allow for discrete calculation of the diffuse transmittance of the blind throughout the year, for all blind angles.

2. Implement a controlled full-scale experimental setup and compare the actual measured transmittance to the simulated results. In combination with the controlled venetian blinds, dimmable lighting in the perimeter zone will be investigated and the reduction in lighting energy is to be measured.

3. Investigate the use of the numerical model in an open-loop control strategy whereby maximum and minimum allowable transmittance values are used to determine the optimal blind angle for clear-sky conditions. Transmittance thresholds are to be based on the minimum amount of daylight required on the work-plane, and the maximum transmittance allowable in order to ensure visual comfort. This model could be ultimately programmed into a blind motor controller.

Chapter 2: Literature Review

2.1 Introduction

This chapter presents a review of relevant literature related to the control of shading devices integrated into commercial building façades. The focus for this study is the control of motorized venetian blinds that are used as a dynamic element within the fenestration system in order to control the transmittance of solar radiation into the occupied building space. The challenge is to allow daylight to penetrate into the interior space while mitigating the risk of excessive solar heat gain and occupant discomfort due to glare.

This review also explores the relevant properties of light, the human factors related to visual comfort, and the use of manually operated shading devices which are the norm in today's buildings.

2.2 Dynamic Façades

The façade of a building consists of various components and is designed to separate the exterior and the interior conditions. This building "skin" contains the thermal insulation with the exterior, the fenestration that allows for daylighting and views to the exterior, and serves as a barrier to the natural elements such as wind and rain. Aside from the practical purpose of protecting the occupants, façades are an architectural component of the building itself: the shape, form, texture and colour often communicate an architectural theme or corporate image.

Building design often ignores the climatic boundary conditions for the sake of visual impression (Voss, 2000). Dynamic façades are intended to take advantage of the natural environment conditions, and use the exterior conditions as either an energy source or sink. In other words, they adapt to the available energy from the exterior. "Dynamic" encompasses motorized louvers, venetian blinds and shades, controllable openings, as well as advanced glazing, i.e.: electrochromics and electrically heated glazing (Lee et al., 1998). A static façade – one that is designed for a unique set of boundary conditions – does not consider the seasonal temperature and solar radiation changes throughout the year. Façade systems must be dynamic and flexible in order to accommodate changes in the exterior conditions and the building occupants' needs (Selkowitz, 2001).

Mechanical equipment sizing is dependent on the amount of heat gain from solar energy transmitted though the façade fenestration (ASHRAE, 2005). Designing a façade that regulates the amount of energy flow from the exterior to the interior may reduce the size of mechanical equipment, peak loads and annual energy consumption. However, since HVAC systems are traditionally designed to be able to meet peak loading conditions, if the equipment is sized dependent on the ability of the solar control, it is important that the dynamic façade system be reliable (Selkowitz, 2001).

For commercial buildings, the internal load is noticeably increasing as more electrically powered equipment is being used (Voss, 2000). Also, the trend in buildings, and often the legislation in European countries, is to allow higher levels of daylight in the office environment. As mentioned by Lee et al. (2004), the design ideology of highly glazed buildings originated in Europe, and there is now a growing interest in North America to construct buildings with large portions of their façades covered with high

transmittance glazing. This change in architectural design is leading to an increased demand in sun control systems, including dynamic façades (Lee et al., 2004). As an example of the necessity of solar control, Kuhn (2006) cites a highly glazed building in Germany having up to 70% of the peak cooling loads caused by solar gains.

2.3 Daylight

When discussing the concept of solar control and daylighting, it is important to look at the source of this light: the sun. It is well known that the sun emits radiant energy over a range of wavelengths, as presented in Figure 2-1 (Gueymard, 2002). The extraterrestrial irradiance, which is approximated by blackbody radiation at 5800 K, is attenuated as it travels through the earth's atmosphere. Shorter wavelengths (ultraviolet) are lost due to the ozone layer, and losses in the higher wavelengths (infrared) are caused by gases in the atmosphere, such as water vapour and carbon dioxide (Webb, 2006). The peak of the solar spectrum occurs between wavelengths of 380 – 770 nm, which also corresponds to the visible range of the human eye. The relationship between irradiance (W/m^2) and the corresponding lighting metric 'illuminance' (lm/m^2 or lux) is due to the spectral sensitivity of the eye (Murdoch, 2006).

In a paper by Webb (2006), which explored the non-visual effects of lighting in the built environment, it was pointed out that the design for artificial lighting systems only takes into account the visual needs of the occupants, whereas the additional benefits of natural light are often not considered. These non-visual effects include the control of the circadian rhythm, which dictates hormone secretions and has an effect on the sleep/wake cycle.

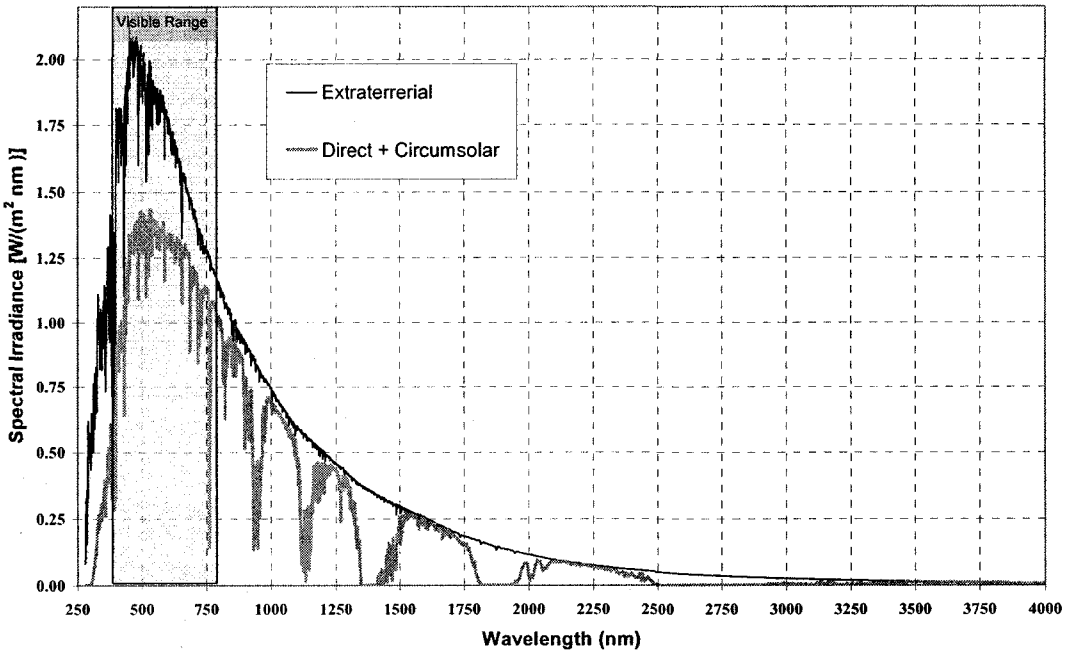

Figure 2-1: *Extraterrestrial and Direct + Circumsolar radiation, ASTM G-173-03 Standard Solar Reference Spectra, (Gueymard, 2002)*

According to Noguchi et al. (as cited by Veitch, 2006) bright natural lighting on the office work-plane – 2500 lux compared to 750 lux – can increase the alertness of occupants and enhance their mood. Illuminance levels exceeding 2000 lux are said to be quite common in workplaces using daylight, whereas artificial lighting design levels are significantly lower (Nabil et al., 2005). Webb concludes that the increased use of daylight has the potential to increase safety and productivity in the workplace, and can also benefit human health.

From an energy-conservation standpoint, daylight – or the visible portion of solar radiation – has a high efficacy between 100 to 120 lumens per watt at the earth's surface (Rosenfeld et al, 1977). Table 2-1 displays the efficacy of different sources of light. As seen, the efficacy of diffuse skylight is higher than the widely used standard fluorescent (T8) lamps, as well as the more recent high efficiency T5 fluorescent lamps.

Table 2-1: *Comparison of Light Sources (Murdoch, 2003; *Rosenfeld et al., 1977)*

	Lamp	Type	Colour Temp. (K)	Initial lm/W	Life (hr)
1	Incandescent	60 W Standard	2770	14.8	1000
2	Tungsten-Halogen (TH)	100 W T3	2800 - 3400	16	2000
3	Fluorescent	40-W T8	3500 - 5000	94	20,000
4	Fluorescent	35-W T5	3500 - 5000	104	16,000
5	Direct Beam Sunlight	---	5800	100*	---
6	Skylight on Vertical	---	5800	120*	---

It is important reiterate that that light itself is radiant energy. The amount of radiation outside of the visible spectrum contributes only heat to the interior environment, and hence it is undesirable for cooling-dominated commercial buildings. As such, the sun is an efficace source of light that may enhance health and productivity, and also offset the use of less efficient artificial light sources. However, excessive levels of natural light can cause unnecessary cooling loads in buildings and may also cause discomfort due to glare.

2.4 Glare

Perhaps the most important variable in the control of automated blinds, whether venetian or other, is the mitigation of daylight glare. Maintaining visual comfort is fundamental if a shading system is to meet the demands of the user (Kuhn et al., 2000). This is especially important in day-lit office spaces, particularly those with computer workstations with visual display terminals.

There are two important types of glare: Disability and Discomfort. Both impact human visual comfort in different ways. Disability glare is caused by bright light sources,

such as direct sun, and there is an immediate reduction in the ability to see or perform a visual task. Discomfort glare is a more subjective phenomenon that is caused not only by the brightness of the source, but by source size and contrast with other luminous surfaces. This type of glare may not be immediately perceived, but can lead to headaches and reduced work performance. Discomfort glare is considered a psychological effect, whereas disability glare is a physiological and immediate effect (Osterhaus, 2005).

Due to the fact that the perception of discomfort glare is subjective, there has been significant work in attempting to define indices in order to predict the human response. Osterhaus (2005) conducted work to evaluate the existing assessment and prediction models, and he concluded that the available methods are of limited practical use for day-lit offices, and that there has been no method developed to combine both daylighting and electric lighting into these models.

Nazzal (2001) modified the daylight glare index formula (*DGI*) that was based on the Cornell large-source glare formula. Nazzal proposed a new evaluation method for daylight discomfort glare, the DGI_N. As Osterhaus concluded, Nazzal also states that there is a need for a proper glare prediction method in order to promote visual comfort in workplaces. The general argument is that the previously developed glare evaluation methods work only for artificial sources.

Fisekis et al. (2003) carried out field experiments to compare the original *DGI* to the modified DGI_N proposed by Nazzal. This study used the surveyed response from occupants as well as sensors to measure the variables in the DGI_N formulation, and compare the calculated DGI_N index to the response of the subjects. The results showed that the method proposed by Nazzal is more effective at predicting mild degrees of glare

(up to 22 on the *DGI* scale), but it underestimates the comfort index beyond this level when compared to the standard *DGI* formulation. Table 2-2 displays the *DGI* scale and corresponding perception of comfort.

Table 2-2: *Discomfort Glare Index (DGI) Multiple Criterion Scale (Fisekis et al., 2003)*

	Described Criteria	Designated regions between criteria	DGI Scale
		Intolerable	
Discomfort zone	Just intolerable	Just intolerable	28
		Uncomfortable	26
	Just uncomfortable	Just uncomfortable	24
	Just acceptable	Acceptable	22
Comfort Zone		Just acceptable	20
		Noticeable	18
	Just perceptible	Just perceptible	16

As mentioned by both Osterhaus and Fisekis, no universal generic formulae currently exist; hence the glare indices should be used as a guide only.

A different approach was recently taken by the International Energy Agency's (IEA) Solar Heating and Cooling Task 31. In Subtask 'A' of Task 31, the Daylight Glare Probability (*DGP*) index was developed in order to model occupant use of lighting and shade controls (Ruck, 2006). This method calculates the probability that a person will be disturbed, instead of a fixed glare magnitude index such as presented for the *DGI*. In this particular study, the surveyed responses from users were correlated to measurements of a CCD camera in order to develop probabilities of discomfort. However, as this method is new, the authors caution that their results should be confirmed by additional assessments,

and that the probability model should be tested with other shading systems (Wienold et al., 2006).

The work in the glare prediction field allows one to evaluate the discomfort that may result from a certain façade design, but it may also be used for a control application. The maximum fenestration illuminance threshold could be set based on the *DGP* or *DGI* scale, but it may also be later commissioned and adjusted to better respond to the occupants' needs. The minimum illuminance from the fenestration could be programmed to meet the minimum indoor illuminance requirement on the work-plane which, according to Voss (2000), is the basic requirement of a solar gain management system for façades.

2.5 Fenestration

The term fenestration refers to the arrangement, proportion and design of windows, skylights and door systems in a building. Fenestration is a system of components that include the transparent glazing material, most commonly glass; opaque portions such as the framing and mullions, and may include external or internal shading devices. In general, fenestration affects building energy use through four basic mechanisms: thermal heat transfer, solar heat gain, air leakage and daylighting (ASHRAE, 2005).

When considering the effectiveness of a fenestration product in managing the energy flow from solar radiation flux, two parameters are often cited: the solar heat gain coefficient (SHGC) in North America, and the total solar energy transmittance or G-Value in Europe (ASHRAE, 2005; Kuhn et al., 2000). In fact, these two quantities

describe the exact same phenomena: the percentage of total incident solar radiation transferred to the interior through the complete fenestration system. The energy flux includes the transmitted portion through the glazing, as well as the inward flowing portion that is first absorbed by the opaque components and then transferred to the interior via conduction, convection and radiation (ASHRAE, 2005). Because of the interaction of different components and materials from a large variety of manufacturers, determining the inward flowing component is currently not a straightforward process, and relies on measuring scale-models using calorimetry or fenestration empirical models (McCluney, 1998).

2.5.1 Glazing

Advances in the last 30 years in glazing technology have been quite significant. Specifically, spectrally selective coatings applied to glazing are capable of reflecting the ultraviolet and infrared radiation (McCluney, 1998). The term 'low-e glass' is often used to describe these coatings due to the fact that as the reflectivity at a certain wavelength increases, the absorptance decreases (Kirchoff's law states that the absorptance and emissivity of a material are equal for any given wavelength and incidence angle). Architectural glass is mostly opaque to radiation in the longer wavelengths, such as that emitted by objects at room temperature. Without a coating the emissivity is near 0.86 due to absorbed radiation, and with a coating it can be lowered to 0.10 (ASHRAE, 2005). The result is a reduced U-Value of the fenestration since glass at lower temperatures radiates less heat to the exterior.

The optimum spectral selectivity of incident solar radiation is climatic dependent. Figure 2-2 displays the ideal transmittance of spectral selective coatings for hot and cold climates (ASHRAE, 2005).

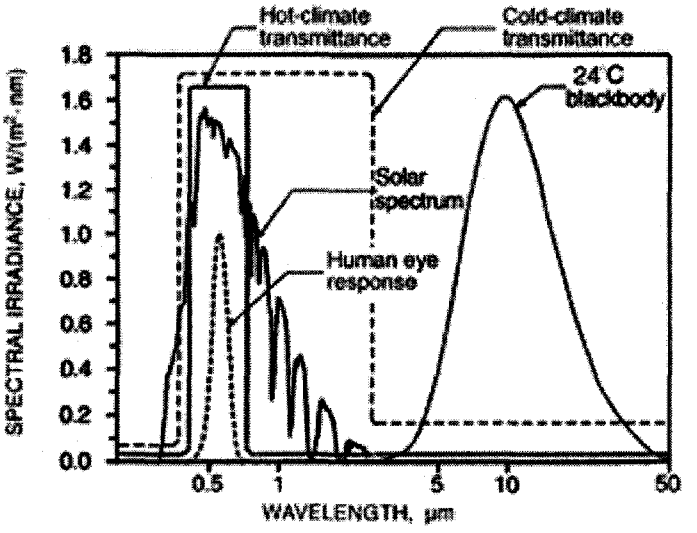

Figure 2-2: *Demonstration of Two Spectrally Selective Glazing concepts, Showing Ideal Spectral Transmittances for glazing intended for Hot and Cold Climates (ASHRAE, 2005)*

Spectrally selective coatings influence greatly the SHGC of a window as they can drastically limit heat gains, especially those in the non-visible range. However, as it was discussed earlier, about half of solar radiation energy is contained within the visible spectrum. Thus, for clear glass, it is equally important to include shading devices within the fenestration system in order to limit overheating.

2.5.2 Properties of Shades and Blinds

> ***shade (noun) :*** *a flexible screen usually mounted on a roller for regulating the light or the view through a window*
>
> ***blind (noun):*** *something to hinder sight or keep out light: as* ***a :*** *a window shutter* ***b :*** *a roller window shade* ***c :*** *venetian blind*
>
> - Merriam-Webster Dictionary (2005)

It is well accepted, from both an energy conservation and a comfort standpoint, that solar shading is absolutely necessary in buildings with large glazing areas. The view, daylight and connection to the outdoors provided by windows is desirable, however the fenestration product must control glare, solar transmittance and maintain thermal and visual comfort. Glazing alone rarely can provide this level of control, and thus some form of shading device is necessary (Selkowitz, 2001).

Shading devices vary from exterior fixed objects such as overhangs, louvers, shutters and awnings; to roller and venetian type blinds, which may be positioned in an intermediate zone such as between multiple-glazing, within a double-façade or internally in the conditioned space. Shading may also be provided by a building's geometry, as well as by other surrounding structures or geographical features.

Extensive work to develop numerical models of the transmittance of blinds and shading devices has been carried out over the years. This work has mostly focussed on developing building energy simulation models, and the determination of the SHGC or G-Values. The European Union JOULE programme (van Dijk et al., 1998) had the goal of developing detailed product information of novel glazing and solar shading devices. This project involved creating a database and software tool to allow designers to calculate the daylight distribution and to design for glare avoidance. This led to the development of the European software tool WIS (van Dijk et al., 2003), which looks at slat-type solar shading devices and can calculate the G-value of the fenestration system.

The *Solar Shading Project* at Lund University, with phase 1 focussing on exterior and phase 2 on interior and inter-pane devices, studied the performance of solar shading

devices in order to develop comparable G-values. The general conclusion was that external shading products are twice as effective as internal products with respect to reducing the peak cooling loads. A computer software *ParaSol* was developed, which is used to determine the solar transmittance properties of glazing and shading systems, with the blinds at fixed angles (Bülow-Hübe et al., 2001)

Optical and thermal properties, including the G-Value and SHGC, depend greatly on the fenestration component as a system. The radiation exchanges are a complex process, especially when taking into account the variable angle-dependent transmittance when using venetian blinds (Kuhn, 2006). SHGC values listed by ASHRAE for venetian blinds apply for incidence angles of 30 degrees or less, and a warning is given that these values do not consider important azimuthal angle effects (ASHRAE, 2005).

Klems et al. (1997) developed numerical models and conducted spatial-averaged measurements to determine the SHGC of fenestration with a venetian blind layer. The European ALTSET project (Rosenfeld, J. et al., 2001) compared modelled and measured values of complex glazing, including fixed and variable venetian blinds. They treated the fenestration as a system composing of layers, with the normal reflectance as the input to the model. They concluded that their models, used with caution, are suitable for use in building energy simulation tools. Breitenbach et al. (2001) explored the optical and thermal performance of primarily diffuse reflecting venetian blinds integrated within a double-glazed window unit.

Kotey et al. (2006) developed a simplified layer-based model of fenestration with venetian blinds similar to the work of Klems, but not as computationally intensive.

As seen, research in the area of modelling venetian blinds is quite extensive. However, the variations of venetian blind products, the lack of detailed optical properties available from manufacturers, and the issues involved with the human interaction continue to present challenges from both a modelling and an implementation point of view.

2.5.3 Venetian Blind Variations

> ***venetian blind (noun) :*** *a blind (as for a window) having numerous horizontal slats that may be set simultaneously at any of several angles so as to vary the amount of light admitted.*
>
> - Merriam-Webster Dictionary (2005)

This current study focuses on the control of venetian blinds. In the literature, it is often pointed out that venetian blinds offer more control over fenestration transmittance than their most common counterpart, roller shades (Lee et al., 2002). Venetian-type blinds, with angle-adjustable horizontal slats, louvers or lamallae, are often more accepted in commercial or institutional settings because the practicality and utility of the product outweigh aesthetic design criteria (French, 1941).

There are various venetian blind products on the market. The most common are extruded aluminum blinds with a concave feature. It is convention that the inward curving side of the venetian slat face towards the interior. This results in an overlapping of the blind slats, when fully closed, so that light transmission is limited.

The reflectance and angle of the horizontal slats are the most important parameters for determining transmittance, with the latter more deterministic than the former (Bülow-Hübe et al., 2001). Whether the horizontal slats are specular reflective or

diffuse reflective will change the functionality of the device. For example, A. Rosenfeld and Selkowitz (1977) proposed the novel use of a combined system of venetian blinds. Reflective blinds are positioned in the upper "beam reflecting" section of the fenestration unit. The intent is to have the slats orientated to reflect the sun's rays deep into the space. This is practical only if the blinds are positioned at the top part of the window since direct reflectance towards occupants' eyes is highly undesirable.

Rosenfeld and Selkowitz (1977) also suggested that the lower 'view' portion of the window should be covered by light coloured, opaque venetian blinds. The diffuse reflecting characteristics of this shade would allow for it to be operated as a diffuse emitting side-light, as presented in Figure 2-3.

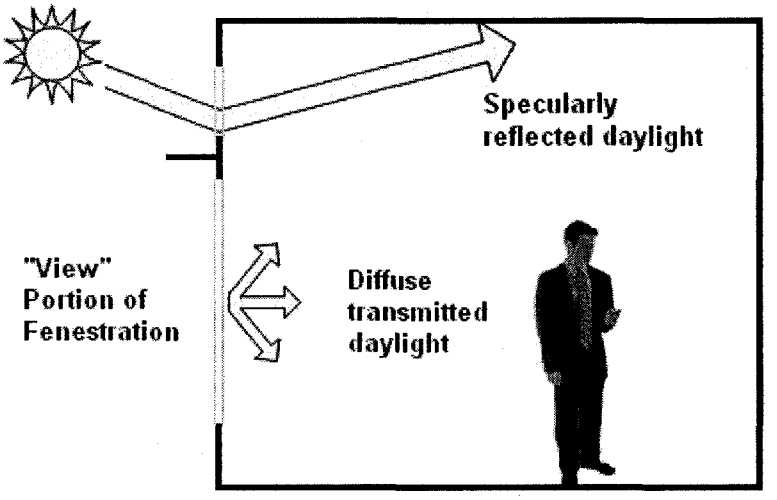

Figure 2-3: *"Beam reflecting" blinds in upper portion of fenestration; Diffuse emitting side-light in lower "view" portion. (Rosenfeld et al., 1977)*

Other innovative horizontal lamellae venetian-blind-type shading devices have also been developed. These include slats with micro-prismatic features that change the

direction of the blind reflectance, as well as slats with W-shaped profiles, as shown in Figure 2-4 (Retrosolar[1]).

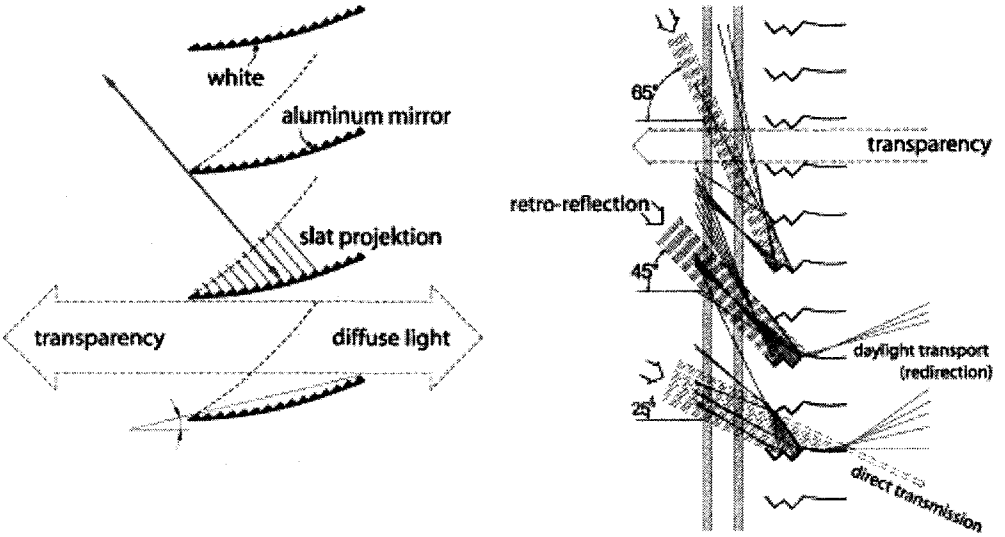

Figure 2-4: *Innovative Retrosolar © Mico-Prismatic and W-Shaped Blind Profiles*

2.6 Blind Control

The intent of this study is to control the 'view' portion of a venetian blind shading system, described by Rosenfeld et al. (1977), where the venetian blinds are primarily diffuse reflecting, and of a standard concave design. Other studies have been conducted for innovative control strategies of reflective venetian blinds (McGuire, 2005), and also roller blinds. This review specifically looks at the issues surrounding the control of interior blinds, and specifically the issues related to venetian-type blind control.

[1] www.retrosolar.de

2.6.1 Occupant Behaviour / Manual Control

It is well recognised that shading devices are capable of controlling glare, reducing cooling load, and providing privacy. The latter is a human factor that is subjective, and from an engineering perspective can be solved only by allowing manual user override to any shading system.

Occupant behaviour relating to shade control has been studied by various researchers, especially those concerned with modelling the energy performance of buildings. Reinhart (2004) reviewed the closing criteria of manual operated blinds. He notes that different criteria have been used for a variety of energy modelling procedures. The approaches vary from modelling blinds to be closed when direct sunlight is present (Vartiainen, 2001); assumed presence of glare (i.e.: Lee and Selkowitz (1995) equalized glare with transmitted direct solar radiation of 94.5 W/m^2); and overheating in non-air-conditioned spaces (i.e.: Goller (1998) assumed blinds closed when the internal temperature exceeds 26°C). Newsham (1994) assumed that initially blinds are open at the beginning of the day, but closed for the rest of the day if the façade of the workspace has been exposed to irradiance values above 233 W/m^2.

This assumption that blinds are closed and are not again opened corresponds to the work cited by Bülow-Hübe (2001), where it was found that occupants may not open shading devices once they are closed, especially if they expect to be uncomfortable. It was noted that these habits may be changed through education or if the occupant has strong environmental values. Reinhart (2003) also mentions that work by Lindsay et al. (1993) and Inoue et al. (1988) point to the fact that the general motivation of occupants to actuate blinds is to avoid glare rather than to prevent overheating.

Reinhart (2004) concluded that manual control is more of a stochastic nature when considering lighting and blind control. This led to the development of the *LIGHTSWITCH* software for evaluating electric lighting and daylight controls.

These findings show that manually operated shading devices are quite commonly misused. For example, Foster et al. (2001) found that blinds may be left untouched in single offices for periods of weeks, or even months. Considering the potential energy savings and comfort improvements, especially in shared office spaces where no true ownership of the blind control is exerted, the potential for automated blinds is quite good.

2.6.2 Automated Control Strategies

Due to the fact that manual shading devices are rarely used as designed (Kuhn et al., 2000), the initial design assumptions of the façade and associated shading coefficients may not be congruent with the actual operating conditions. The anomaly between design and actual conditions can affect the energy consumption estimates, and thus the corresponding sizing of a variety of a building's mechanical equipment (Foster et al., 2001).

Extensive work has been done on investigating automated control strategies of shading devices. The challenge has been to balance the thermal requirements of the building with the visual and thermal comfort of the occupant, as well as the psychological constraint that the occupant desires a view to the exterior. Depending on the exterior view, the user of the shading system may have a higher tolerance to the effects of glare and thermal discomfort (Bülow-Hübe, 2001).

Closed-loop systems are the most prevalent type of control applications for venetian blinds. A generalized schematic of this control is presented in Figure 2-5.

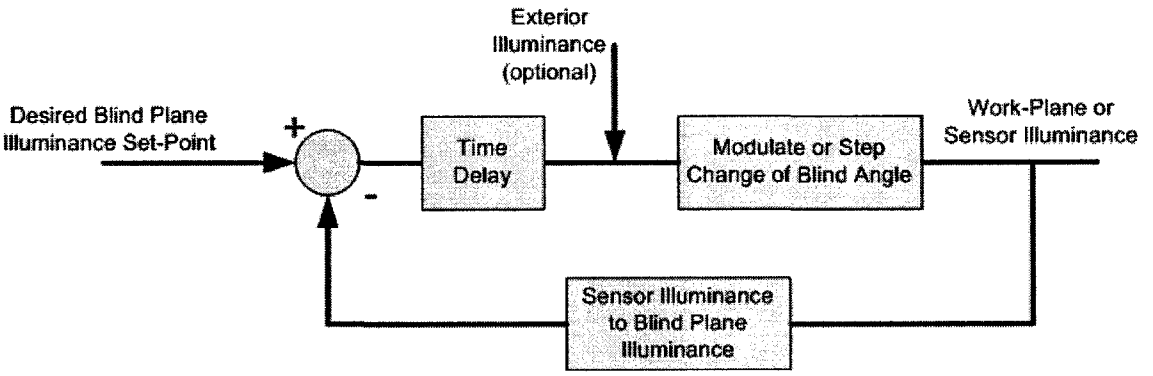

Figure 2-5: *Generalized Closed-Loop Blind Control Schematic*

A modulating control based on the measured exterior illuminance or irradiance on the window plane was tested by Galasiu (2004). The system employed an interior sensor measuring the transmitted illuminance at the glazing. During a one-year monitoring period, in conjunction with dimmable fluorescents, it was found that electric lighting energy savings were greater with this photo-control application, compared to static blinds.

DiBartolomeo et al. (1996) developed a closed-loop proportional control system that controls the daylight transmitted through venetian blinds based on the measurements of a calibrated ceiling mounted sensor. The algorithm was designed to always block direct sun, and adjust the blind angle to maintain the design work-plane illuminance with daylight, if possible. The blinds were positioned at one-minute intervals. An innovative sun angle sensor was also developed for this study that determines the sun altitude when the sun is in the window plane, eliminating the need for calculations with a real-time clock and site-dependent commissioning. Dimmable electric lighting was used to supplement insufficient quantities of daylight. Lighting energy savings of 62-83% were realized compared to a system with no daylighting controls. Changing the time step from one minute to five minutes decreased lighting savings by 1-2%. The author does note,

however, that while the control objectives were met, visual comfort for occupants may not have been optimal.

A method to calculate the correlation between interior mounted illuminance sensors and the daylight contribution was developed by Park et al. (2003). This method allows for the development of closed-loop proportional control strategies that can be used to adjust the venetian blind angle in order to increase the daylight contribution to the work-plane.

Kuhn et al. (2000) investigated two different control strategies for venetian blinds in order to aid the planning process to assess overheating. They modelled the performance for the venetian positioned on the exterior side of the glazing. When the façade is illuminated by the sun, the venetian blinds were modelled to be either closed or positioned at the "cut-off" angle to block direct beam radiation. The cut-off angle strategy was identified as the worst-case for overheating protection, but that it optimizes view to the exterior while protecting against glare from direct irradiation. Using real weather data, the calculated annual G-Value of the closed strategy was 0.04, compared to 0.2 for the cut-off strategy.

Open-loop control for shading devices found in the literature involved roller blind systems. An example of open-loop control is presented in Figure 2-6 .

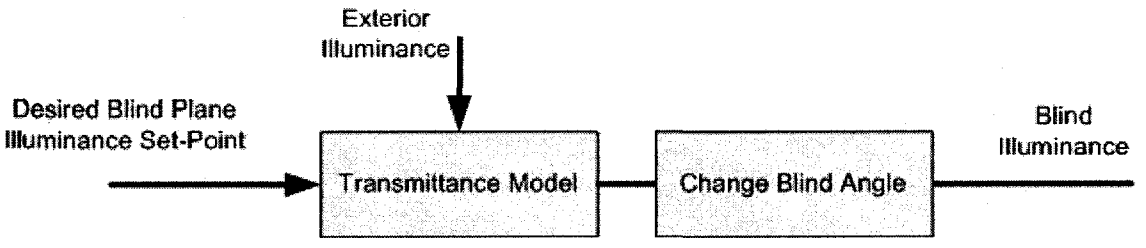

Figure 2-6: *Generalized Open-Loop Blind Control Schematic*

Roche (2002) developed an open-loop control algorithm that determined whether direct sun was incident on the façade: an empirical formula was used to compare the measured exterior vertical illuminance to that of the predicted exterior illuminance for clear-sky conditions. The shades were automatically positioned to allow beam radiation to penetrate a maximum of 1 metre from the façade.

An open-loop control system provided by *Mechoshade* was tested (Pedersen, 2004) for the recently completed New York Times Building, in New York city. The design team constructed a one-floor scale mock-up equipped with automated roller blinds and dimmable lighting (Lee, 2006). Similar to the strategy implemented by Roche, the *Mechoshade* system measures exterior illuminance, with three sensors in this case, and determines the sky-condition compared to an ASHRAE clear-sky. Solar geometry is calculated and the shades are then positioned based on the maximum allowable direct beam penetration.

Another example of an innovative control strategy for roller blinds involved the use genetic or fuzzy-logic algorithms in order to adapt the control algorithm to better suit user preferences (Guillemin et al., 2002).

There were no cases of open-loop (model-based) control systems for venetian blinds found in the literature review.

2.7 Integrated Daylight and Lighting Control

The instantaneous nature of the changes in exterior sky conditions and the variable transmittance of the fenestration system can cause fluctuating illuminance levels on the interior work-plane. It is desired to maintain or control the interior illuminance levels such that they do not fall below design levels, exceed a certain maxima, or disturb

occupants. In response to the changes in transmitted daylight, the electric lighting system may also have an adjustable luminous output.

Daylight responsive lighting systems are capable of reducing lighting electricity consumption by 20 to 50% (IEA, 2001) due to either dimming technology or on/off switching. The reduced use of electric lighting can also significantly reduce the cooling load of the building (Tzempelikos et al., 2007).

Ideally, an integrated shading and lighting control system would work together to continuously maximize the daylight contribution to the work-plane illuminance while minimizing the use of electric lighting. In the heating season, the maximum allowable daylight based on comfort requirements would be desirable; in the cooling season, the minimum required daylight to allow optimal dimming of perimeter electric lighting. These shading controls could be linked with the building control system in order to determine the state of the HVAC demand, the occupancy, and the scheduling.

2.7.1 Electric Lighting Control

Electric lighting controls have been available on the market for almost two decades, but their application has been limited (Lee, 2006; Escuyer, 2001). In order for the transmitted daylight into an office space to make a contribution to energy efficiency, the appropriate control of the electric lighting system is essential (Littlefair, 1998).

Fluorescent lighting is predominant in the commercial building sector due to its high efficacy (Murdoch, 2003), as was seen in Table 2-1. As fluorescent lamps require high voltages during start-up, ballasts are required for their operation. High frequency electronic dimmable ballasts are a technology that has been replacing conventional magnetic ballasts as they are more efficient and operate at higher frequencies, resulting in

less stroboscopic effects (To et al., 2002). As an added advantage, they may also be used to dim the luminous output of the lamp using pulse-width modulation.

Dimmable ballasts that receive an analogue control signal, such as 0-10V, were the first on the market and are still prevalent. The advent of digital controls and the standardized Digital Addressable Lighting Interface (DALI) open-protocol has resulted in a more flexible and robust technology. DALI controlled ballasts receive a digital 8-bit signal which corresponds to a standard percent reduction in luminous output. This allows for various DALI capable lighting fixtures to consistently dim at the same rate and magnitude (Pflaum, 2001).

The work-plane illuminance is the basic criterion that is used for lighting control. The amount of electric lighting needed to compensate the daylight contribution is relative to the relationship between the photo-sensor position used for control and the lighting fixture arrangement and properties (Park et al., 2003). Most applications of interior daylight-linked lighting control use an interior photo-sensor and a mathematical relationship to determine the work-plane illuminance (IEA, 2001).

2.7.2 Target Work-Plane Illuminance

The design illuminance level to be maintained on the work-plane is dependent on the needs of the occupants. This quantity may differ between individuals and their tasks, and also whether the source of light is artificial or natural.

Love (1998), in a survey of offices, found that occupants may be satisfied with lower illuminance levels provided by daylight than those required by electric lighting design. Another field study of office workers by Escuyer (2001) found that the preference of illuminance varied greatly, ranging from 100 – 600 lux. For those working primarily

on computers, low illuminance levels (100-300 lux) were preferred. In a case study of the New York Times building, the work-plane illuminance set-point when using occupant adjustable dimmable electric lighting was 400 lux, even though the design set-point range was 484-538 lux (Lee, 2006).

Dimmable lighting that allows user control may be able to overcome the design ideal of fixing the work-plane illuminance at a single value. Galasiu (2006) conducted an extensive literature review on occupant satisfaction with control systems in day-lit offices. She states that fully automated lighting control systems have low occupant acceptance, and thus allowing individual override is preferable. Escuyer (2001) also concluded that the ideal lighting control system for office environments, and from a comfort point of view, should allow the electric light illuminance to be chosen and changed throughout the day.

These studies show that a set work-plane illuminance is not required for occupant satisfaction. On the contrary, just like the natural cycle of exterior light levels, the occupant should be allowed to change the illuminance levels throughout the day. Increasing the use of natural light, while allowing control and user input, could satisfy the illuminance levels desired by the occupant.

Chapter 3: Numerical Model of Venetian Blind Transmittance

3.1 Introduction

A numerical model based on radiosity theory (Murdoch, 2003) was created and programmed in *MathCAD 2001i* (PTC Inc.[2]) software. This model was developed in order to predict the transmittance of the fenestration system – including glazing and blind – for clear sunny days. The important input parameters are geographic location, façade orientation, sky conditions and blind and glazing properties. The model may be used for standard venetian blinds and glazing systems, and at any geographical location and façade orientation. However, the validation was carried out only with one type of motorized venetian blind system.

3.2 Blind Properties

The model developed for this study was specifically created for standard concave venetian blinds with horizontal slats that have primarily diffuse reflecting surfaces. Physical blind properties required for this model include the slat width and separation distance between slats, as well as the average reflectance of the slat throughout the visible wavelengths.

[2] www.ptc.com

3.2.1 Blind Reflectance

The 'view' portion of the fenestration requires that shading devices are diffuse reflecting into the interior space (Rosenfeld et al., 1977). Thus, diffuse reflection was only considered in this model, and the surface was considered to be ideal Lambertian. This assumption was made in order to simplify the calculation procedure, and has been used by others when considering total solar radiation blind transmittance (van Dijk, 2003).

The average reflectance through the visible wavelengths may be calculated for a given blind surface. For example, the measured reflectance of the blind slats used in this study for experimental validation is presented in Figure 3-1.

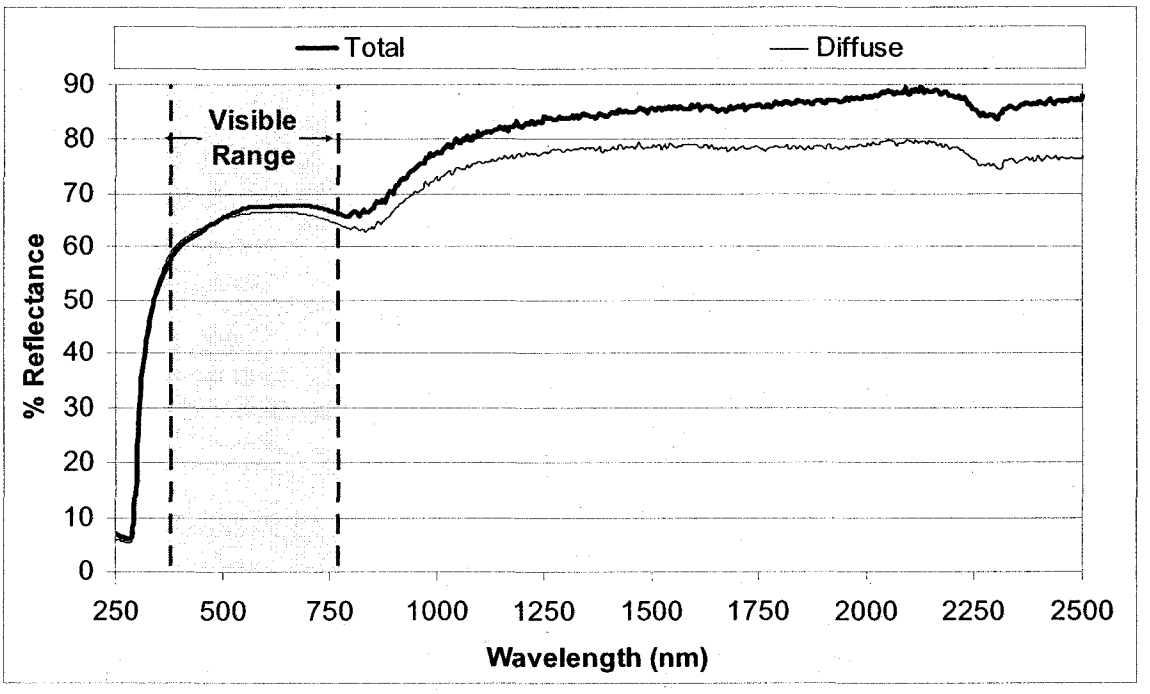

Figure 3-1: *Spectral reflectivity of a grey venetian blind slat (M. Collins)*

The average spectral reflectance calculation considers the spectral power density $P(\lambda)$, the spectral sensitivity of the eye, $V(\lambda)$, as well as the spectral reflectivity of the surface $\rho(\lambda)$, and is calculated as follows:

$$\rho_{avg} = \frac{\int_{380nm}^{770nm} \rho(\lambda) \cdot P(\lambda) \cdot V(\lambda) \cdot d\lambda}{\int_{380nm}^{770nm} P(\lambda) \cdot V(\lambda) \cdot d\lambda} \qquad (3\text{-}1)$$

The average specular reflectance at varying incidence angles for the experimental venetian slats is shown, as a percent of total reflectance, in Table 3-1. As seen, the specular reflectance at normal incidence is quite small, and increases with incidence angle. Due to this, the diffuse reflectance assumption will not be as valid when the blind is not positioned at the 'cut-off' angle, or near normal to the sun rays (See Figure 3-2).

Table 3-1: *Average blind slat specular reflectance for varying incidence (M. Collins)*

Incidence Angle (Degrees)	Average specular reflectance (% of Total)
0	0.9
30	3.4
45	3.0
60	2.2

3.2.2 Blind Geometry and Cut-Off Angle

When direct irradiance is incident on the façade, the 'cut-off' angle is the minimum angle that the blind may be opened while still blocking direct beam radiation (ASHRAE, 2005). Figure 3-2 presents a side-profile of two opposing venetian blind slats positioned to be in the cut-off angle relative to the sun. The width of the slat, w,

separation distance, *s*, and blind slat angle, β, are shown. The profile angle, *d*, of the sun must also be calculated. (See Section 3.4 for profile angle discussion)

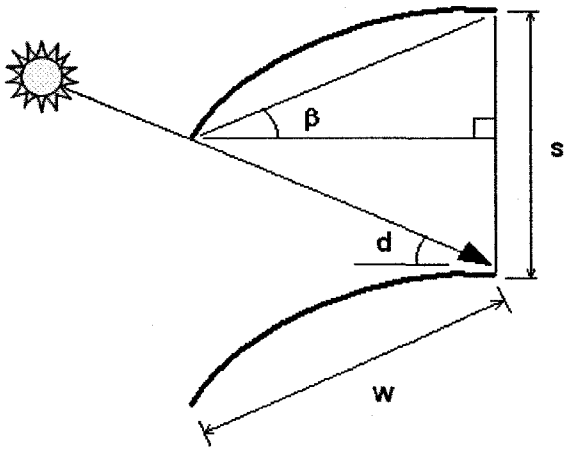

Figure 3-2: *Blind geometry nomenclature*

The relation between *s*, *w*, *d*, and β may be determined using the Sine Law:

$$\beta = \sin^{-1}\left[\cos(d)\cdot\frac{s}{w}\right] - d \qquad \textbf{(3-2)}$$

The cut-off angle is to be used as the minimum blind angle, however if restrictions exist on the maximum allowable interior blind illuminance, higher blind angles can be calculated and implemented in order to ensure user preference or visual comfort.

As shown in Figure 3-3, the calculated blind angle, β, for the experimental blinds approaches zero degrees as the profile angle, *d*, approaches 37.5 degrees. In order to maintain visual contact with the exterior while still blocking direct luminance, the minimum slat angle may be set to zero degrees, essentially horizontal, for high profile angles.

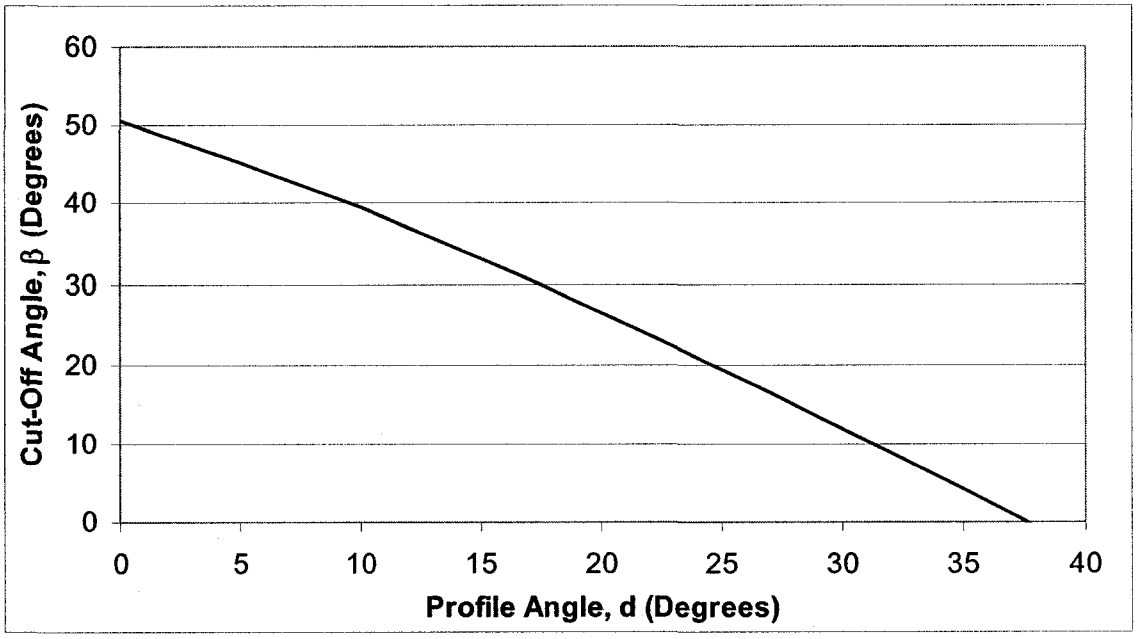

Figure 3-3: *Venetian slat cut-off angle, β, as a function of profile angle, d, for venetian blind used in experiment*

Negative blind angles would result in views of the sky, which is also undesirable for glare purposes (Bülow-Hübe, 2001), and are thus avoided.

3.3 Glazing Properties

The glazing is represented in this model by its diffuse and direct beam transmittances, respectively τ_{wd} and τ_{wb}. The direct beam transmittance of glazing is dependent on the solar incidence angle, whereas most manufacturers list only normal incidence transmittances (ASHRAE, 2005). As this is the case, the properties of the glazing used for the validation of the model were measured experimentally (See Section 4.5). A function with respect to the solar incidence angle was derived from a curve fitted to experimental data, and then implemented in the model. This is displayed in equation 3.3.

$$\tau_{wb} = -0.294 \cdot \theta^3 + 0.435 \cdot \theta^2 - 0.258 \cdot \theta + 0.769 \qquad (3\text{-}3)$$

where, θ is the solar incidence angle in radians. Measured data for the transmittance of the glazing is plotted in Figure 4-11.

3.4 Solar Geometry

The control of the slat angle is highly dependent on the position of the sun. Also, predicted sky illuminance is also a function of sun position. The calculation procedure for determining the solar coordinates is well defined (Duffie et al, 2006) and depends on the latitude and longitude of the geographic location.

As mentioned earlier, the defining parameter for determining the minimum blind angle is the solar profile angle, *d*. The profile angle is defined as the projection of the altitude angle on the vertical plane perpendicular to the building façade (Duffie et al., 2006). This is calculated as in equation (3-4), where α is the solar altitude and γ is the solar surface azimuth.

$$d = \tan^{-1}\left[\frac{\tan(\alpha)}{\cos(\gamma)}\right] \qquad (3\text{-}4)$$

The solar surface azimuth calculation requires that the azimuth angle of the façade is known and inputted into the model. Figure 3-4 displays the parameters used to define the solar position relative to the surface (façade) normal.

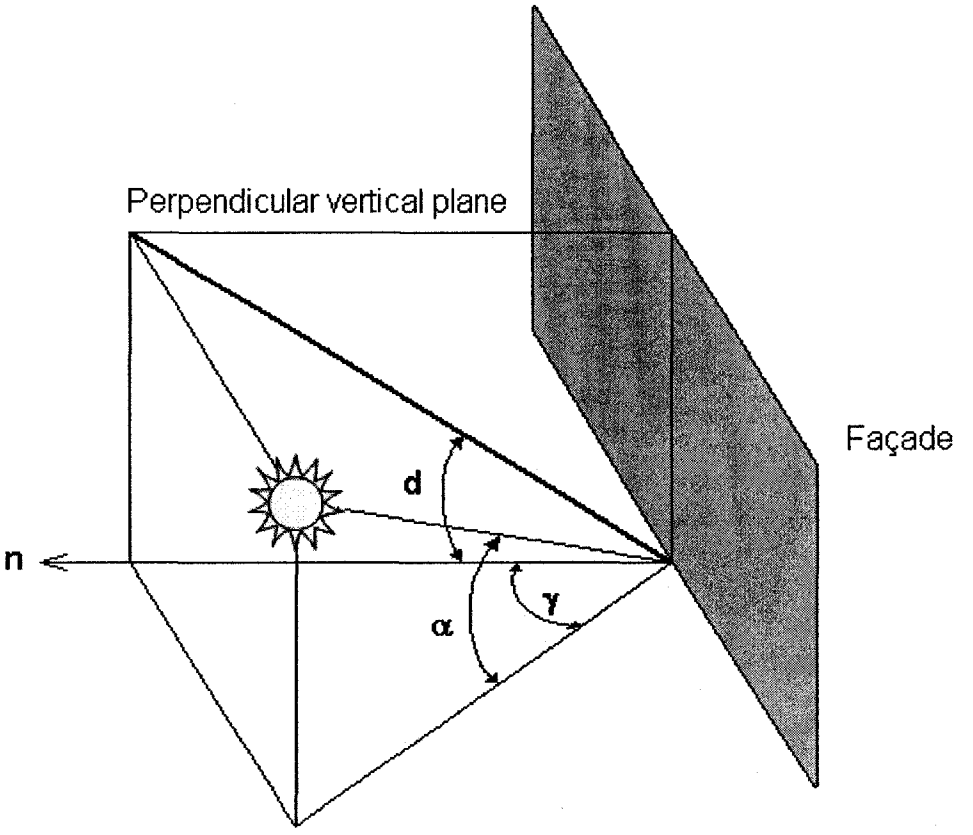

Figure 3-4: *Solar Geometry Nomenclature*

3.5 *Exterior Clear-Sky Illuminance – Modelling*

In order to model the transmittance of the fenestration system on a clear day, the components of the sky radiance must be separated and used in the calculation. The goal of calculating the components of the illuminance, diffuse and direct beam, on a clear day was to first evaluate the effectiveness of the sky illuminance model, but also to determine the feasibility of using a single exterior sensor to determine whether the sky is in fact clear or not. The assumption is that if a modelled clear sky vertical illuminance is significantly higher than the actual measured value, then the sky may be considered overcast and the blinds subsequently opened.

3.5.1 Sky and Solar Illuminance

Exterior diffuse vertical illuminance and direct normal beam illuminance were estimated using a combination of the CIE Clear Sky Model (Duffie et al., 2006) and the ratios of horizontal diffuse illuminance to vertical diffuse illuminance developed experimentally by Perez (Perez et al., 1990).

The CIE model predicts the horizontal sky illuminance using the following formula:

$$E_{hc} = 1000 \cdot \left[A + B\sin^{C}(\alpha)\right] \cdot lux \qquad (3\text{-}5)$$

where for clear-sky conditions, the constants are displayed in Table 3-2.

Table 3-2: *CIE Sky Illuminance Model Constants (Murdoch, 2003)*

Sky Type	A	B	C
Clear	0.8	15.5	0.5
Partly-Cloudy	0.3	45	1
Overcast	0.3	21	1

For estimating the direct normal solar illuminance, the solar illuminance constant, E_{sc}, is used. This value is equal to 127.5 klux. The extraterrestrial illuminance, for any given day, is thus adjusted for the slightly elliptical shape of the earth's orbit around the sun (Murdoch, 2003). Equation (3-6) displays this result:

$$E_{xt} = E_{sc} \cdot \left[1 + 0.034\cos\left(\frac{360}{365} \cdot (n-2)\right)\right] \qquad (3\text{-}6)$$

Where n is the julian day number.

Finally, atmospheric attenuation is accounted for and direct normal solar illuminance at sea-level, E_{dn}, may be expressed as:

$$E_{dn} = E_{xt} \cdot e^{-cm} \quad (3\text{-}7)$$

where c is the optical atmospheric extinction coefficient, with a value of 0.21 for a clear sky (0.8 for a partly-cloudy sky), and m is the ratio of the mass of atmosphere in the actual earth-sun path to the mass when the sun is directly overhead at sea level. It is defined as the inverse of the sine of the solar altitude angle:

$$m = \frac{1}{\sin(\alpha)} \quad (3\text{-}8)$$

3.5.2 Horizontal to Vertical Illuminance Ratio

The relationship between the horizontal and the vertical clear-sky illuminance changes throughout the day, and throughout the year. The Perez (1990) model was developed to extrapolate the components of sky illuminance and irradiance from measurements of global horizontal and direct beam irradiance. In place of measurements of global and direct beam, calculated values from the CIE Clear Sky Model were used and the ratio of diffuse horizontal to diffuse vertical calculated.

The ASHRAE Fundamentals Handbook (2005) also contains diffuse horizontal to diffuse vertical irradiance ratios, Y. The formulation for this ratio is defined in equation (3-9).

$$\begin{gathered} Y = 0.55 + 0.437\cos(\theta) + 0.313\cos^2(\theta), if\ \cos(\theta) > -0.2 \\ Y = 0.45, if\ \cos(\theta) \leq -0.2 \end{gathered} \quad (3\text{-}9)$$

However, unlike the ratios determined using the Perez method, the ASHRAE ratios are location and elevation independent. The values of the two different methods differ. Figure 3-5 displays the ratios of vertical to horizontal illuminance for March 28 and May 1, comparing both the ratios of Perez and those from ASHRAE.

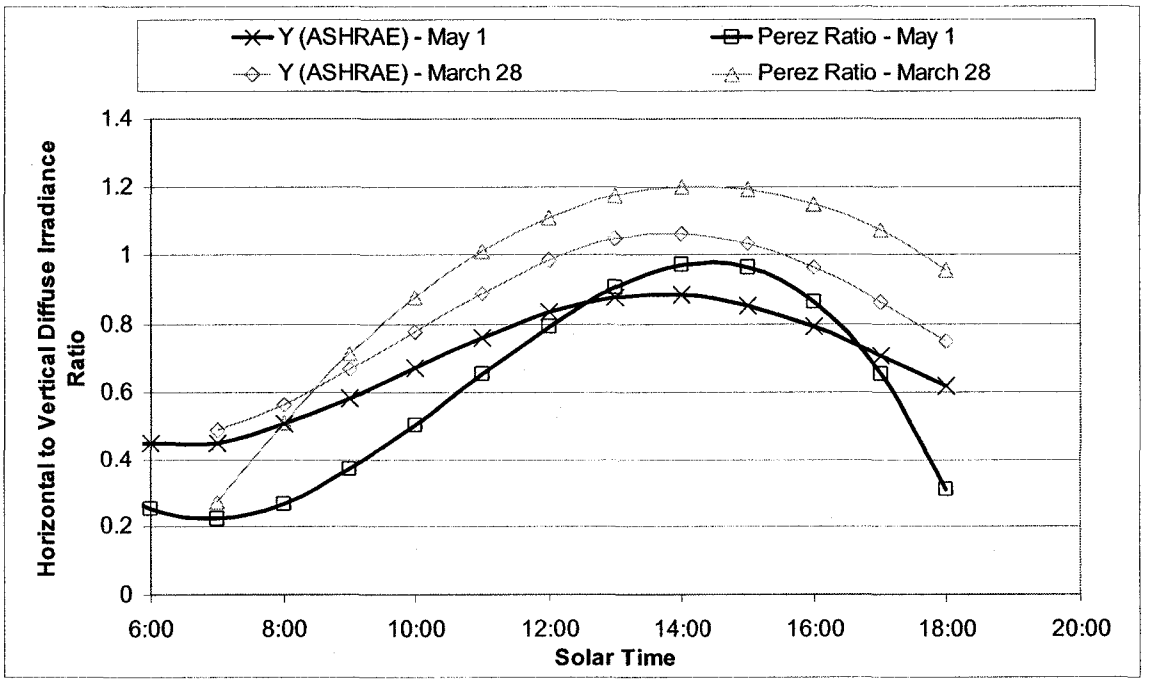

***Figure 3-5**: Vertical to Horizontal Ratios from ASHRAE and Perez Model*

Due to the fact that they consider the site location and elevation, the Perez ratios were used within the exterior illuminance model rather than the ASHRAE ratios.

3.5.3 Reflected Ground Light

Illuminance due to light reflected from the ground was considered in this model, and is a contribution to the total vertical illuminance on the façade. The horizontal illuminance on the ground, E_g, was calculated by including the contributions from the horizontal sky illuminance, E_{hc}, and the direct normal beam illuminance, E_{dn}, as follows:

$$E_g = E_{hc} + E_{dn} \cdot \sin(\alpha) \qquad \textbf{(3-10)}$$

where α is the solar altitude.

As the ground is assumed to be a horizontal flat diffuse-emitting surface infinitely long in both horizontal directions, the view factor between two surfaces at right angles is 0.5

(Murdoch, 2003). The resulting illuminance on the vertical surface, E_{wg}, from the illuminated ground is given by:

$$E_{wg} = \frac{\rho_g \cdot E_g}{2} \qquad \textbf{(3-11)}$$

where ρ_g is the ground reflectance. The ground reflectance was set at 0.2 (concrete) when no snow cover was present, and 0.7 when there was snow.

3.6 Radiosity Theory

Radiosity theory is a method for calculating the transfer of radiant energy between surfaces. The analysis may also be referred to as multiple-bounce flux transfer (Murdoch, 2003). The basic method assumes diffuse reflecting surfaces and the calculation of the form, or view, factors between surfaces is required. The basic flux transfer in a diffuse enclosure is:

$$M_i = M_{i,o} + \rho_i \sum_j M_j F_{ij} \qquad \textbf{(3-12)}$$

where:

- M_i is the final luminous exitance of surface i (lux).
- $M_{i,o}$ is the initial luminous exitance of surface i (lux).
- ρ_i is the diffuse reflectance of surface i.
- M_j is the final luminous exitance of surface j.
- F_{j-i} is the view factor between surfaces j and i.

Essentially, the sum of the inter-reflections from all surfaces is considered, and the final luminous exitance, M_i, of each surface may be calculated.

3.6.1 View Factor Calculation

The view factor calculations used in this model are based on Hottel's Crossed-String Method (Kreith, 1986). Referring to Figure 3-6, the blind system was simplified to be composed of a series two overlaying venetian slats. Four surfaces were assumed: the two slats, and the interior and exterior openings.

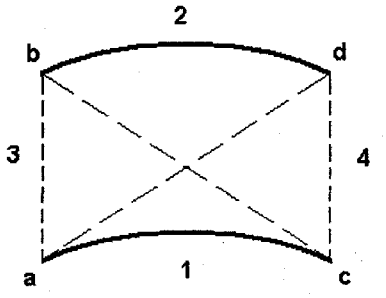

Figure 3-6: *Hottel's Crossed-String Method employed for venetian blinds*

The general form of the view factor equation, with L referring to surface length, is presented in equation (3-13).

$$F_{1-2} = \frac{\overline{ad} + \overline{cb} - \overline{ab} - \overline{cd}}{2 \cdot L_1} \qquad \textbf{(3-13)}$$

The position of the blind slats with respect to one another changes when the slat angle is adjusted. As such, the view factor must be calculated for each blind angle increment.

3.6.2 Blind Illuminance

In this model, the illuminance of the venetian slat was calculated based on the contributions of the transmitted diffuse clear sky illuminance, E_{vc}, the ground reflected illuminance, E_{wg}, and the component of the beam radiation, E_{dn}, normal to the slat surface. The slats were assumed to reflect incident radiation as an isotropic diffuse surface (i.e.: equal properties in all directions). At the cut-off angle, direct incidence is near normal. However, it has been noted from other research that at greater incidence angles, such as when the blinds are maintained at horizontal, the specular reflectance is higher and the diffuse surface assumption may lead to inaccuracy (Kuhn et al., 2000).

Figure 3-6 showed the modelled blind surface layout. It was assumed that the glass, surface *3*, was adjacent to the blind slats, *1* and *2*, and view factors were calculated depending on the calculated blind angle, β. Similarly, view factors were calculated between the lower slat, 1, and the upper slat, *2*, and also between the two slats and the interior open edge of the venetian blind, surface *4*. The view factor calculated between surfaces *3* and *4* allows for the calculation of the transmittance of diffuse exterior daylight directly into the room.

The initial equivalent source exitance of surface *3* (window) was modelled as being the diffuse sky and ground reflected daylight transmitted through the glazing. The initial source exitance of surface *1* is due to the reflected incident direct beam rays, transmitted through the glazing. Figure 3-7 displays the initial sources.

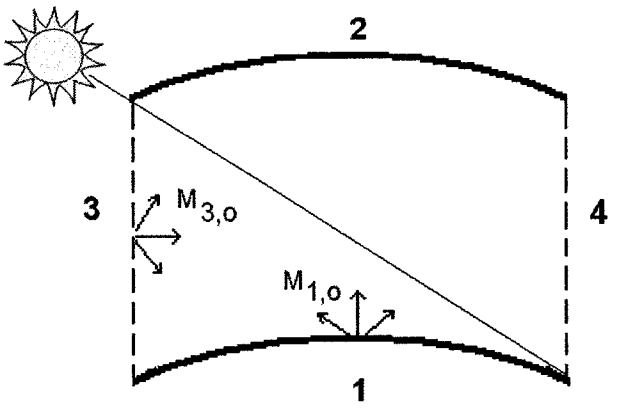

Figure 3-7: *Initial Equivalent Source Exitance of Blind Surfaces*

Numerically, the initial exitance terms are defined in equations (3-14) and (3-15).

$$M_{1,0} = \tau_{wb} \cdot E_{dn} \cdot \cos(\theta_{slat}) \cdot K_{frame} \cdot K_{slat} \qquad \textbf{(3-14)}$$

$$M_{3,0} = (E_{vc} + E_{wg}) \cdot \tau_{wd} \qquad \textbf{(3-15)}$$

where θ_{slat} is the incidence angle from the slat surface normal, and τ_{wd} and τ_{wb} are the diffuse and beam transmittances, respectively, of the glazing. The correction factors, K_{frame} and K_{slat}, are used to account for the shading from the window frame, and also when the slats are not fully illuminated. Both of these factors are the ratios of the illuminated to shaded areas of the blind slat, and are explained in section 3.6.3.

Assuming that the reflectance of the glazing (surface 3) is zero, the flux transfer equation (3-12) can be expressed in matrix form as:

$$\begin{bmatrix} M_1 \\ M_2 \\ M_3 \\ M_4 \end{bmatrix} = \begin{bmatrix} M_{1,0} \\ 0 \\ M_{3,0} \\ 0 \end{bmatrix} + \begin{bmatrix} M_1 & M_2 & M_3 & M_4 \end{bmatrix} \cdot \begin{bmatrix} \rho_1 \cdot F_{1-1} & \rho_2 \cdot F_{2-1} & 0 & \rho_4 \cdot F_{4-1} \\ \rho_1 \cdot F_{1-2} & \rho_2 \cdot F_{2-2} & 0 & \rho_4 \cdot F_{4-2} \\ \rho_1 \cdot F_{1-3} & \rho_2 \cdot F_{2-3} & 0 & \rho_4 \cdot F_{4-3} \\ \rho_1 \cdot F_{1-4} & \rho_2 \cdot F_{2-4} & 0 & \rho_4 \cdot F_{4-4} \end{bmatrix} \qquad \textbf{(3-16)}$$

Since the system is not exactly an enclosure, further adjustments to the formulation must be made. The final exitance of surface 4, M_4, is the actual illuminance on the interior plane of the blinds, directed towards the interior space. The reflectance of this surface was set to equal unity, and no reflected illuminance from surface 4 was added to the other surfaces. Accounting for this adjustment, and knowing that the view factors F_{i-i} are equal to zero, the equation can be reduced to:

$$\begin{bmatrix} M_1 \\ M_2 \\ M_3 \\ M_4 \end{bmatrix} = \begin{bmatrix} M_{1,0} \\ 0 \\ M_{3,0} \\ 0 \end{bmatrix} + \begin{bmatrix} M_1 & M_2 & M_3 & M_4 \end{bmatrix} \cdot \begin{bmatrix} 0 & \rho_2 \cdot F_{2-1} & 0 & F_{4-1} \\ \rho_1 \cdot F_{1-2} & 0 & 0 & F_{4-2} \\ \rho_1 \cdot F_{1-3} & \rho_2 \cdot F_{2-3} & 0 & F_{4-3} \\ 0 & 0 & 0 & 0 \end{bmatrix} \qquad \textbf{(3-17)}$$

Equation (3-17) can also be simplified as follows:

$$\left(I - \begin{bmatrix} 0 & \rho_1 \cdot F_{1-2} & \rho_1 \cdot F_{1-3} & 0 \\ \rho_2 \cdot F_{2-1} & 0 & \rho_2 \cdot F_{2-3} & 0 \\ 0 & 0 & 0 & 0 \\ F_{4-1} & F_{4-2} & F_{4-3} & 0 \end{bmatrix} \right) \begin{bmatrix} M_1 \\ M_2 \\ M_3 \\ M_4 \end{bmatrix} = \begin{bmatrix} M_{1,0} \\ 0 \\ M_{3,0} \\ 0 \end{bmatrix} \qquad \textbf{(3-18)}$$

where the 4 x 4 identity matrix is denoted as I. The solution is thus:

$$\begin{bmatrix} M_1 \\ M_2 \\ M_3 \\ M_4 \end{bmatrix} = \begin{bmatrix} 1 & -\rho_1 \cdot F_{1-2} & -\rho_1 \cdot F_{1-3} & 0 \\ -\rho_2 \cdot F_{2-1} & 1 & -\rho_2 \cdot F_{2-3} & 0 \\ 0 & 0 & 1 & 0 \\ -F_{4-1} & -F_{4-2} & -F_{4-3} & 1 \end{bmatrix}^{-1} \begin{bmatrix} M_{1,0} \\ 0 \\ M_{3,0} \\ 0 \end{bmatrix} \qquad \textbf{(3-19)}$$

By substituting the reflectance for all surfaces as the slat reflectance, ρ_{slat}, the solution of final illuminous exitance of each surface, as in equation (3-19) may be solved by matrix inversion. Particularly, the solution of the exitance of surface *4*, M_4, is the estimated illuminance of the interior plane of the venetian blinds.

3.6.3 Correction Factor due to Shading

Two correction factors were applied, as was seen in equation (3-14), due to shading from both the window frame and the upper venetian slat. The assumption that the venetian blind is directly adjacent to the glazing does not account for possible shading due to the window frame and the gap between the venetian slat edge and the glazing. Furthermore, the upper venetian slat will shade the lower slat when the blind angle is not positioned exactly at the cut-off angle. Correction factors were used in order to simplify the calculation procedure. That is, when the slats are not fully illuminated from direct beam illuminance, it was decided to reduce the total slat illuminance, E_{slat}, by the percentage of the area that is shaded.

Figure 3-8 shows a plan view of a single venetian slat. The distance between the glazing and the venetian blind, D_g, and the shaded length, D_s, that is not illuminated from direct beam illuminance, are defined. The total slat length, L_{slat}, is also shown.

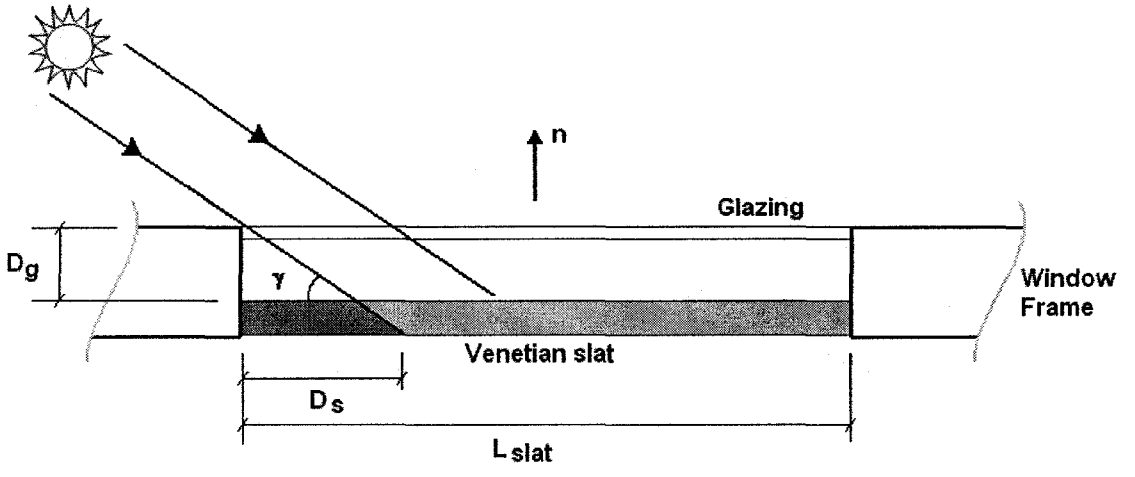

Figure 3-8: *Plan view of venetian slat, showing shaded distance, D_s.*

The correction factor, K_{frame}, is defined as:

$$K_{frame} = 1 - \frac{D_s}{L_{slat}} \qquad \textbf{(3-20)}$$

where:

$$D_s = \frac{D_g}{\tan\left(\gamma + \frac{\pi}{2}\right)} \qquad \textbf{(3-21)}$$

Likewise, the correction factor for shading due to the upper slat, K_{slat}, must be defined. Figure 2-1 shows the side view of two slats. The shaded distance in this case is defined as x. The separation distance between slats, s, is also shown.

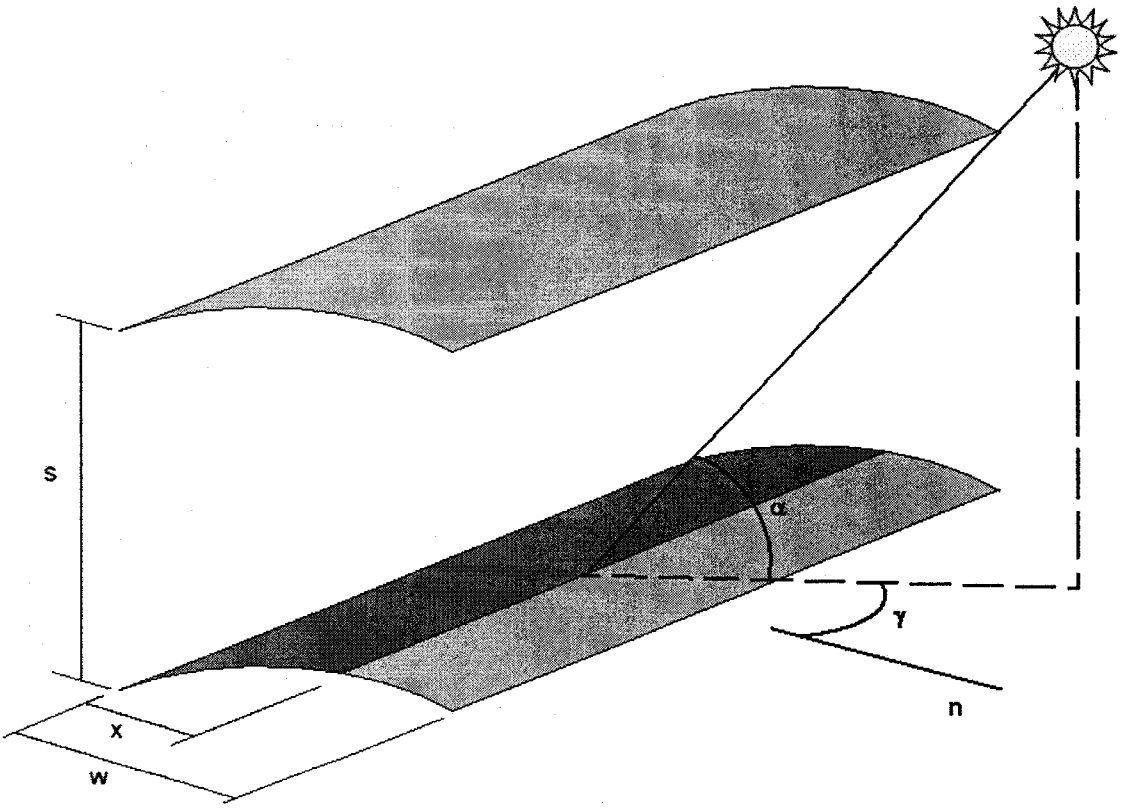

Figure 3-9: *Lower venetian slat shaded by upper slat*

The correction factor, K_{slat}, is defined as:

$$K_{slat} = 1 - \frac{x}{w} \qquad (3\text{-}22)$$

where w is the slat width and the shaded distance, x, is defined as a function of the profile angle, d:

$$x = w - \frac{s \cdot \cos(d)}{\sin(d + \beta)} \qquad (3\text{-}23)$$

The application of these shading correction factors eliminates the need for extensive view factor calculations. This is exemplified in Figure 3-10, where two parallel horizontal venetian slats are shown from the view looking towards the glazing. The bottom slat is shaded by the frame, as was shown in Figure 3-8. To use the view factor method, the system is divided into five surfaces, with surface 5 being an intermediary surface.

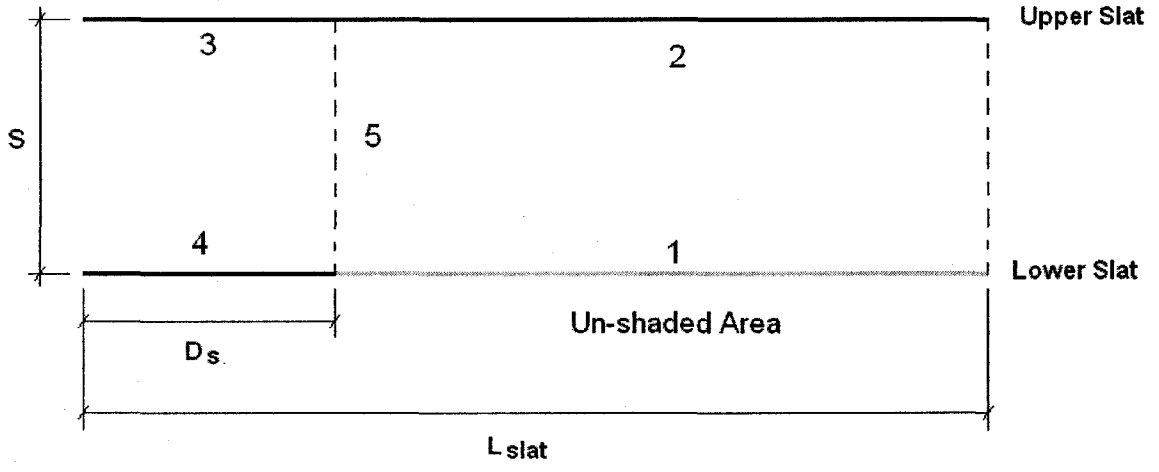

Figure 3-10: *Shaded slat due to frame: View factor calculation*

The system of view factor equations (Incropera et al., 2002) is the following:

$$f_{1-2} = \left[\sqrt{1 + \left(\frac{L_{slat} - D_s}{s}\right)} - 1\right] \cdot \frac{s}{(L_{slat} - D_s)} \qquad (3\text{-}24)$$

$$f_{1-5} = \frac{(1 - f_{1-2})}{2} \tag{3-25}$$

$$f_{5-3} = \frac{1 + \frac{s}{D_s} - \left[1 + \left(\frac{s}{D_s}\right)^2\right]^{1/2}}{2} \tag{3-26}$$

And from the reciprocity theory:

$$f_{1-3} = f_{1-5} \cdot f_{5-3} \tag{3-27}$$

Taking the weighted average of the contribution to each section, in order to have a factor that averages the contribution from surface 1 to the total illuminance of the bottom side of the upper slat, gives the following:

$$factor = \frac{f_{1-2} \cdot (L_{slat} - D_s) + f_{1-3} \cdot D_s}{L_{slat}} \tag{3-28}$$

Of course, averaging the value of illuminance such that it is reduced by the above factor is also a simplification of the process. The alternative would involve discretizing the entire surface and integrating the radiosity calculation across the blind slat, which was considered overly extensive for this application.

The equivalent correction factor, K_{frame}, is compared to the result of the view factor calculation in Figure 3-11. The result shows that the percent reduction, K_{frame}, leads to a similar result to that of the calculation using the view factor method.

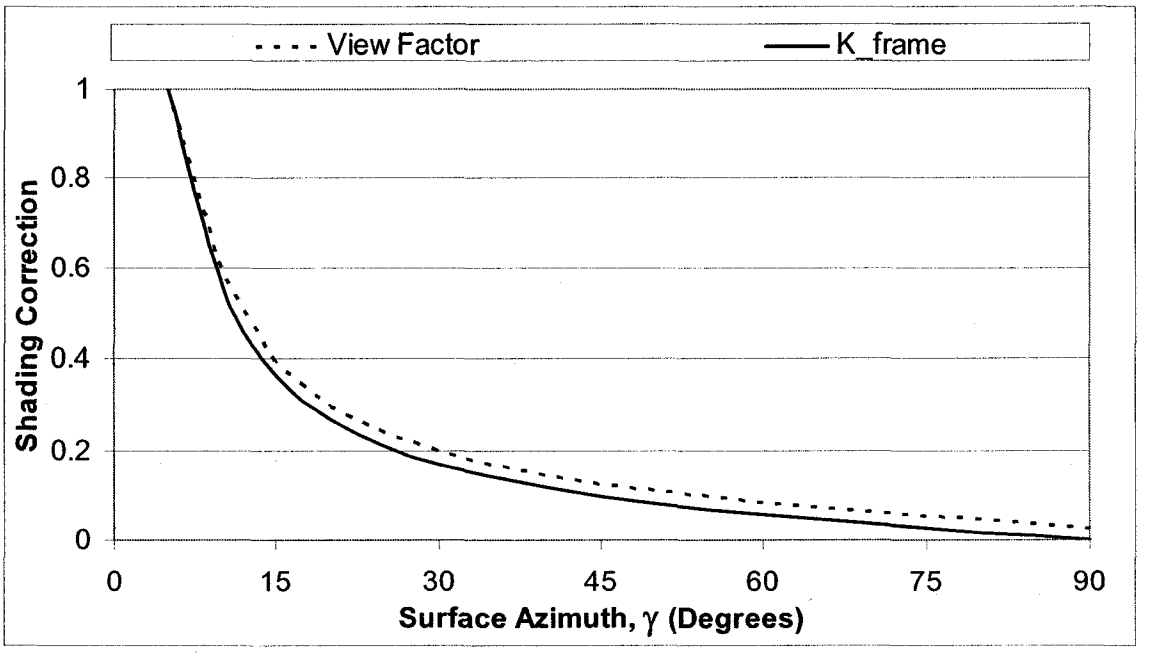

Figure 3-11: *Comparison of correction factor K_{frame} to View Factor Calculation*

Similarly, the view factor calculation method for K_{slat} would involve substituting L_{slat} with the slat width, *w*.

3.7 Numerical Model

The numerical model was employed with time-steps (5-minutes) chosen to correspond to the experimental setup. Selection of the time-step implemented on the control algorithm is important in order to ensure that direct sun is always blocked, dependent on the solar profile angle, *d*. For this experiment, the minimum blind angle increment was 10 degrees due to physical limitations of the blind system, discussed in section 4.3. In order to ensure a correct time step, the rate of change of the required blind angle with respect to time was calculated. For example, for April 20th the required calculated blind angle is plotted in Figure 3-12.

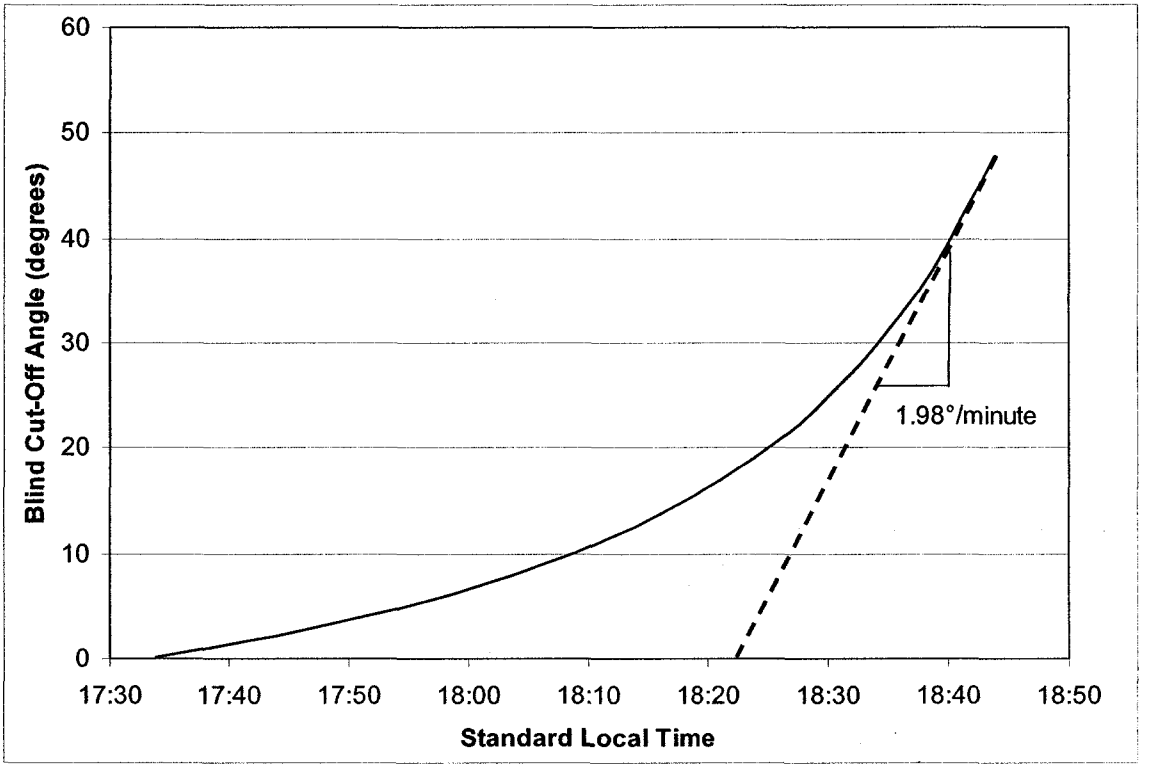

Figure 3-12: *Blind cut-off, rate of change for April 20*

The maximum derivative of the blind angle with respect to time throughout the range is 1.98 degrees per minute. This maximum rate is similar throughout the year. Thus, the blind angle must be incremented 10 degrees at a minimum time-step of five minutes.

Chapter 4: Experimental Setup

4.1 Introduction

In order to test the transmittance model that was developed, a full scale experiment was conducted. This section describes the experimental setup, the equipment used and the procedure of measurement.

4.2 Zone

The experiment was undertaken in the top floor of the Concordia University Engineering and Visual Arts building in Montréal, Canada (45°30' N, 73°36' W). The façade surface azimuth is approximately 20 degrees west of south, and there are no external obstructions to direct solar irradiance (See Figure 4-1).

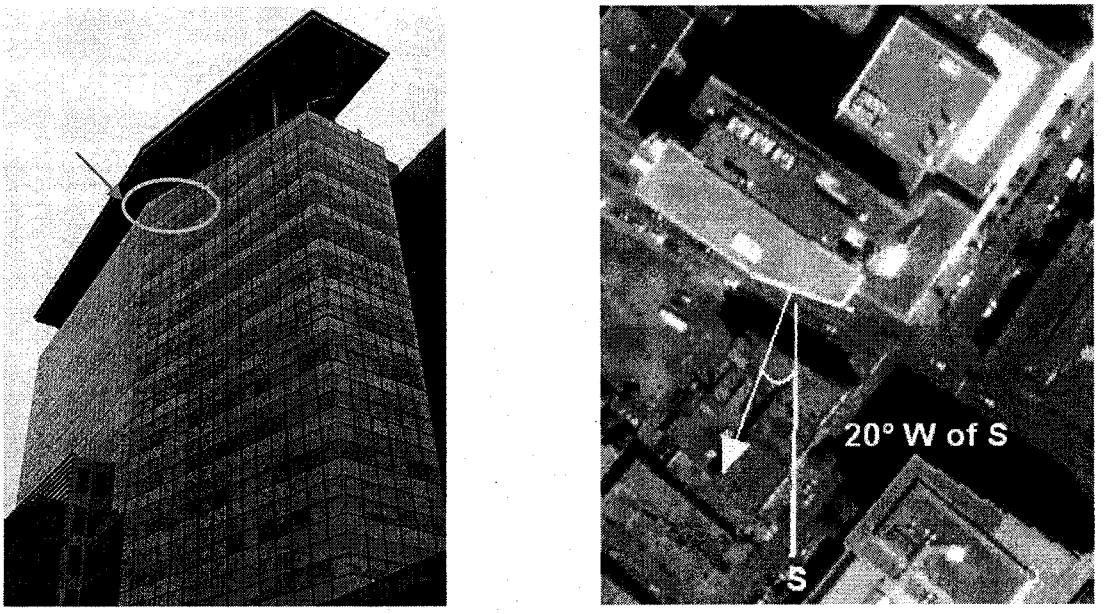

Figure 4-1: *Concordia University EV Building, Montréal, Canada*

One glazing unit of the research lab façade was isolated by enclosing the area with white drapes. A second glazing unit in the zone was blacked out. The zone may be considered as being a small office space with one window. The dimensions of this area are 2.2m perpendicular to the façade, by 1.8m wide and 3m high. Figure 4-2 displays the interior façade of the research lab, without the divisions between windows.

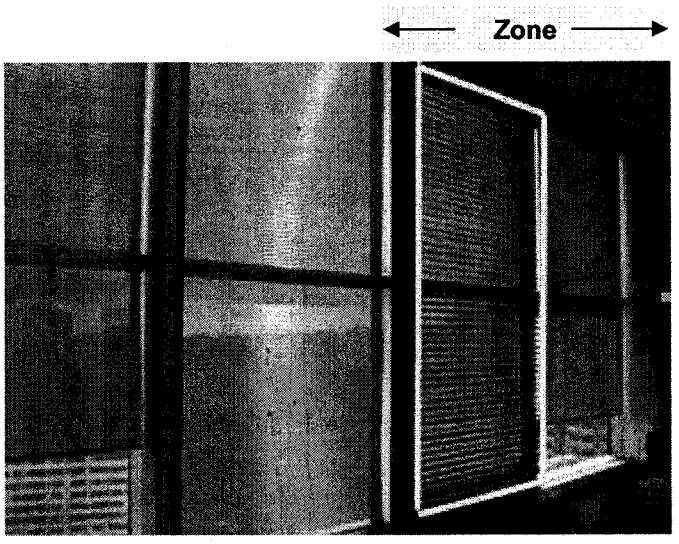

Figure 4-2: *Venetian blind section*

4.3 Venetian Blind

Somfy Canada Inc.[3] provided Concordia University with a motorized venetian blind to be used in the control experiments. The venetian blind was manufactured to specified dimensions and thus covers the complete glazing unit and is well aligned with the window frame. The distance between the glazing and the blind is approximately 15 cm. The individual slat width, *w*, is 47 mm, and the separation distance between the slats, *s*, is 44 mm. The venetian blind used for this experiment is shown in Figure 4-3.

[3] www.somfy.com

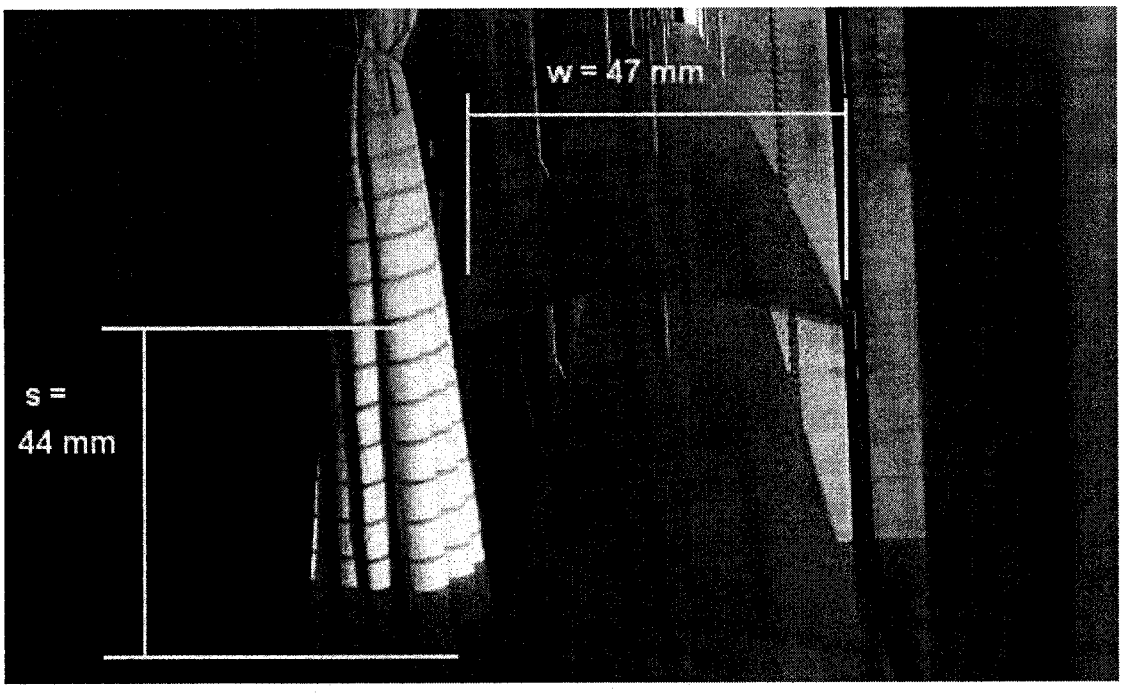

Figure 4-3: *Dimensions of Experimental Venetian Blind*

The blind is actuated by a 24 VDC powered motor. The motor action spools the strings joining all slats. In the upward direction, the slats fully tilt downward, and are subsequently lifted towards the motor. The inverse is true for the downward direction. As such, a change in direction of the blind motor action changes the tilt angle, β, of the horizontal slats.

The slats are grey and, as was shown in Figure 3-1, the slat normal reflectance is highly diffuse in the visible range. Table 3-1 showed the average specular reflectance, as a percent of total, in the visible range and at varying incidence angles.

4.3.1 Venetian Blind Automation

The motorized venetian blind was controlled using the relays of an *Agilent 34907A* data acquisition and control unit (DAQ), as shown in Figure 4-4. An algorithm was programmed in a PC running the control software VEE Pro. The algorithm (Figure

4-5) calculated the real-time solar geometry and the appropriate blind cut-off angle on a continuous loop running every five minutes.

A 24VDC power supply was connected in series with the relays, as well as the DC blind motor. Supplying the blind motor with power involved switching the relay from open to closed state. The maximum switching speed of the relays was the limitation for the minimum pulse size that could be sent to the motor, and hence the smallest blind angle increment. The result of the maximum switching speed of the control unit and the physical properties of these particular venetian blinds was a minimum blind increment of approximately 10 degrees.

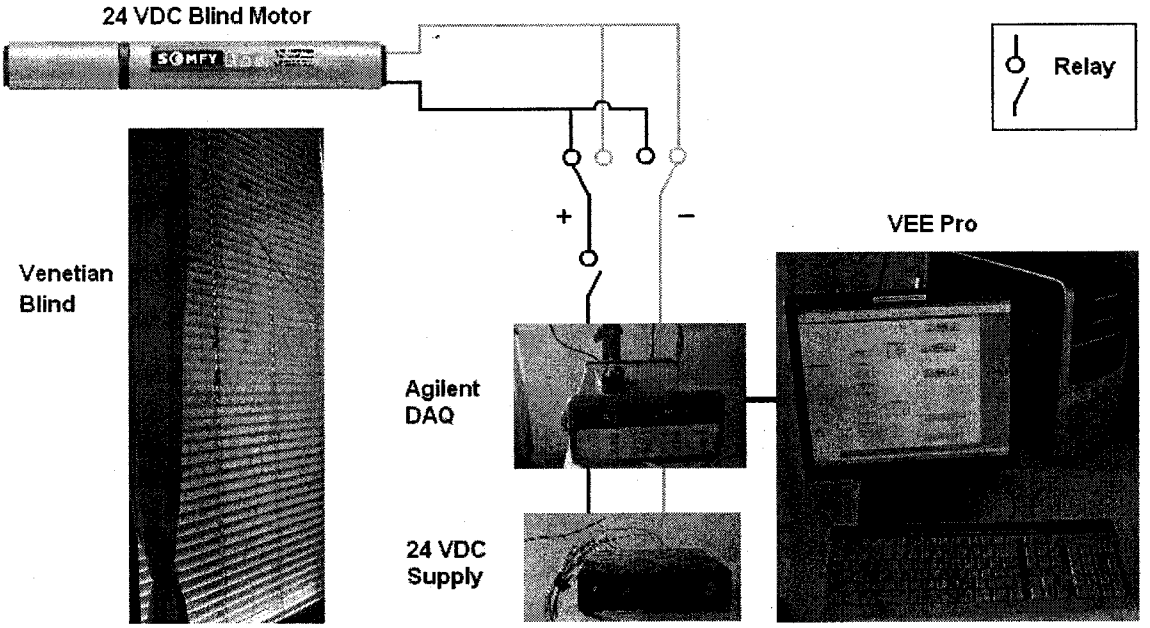

Figure 4-4: *Venetian Blind Control Setup*

The purpose of the control was to test the transmittance model while continuously implementing the cut-off angle, and to determine the corresponding interior blind illuminance levels throughout the day. In order to maintain a consistent control of the

implemented blind angle and to simplify the control structure of the algorithm, the blinds were closed completely at each time step, and the appropriate blind angle was then implemented to the nearest 10 degrees. This eliminated the need for a position memory within the control algorithm loop.

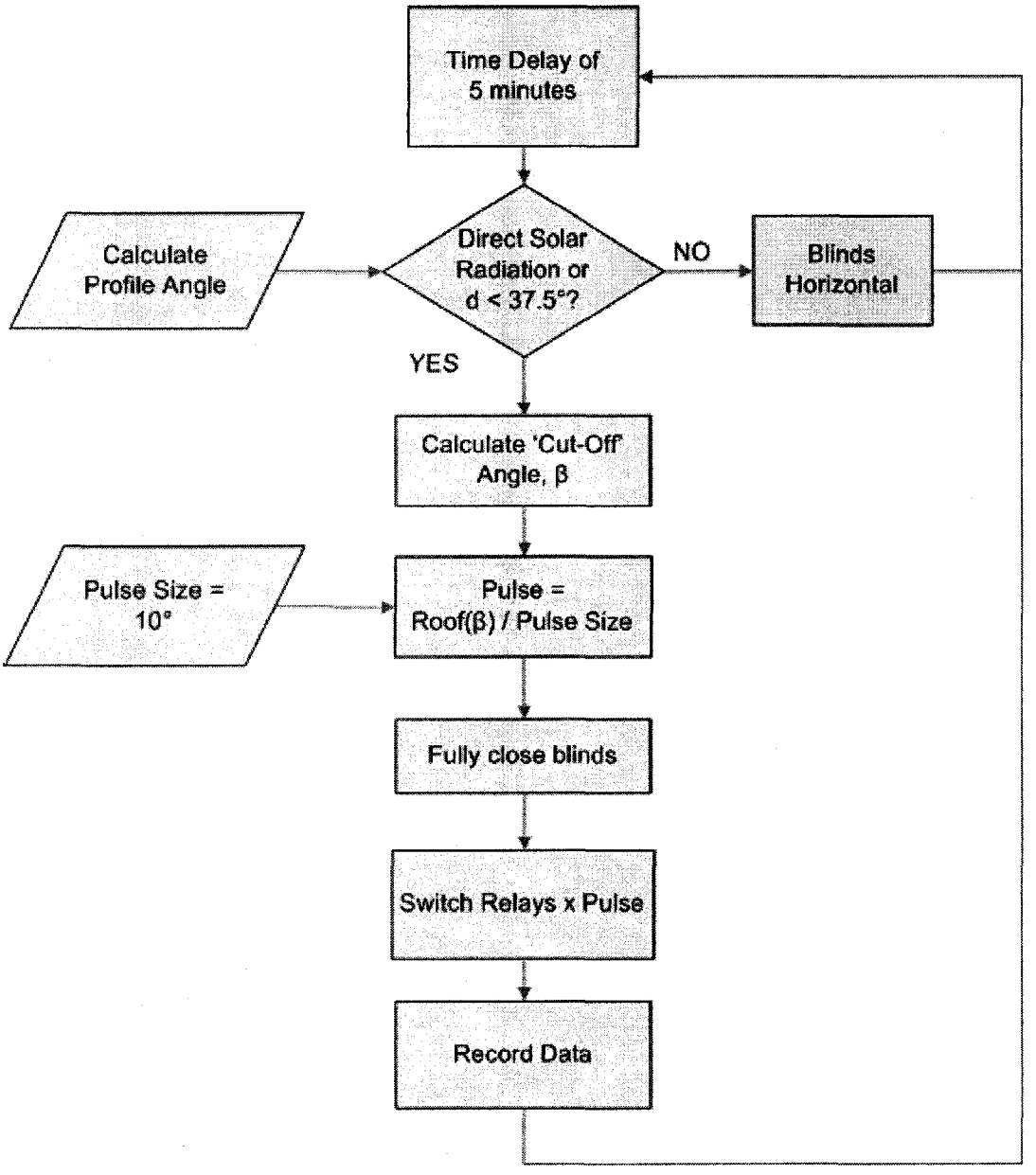

Figure 4-5: *Experimental Cut-Off Angle Algorithm*

4.4 Dimmable Electric Lighting

Canlyte Inc.[4] donated a dimmable fluorescent luminaire to Concordia University for use in the experiments, and this was installed within the zone, parallel to the façade (Figure 4-6). This luminaire contains two 4-foot fluorescent T5 lamps, each with a full-power consumption of 28 W. The ballasts are capable of dimming the lamps from 100% to 1% using the DALI (Digital Addressable Lighting Interface) protocol.

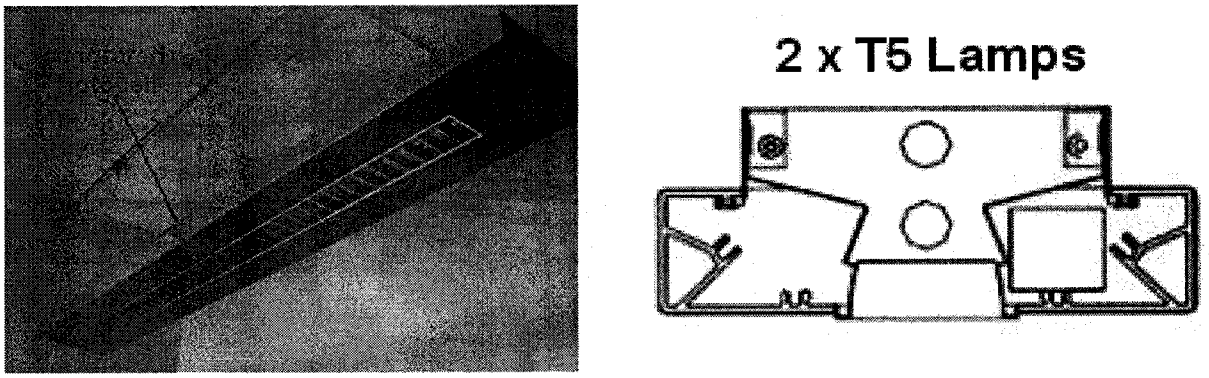

Figure 4-6: *Lightolier Dimmable Fixture with Integrated Photocell*

This luminaire maintained the zone work-plane illuminance at a maximum of 400 lx with no other lighting sources, and has an integrated photocell that measures the upward reflected illuminance. The set-point for the photocell was set to the maximum, so that the illuminance would not drop below 400 lux. The design illuminance for the Concordia EV Building is 375 lux.

The luminaire was positioned at a height of 2.5 m from the ground, and 1.7 m from the façade. At this height, the integrated photocell senses a radius of 1.4 m at ground level (The angle of measurement from the sensor is specified to be 35°). Thus, the

[4] www.canlyte.com

window illuminance was not in the sensor's line of view. The experimental setup is shown in Figure 4-7.

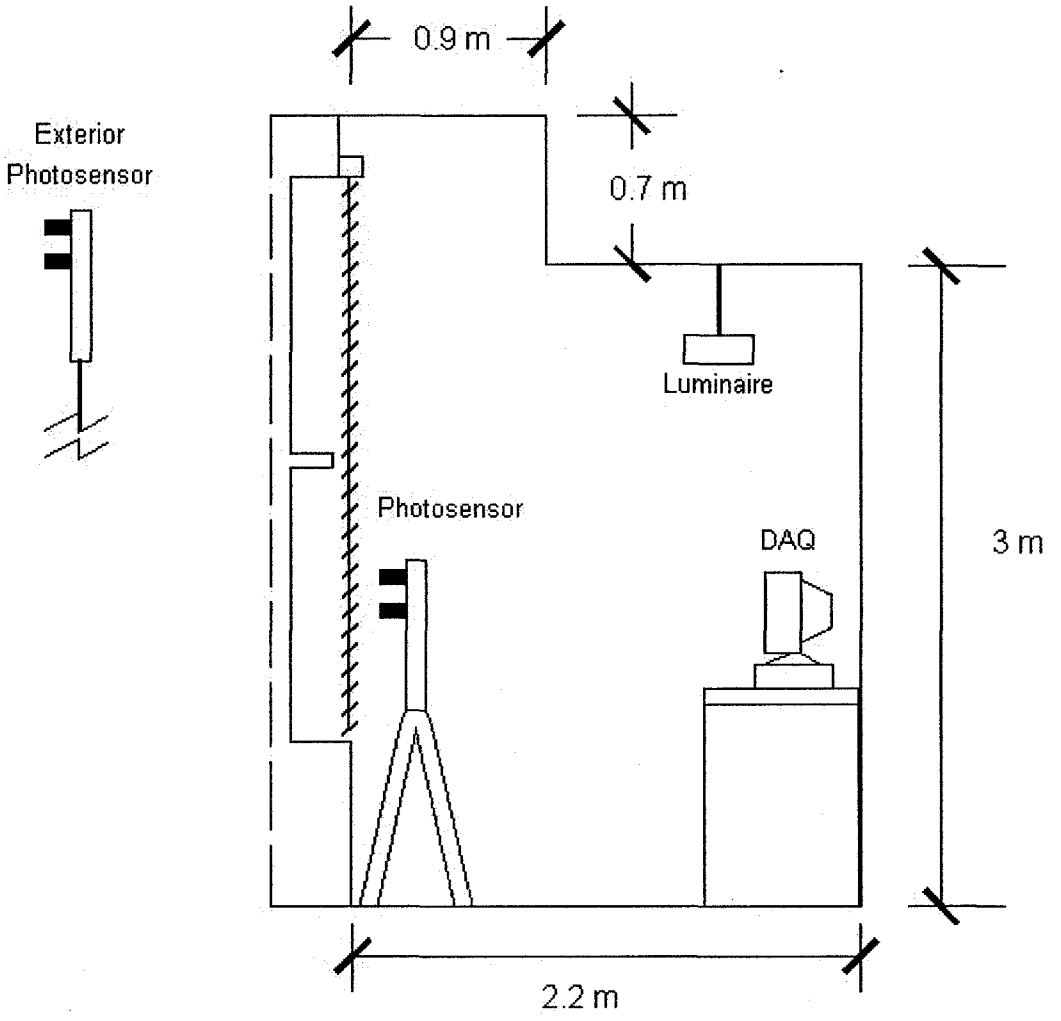

Figure 4-7: *Sensor Placement and Experimental Setup*

The total measured luminaire power consumption is plotted in Figure 4-8 for dimming values from full-scale to 1% of the luminous output. A digital value is sent to the ballast (254 for 100%, and 85 for 1%) via the integrated photocell, and using the DALI communication protocol.

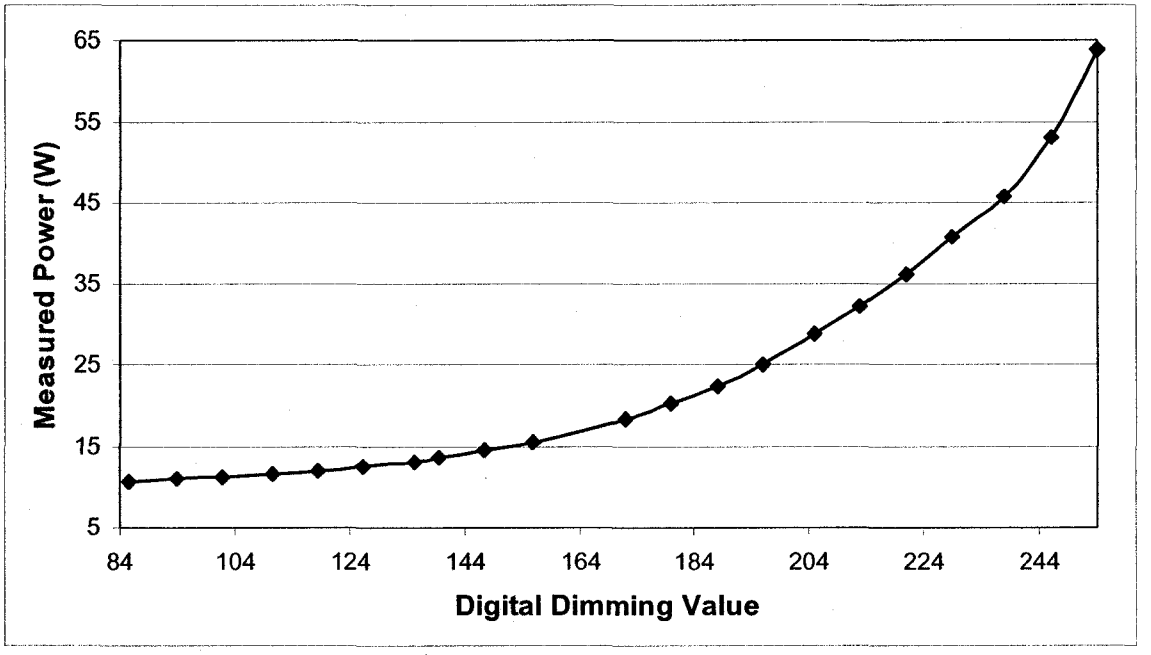

Figure 4-8: *Luminaire Power Consumption versus DALI digital dimming value*

Since all DALI compliant devices dim their luminous output at the same rate (Pflaum, 2001), the power consumption versus percent luminous flux can be calculated. This is shown in Figure 4-9.

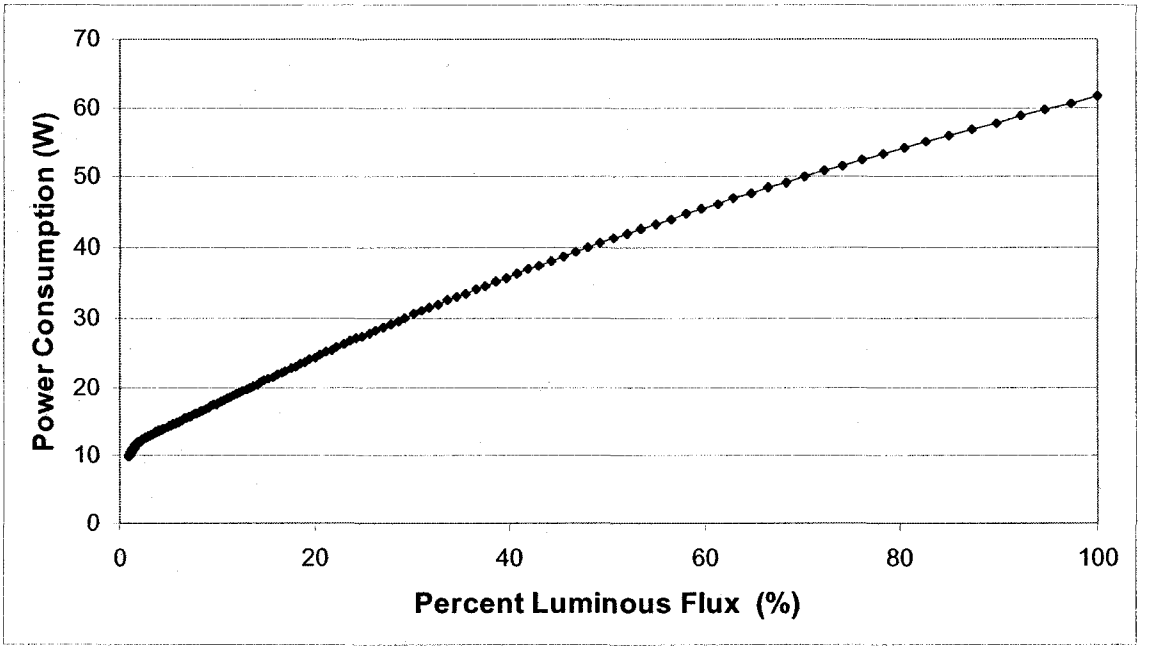

Figure 4-9: *Luminaire power consumption versus percent luminous flux output*

The dimming signal sent to the ballast was recorded using in-house software provided by *Tridonic Inc.*[5], the manufacturers of the photocell. The integrated photocell of the luminaire does not provide data over the DALI bus, and cannot be queried like other DALI devices. Instead, the software queries the ballast level using the DALI bus, and the digital value is recorded with time. The values of the dimming level of the ballast were recorded at 3-minute intervals, and the digital values were converted to the corresponding power value using the measured power profile shown in Figure 4-8. A handheld photosensor was used to verify that the work-plane illuminance was maintained at a value greater than 400 lux.

4.5 Sensor Layout

In order to quantify the transmittance of the fenestration, exterior and interior photocells and pyranometers were installed as shown in Figure 4-7. Vertical illuminance measurements were taken using two Li-Cor LI-210 (Figure 4-10) photometric sensors: one positioned on the exterior of the building façade, and the other placed near the interior plane of the venetian blinds. The sensors have a spectral response from 380nm – 700 nm and are pre-calibrated against a standard lamp using 683 lumens per watt as the value of spectral luminous efficacy at a wavelength of 555 nm. The accuracy of these sensors is 5% for most light sources with a maximum deviation from linearity of 1% up to 100 klux. The sensors are cosine corrected for incidence angles up to 80 degrees.

The Agilent DAQ was used to record the signal from the sensors. The calibrated voltage measurement was programmed into the VEE Pro control algorithm as the final

[5] www.tridonicatco.com

action in the control sequence so that the readings were taken after the blind was set to its position.

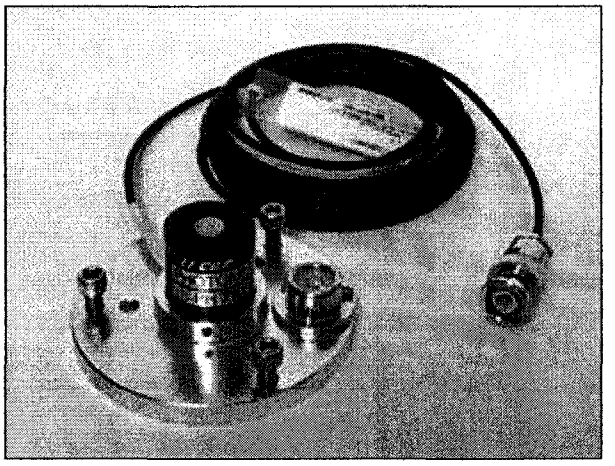

Figure 4-10: *Li-Cor 210 Photometric sensor (Li-Cor Biosciences[6])*

4.6 Glazing Transmittance

To determine the transmittance of the glazing, a photocell was placed on the interior side of the glass. The ratio of interior illuminance to exterior illuminance, when the solar irradiance levels were below 100 W/m^2, was used for the diffuse transmittance of the glazing. The average value from 1900 one-minute measurements was found to be 0.62, with a standard deviation of 0.02.

Figure 4-11 displays the recorded data for the beam transmittance when irradiance values were greater than 300 W/m^2. Note that the incidence angles are relative to the window surface normal.

[6] www.licor.com

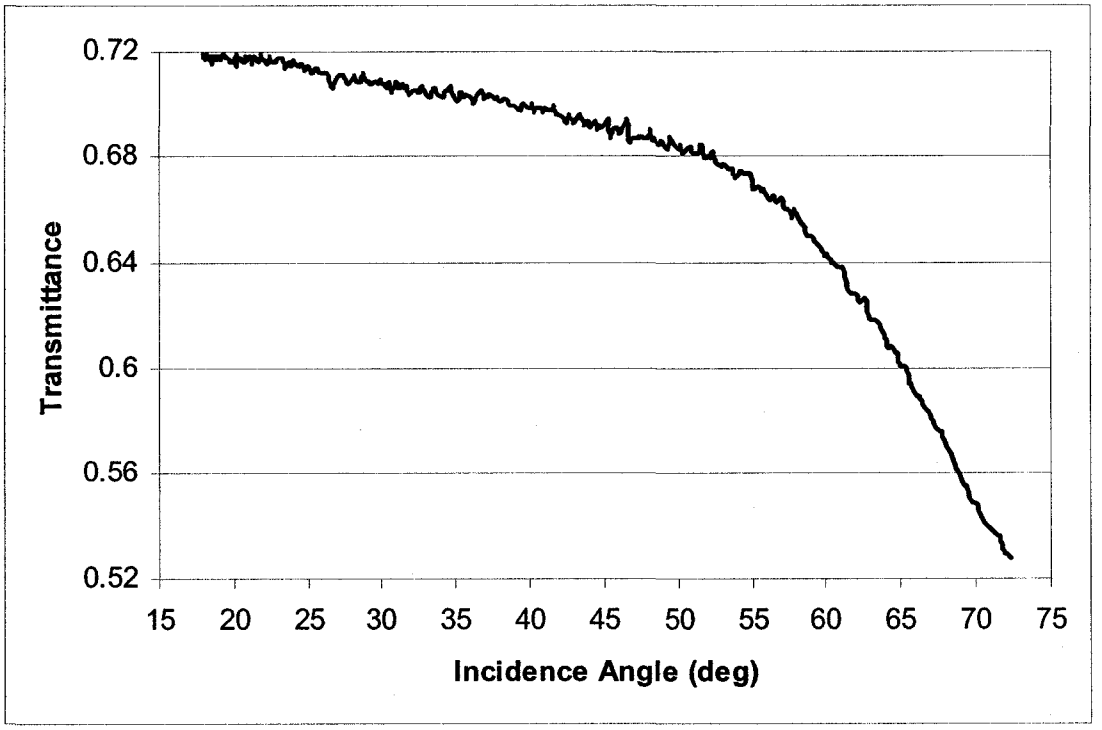

Figure 4-11: *Measured glazing direct beam transmittance,* τ_{wb}

Chapter 5: Experimental Results and Model Verification

5.1 Introduction

The experimental objective of this study was twofold:

1) Compare the modelled prediction of the blind transmittance for clear-sky conditions to the actual measured values. The purpose was to evaluate the venetian blind transmittance model, and whether it would be sufficient for controlling the blinds on clear days.

2) Measure the electrical power consumption of the luminaire installed within the test zone. The objective was to quantify the electrical energy reduction of using daylight controlled luminaires along with controlled venetian blinds. These experiments were conducted on clear days with the blinds controlled to be at the cut-off angle.

5.2 Clear-Sky Model

The clear-sky model described in section 3.5 combined the CIE clear-sky model with the vertical to horizontal sky illuminance ratios developed by Perez (1990). The direct beam, sky and ground reflected daylight on the vertical façade was modelled for each day that experiments were carried out at the Concordia University EV-building in

Montreal. These modelled values were compared to the measured values of vertical illuminance that were taken at the exterior of the building.

The comparison between modelled and measured values for a clear day with dispersed clouds on January 7, 2007 is presented in Figure 5-1. The agreement between the modelled and measured values was quite good, especially when the façade was directly illuminated by the sun. Since there was snow cover on this day, it can be seen that the modelled value depends on the effect of ground reflectance.

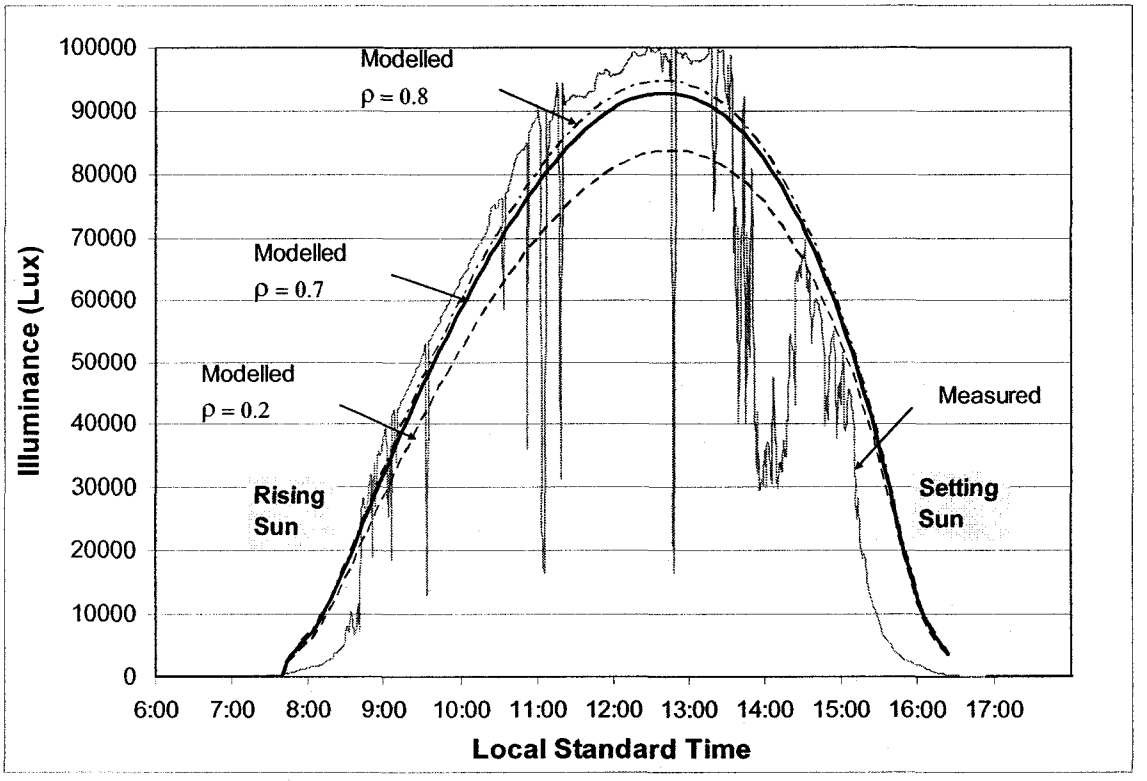

Figure 5-1: *Modelled exterior vertical total hemispherical illuminance compared to measured, and the effect of varying the modelled ground reflectance for January 7, 2007*

The reflectance of fresh snow is about 0.75 (Murdoch, 2003), and for the model 0.7 was used to account for the urban landscape. Other values of reflectance were used as a comparison. The maximum error occurred in the early morning, due to shading from a nearby building, and in the evening when the sun was setting behind Mont Royal. The

percent error for various times throughout the day is displayed in Table 5-1. Sensor error is 5%

Table 5-1: *Error between modelled and measured values (January 7, 2007)*

Time	Percent Error		
	ρ = 0.2	ρ = 0.7	ρ = 0.8
9:14	21.7	**11.7**	9.7
9:59	18.1	**7.6**	5.5
10:59	21.7	**12.0**	10.0
11:59	15.5	**5.6**	3.6
12:59	15.3	**6.3**	4.5
14:54	1.8	**9.7**	11.3

Modelled and measured values of exterior vertical illuminance for a clear day on March 28, 2007 are presented in Figure 5-2. This data shows very good agreement between the modelled and measured values. In this case, there was no snow cover and the ground reflectance was set to 0.2.

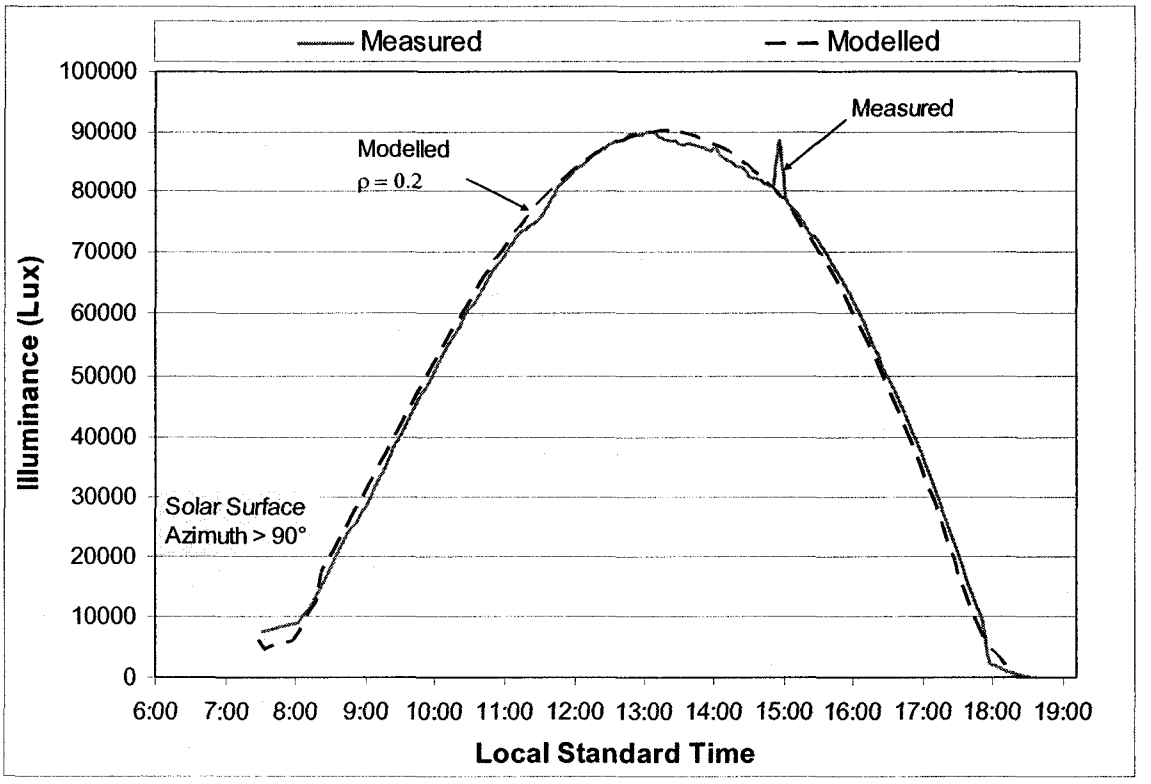

Figure 5-2: *Modelled exterior vertical total hemispherical illuminance compared to measured for March 28, 2007*

One major observation was the reduction in total illuminance when the sun was parallel with the building façade. This can be attributed to the reduced reflectance from neighbouring buildings, as their façades were not directly illuminated. Error from the sensor cosine correction is not expected to be a cause of this decrease as the luminaire photocell also reads a decrease at this time (Figure 5-13). This is further exemplified for data collected on May 3, 2007 (Figure 5-3), where the morning was clear and the large increase when the sun passes in front of the building façade can be easily seen. In order to account for reduction in the modelled values, the ground reflectance was reduced to zero when the solar surface azimuth was between 85 and 95 degrees.

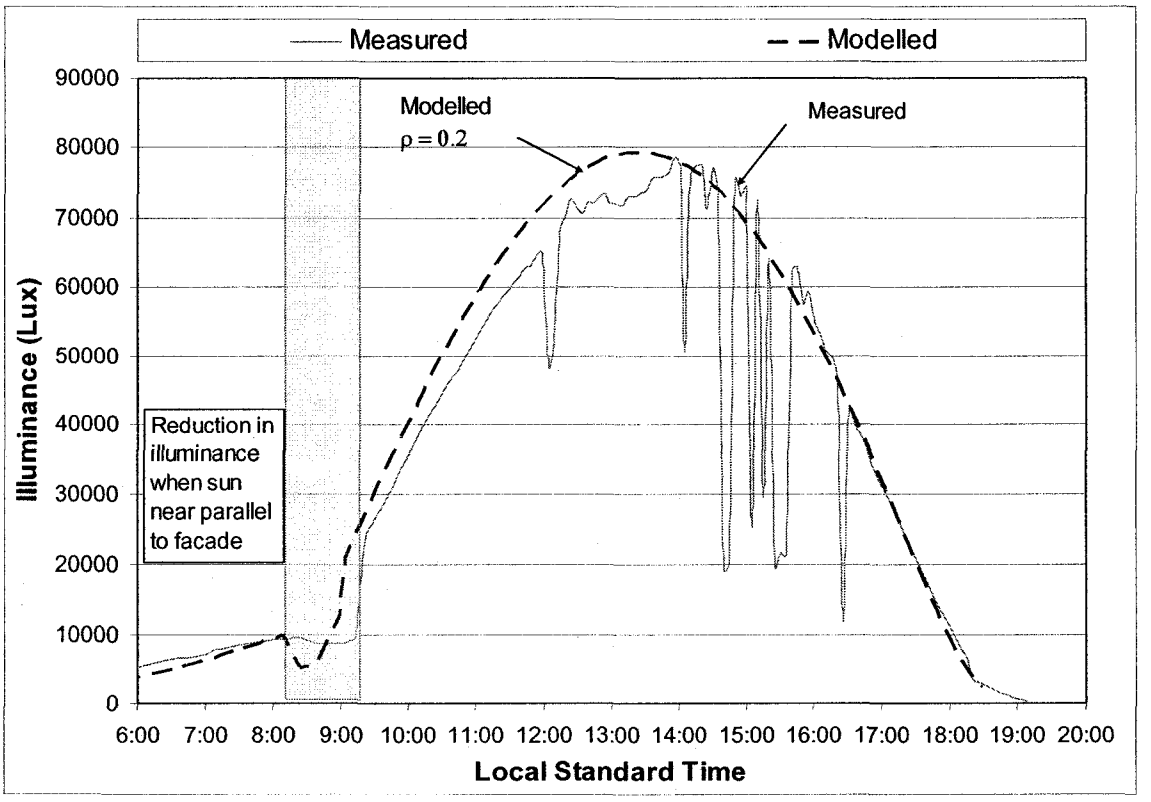

Figure 5-3: *Modelled exterior vertical total hemispherical illuminance compared to measured, showing the effect of the sun passing in front of the building, May 3, 2007*

The changing value of ground reflectance would be difficult to implement in a model-based control algorithm. The goal is to use the modelled exterior illuminance to develop thresholds for when the sky is clear. Since the illuminance from ground reflectance is only a small part of the total illuminance, it is expected that these thresholds can still be developed.

5.3 *Fixed Blind Angle: Model Verification*

Experiments were conducted to record the exterior vertical illuminance and the interior blind illuminance for fixed slat angles. Two separate cases were studied:

1) Clear-sky winter, with slats at 40 degrees;

2) Clear-sky spring, with slats at 70 degrees.

5.3.1 Clear-Sky Winter, Fixed Slat: 40 degrees

Measurements were conducted during a sunny day on January 7, 2007, to quantify the transmittance of visible light through the studied fenestration system with the venetian blind slat angle set at 40 degrees. This angle satisfies the required cut-off angle for the majority of the day, and was chosen as a case where higher transmittance would be desired for the heating season. Measurements were taken of the exterior vertical illuminance and irradiance, as well as the interior transmitted vertical illuminance and irradiance on the interior side of the venetian blinds. The sampling period was one minute. Figure 5-4 displays the modelled and measured results of interior blind illuminance for this day.

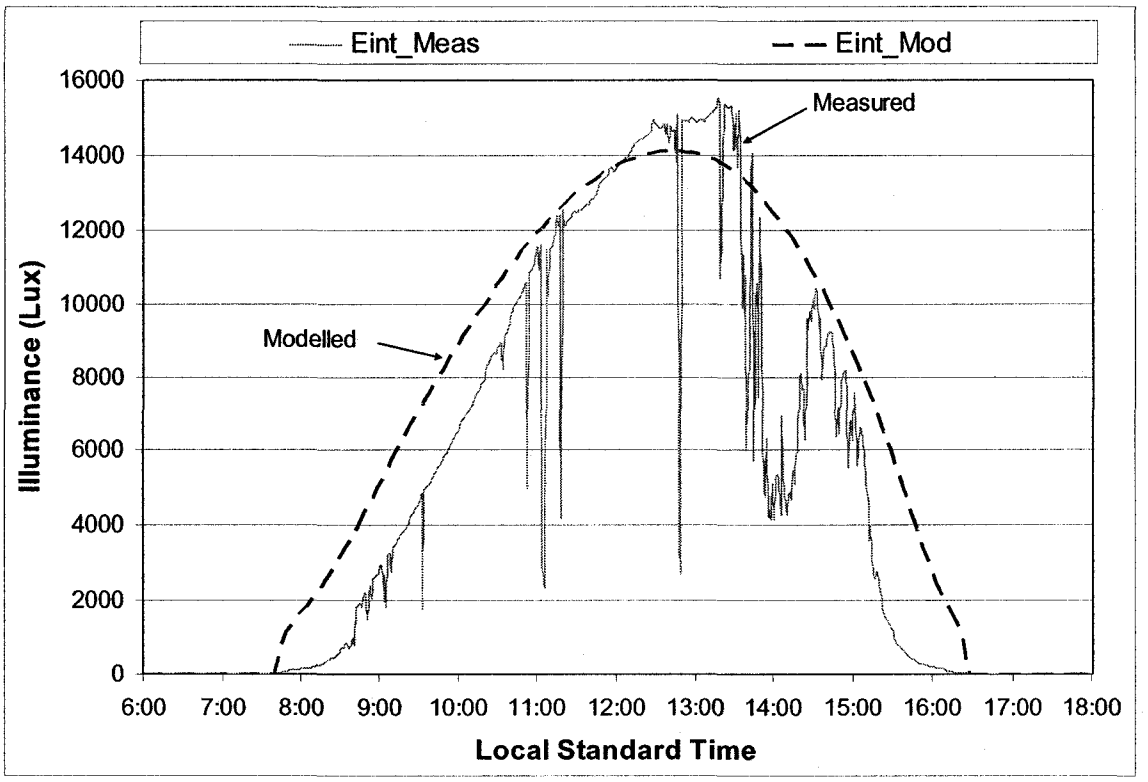

Figure 5-4: *Interior Blind Illuminance, Slat Angle = 40°, ground reflectance = 0.7 (Jan. 7, 2007)*

This data shows that the modelled and measured values are in reasonable agreement when the actual sky conditions were clear. The absolute error at the peak illuminance is in the order of 1,500 lux. Measurement error is +/- 770 lux at this time. Since the actual recorded exterior illuminance was slightly higher than that modelled (Figure 5-1), a comparison of the measured and modelled transmittance of the system was carried out.

Figure 5-5 displays a comparison between the modelled and measured transmittances for January 7, 2007. The maximum absolute error between the modelled and experimental values of transmittance is about 0.05, and this occurs early in the morning. At noon, the predicted versus measured transmittance had absolute errors in the order of 0.015. Accumulated error in the measured transmittance, considering 5% error in both the measured exterior and interior illuminance, is +/- 0.011. It is expected that the

error which occurs may be due to increased specular reflection effects at high incidence angles (62 degrees at 9:00).

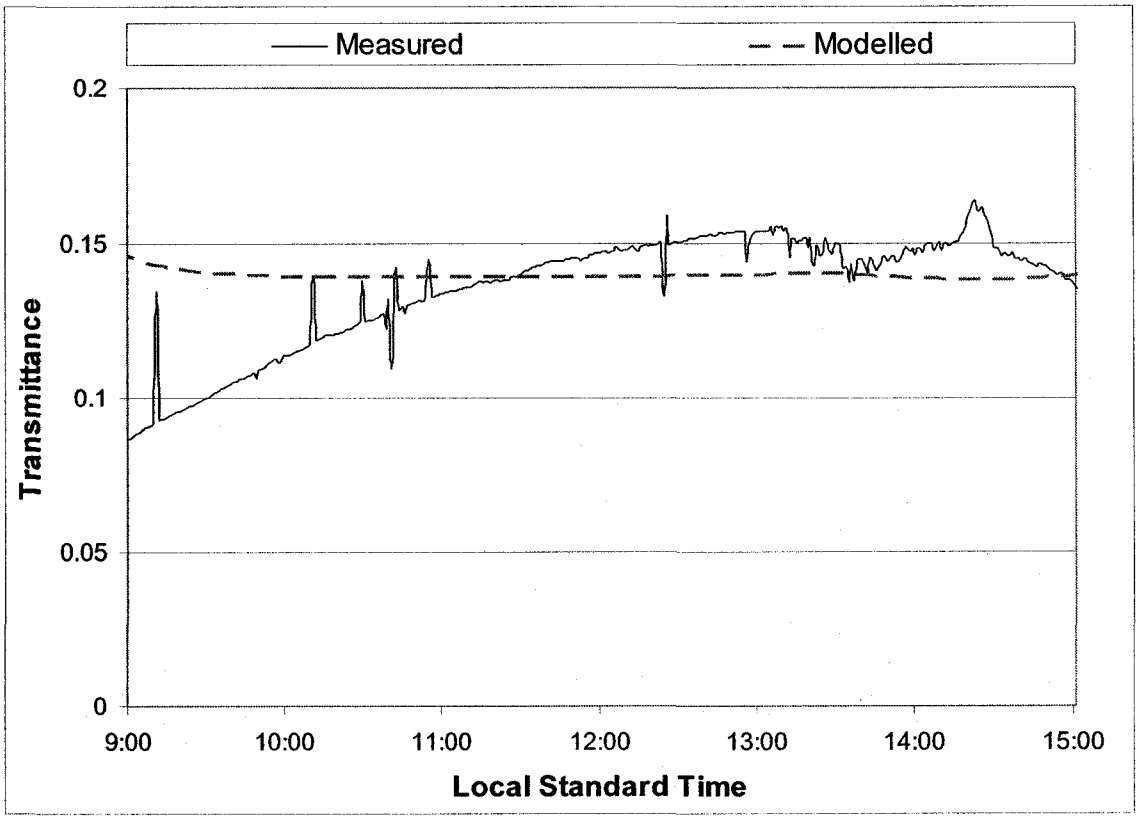

Figure 5-5: *Transmittance, Slat Angle = 40°, ground reflectance = 0.7 (Jan. 7, 2007)*

5.3.2 Clear-Sky Spring, Fixed Slat: 70 degrees

On May 3, 2007, the blind angle was set to 70 degrees throughout the day in order to compare the experimental and predicted results at higher blind angles. This would be comparable to a situation where daylight is desired without excessive solar gains. Results of the modelled versus measured data correspond well at this blind angle, as shown in Figure 5-6. The peak illuminance values, such as observed at 10:25, are the result of direct beam penetration through the string holes of the venetian blind.

The modelled transmittance for this day is displayed in Figure 5-7.

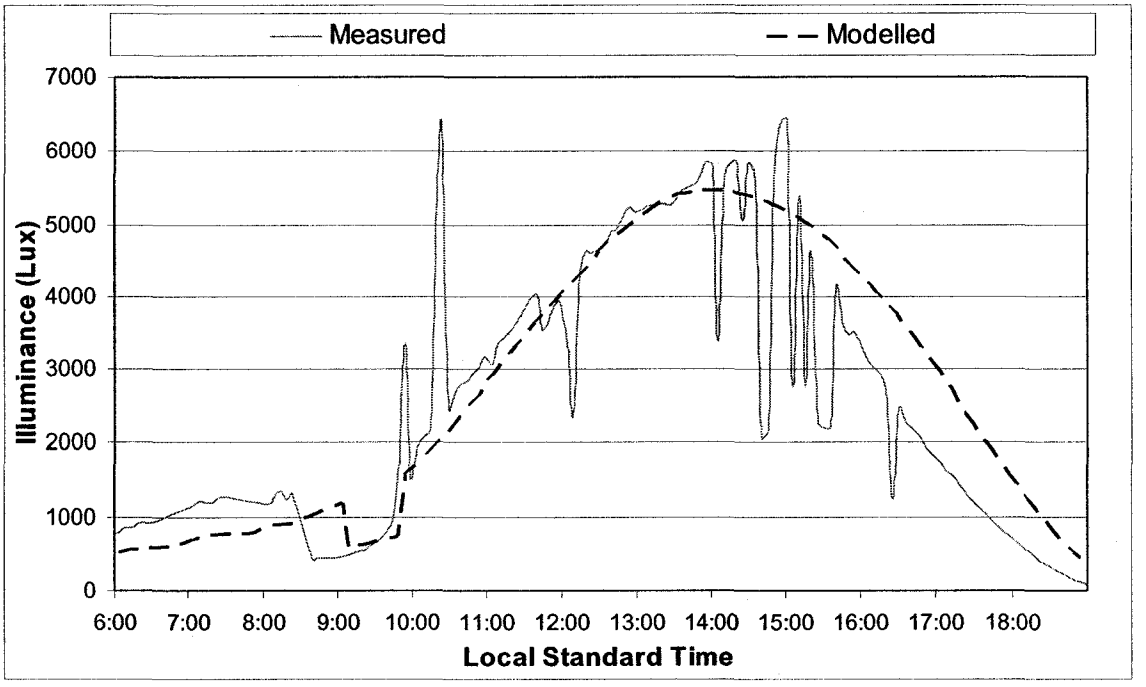

Figure 5-6: *Interior Blind Illuminance, Slat Angle = 70°, ground reflectance = 0.2 (May 3, 2007)*

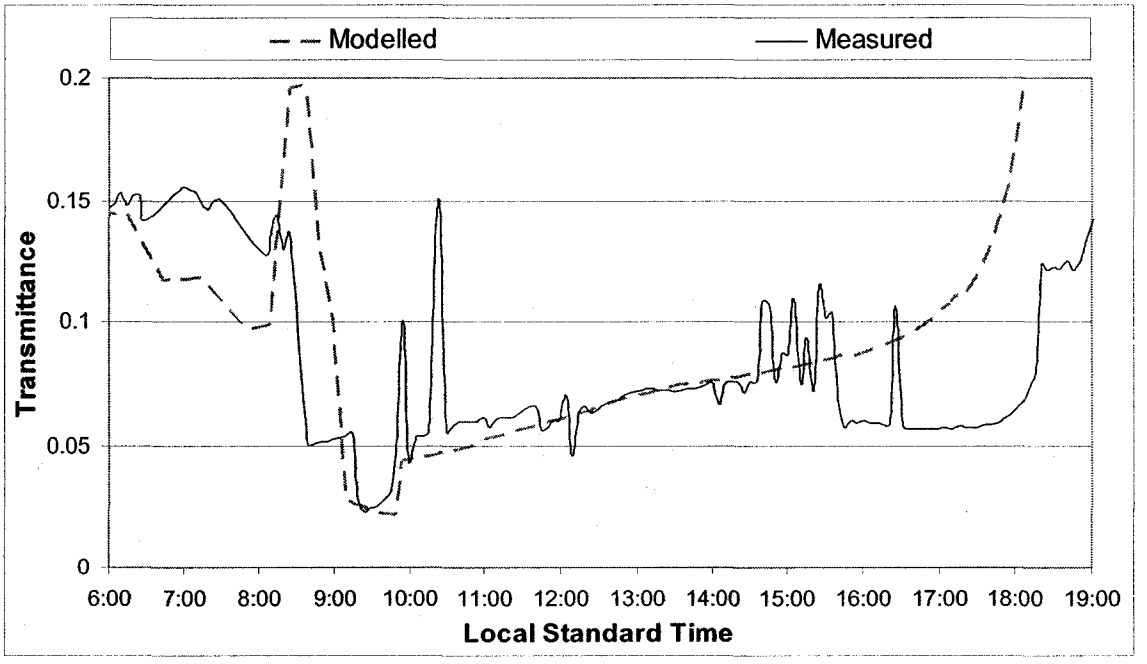

Figure 5-7: *Transmittance, 70° Slat Angle, Modelled vs. Measured (May 3, 2007)*

In this case, the absolute error between the modelled and measured values is of the order of 0.05 during early morning and before sunset. Maximum accumulated error in the measured transmittance is +/- 0.005. The modelled values of transmittance are seen to be quite accurate for the case of the 70 degree blind angle near noon. It should also be noted here that the modelled values do not take into account the reflected illuminance from the interior space, and at low exterior illuminance the electric lighting from the interior space contributes to an error between the measured and modelled values.

These results show that at fixed blind angles the model can predict with good accuracy the transmittance of the fenestration system at peak illuminance values. This is the most important requirement of the model-based control strategy.

5.4 Controlled Blind: Cut-Off Angle

As mentioned in section 4.3.1, the experimental setup allowed for the blinds to be controlled in increments of 10 degrees. The full-scale experiment was carried out with the venetian slat angle controlled to be at the cut-off angle when direct sunlight was present on the façade. As noted before, the blinds were maintained at horizontal when the profile angle was large enough for horizontal slats to block direct beam illuminance.

5.4.1 Daylight Transmittance

Figure 5-8 presents the modelled and measured exterior vertical illuminance values for March 20, 2007. The sky was clear for the entire day, and the modelled values corresponded very well with the measured values.

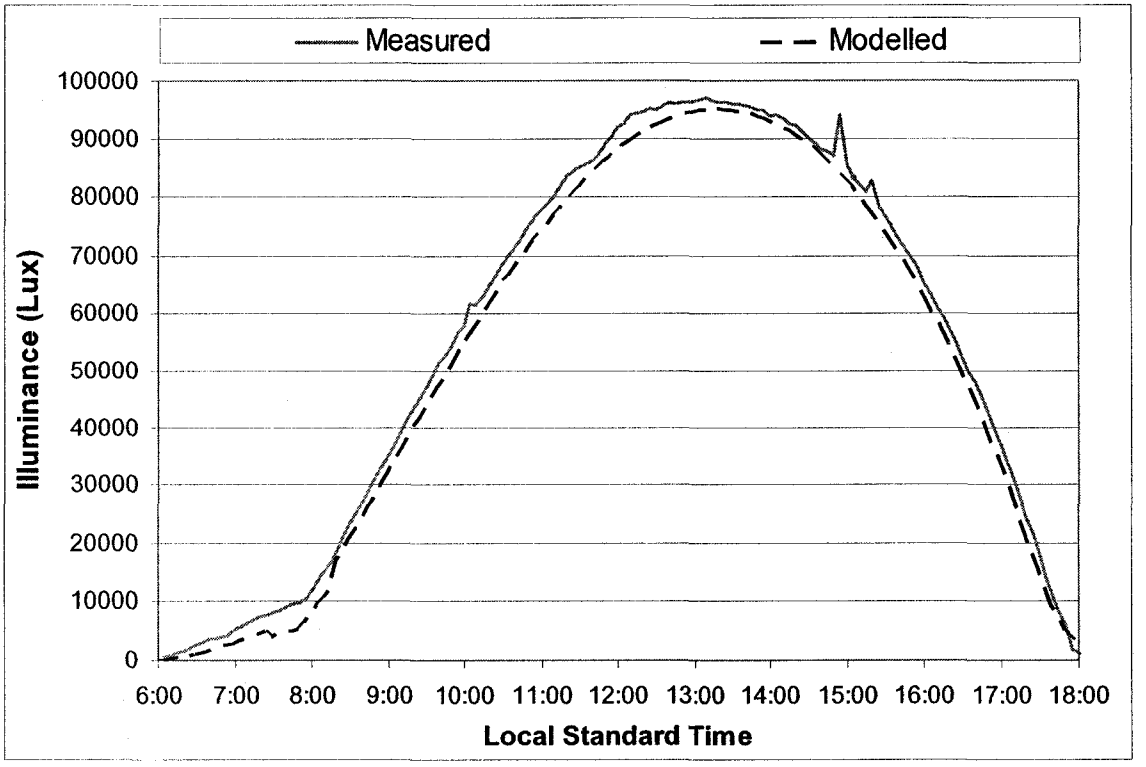

Figure 5-8: *Modelled exterior vertical global illuminance compared to measured (March 20, 2007)*

Figure 5-9 displays the modelled and measured interior blind illuminance for the same day. The results correspond well early in the day and in the evening. However there is a large discrepancy at high solar altitude angles (thus high profile angle) and when the blind angle is near horizontal.

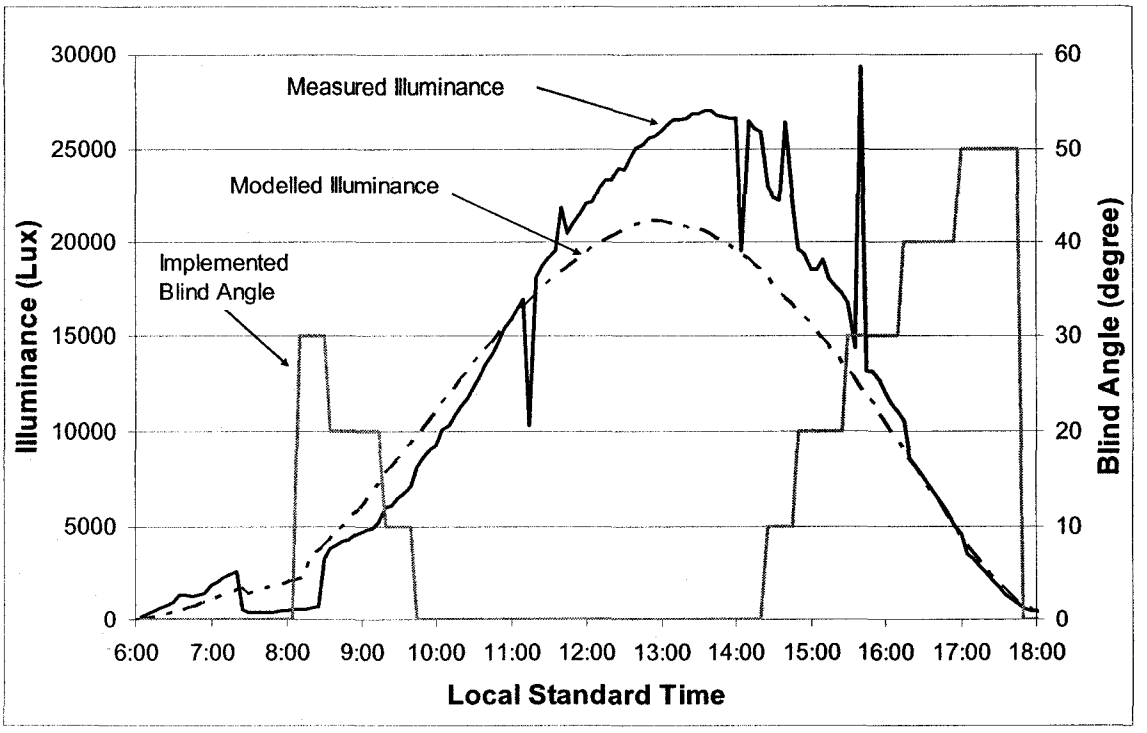

Figure 5-9: *Interior Blind Illuminance, Controlled Slat Angle, Modelled vs. Measured (March 20, 2007)*

The absolute error between the modelled and measured value of approximately 7,000 lux points to a problem in the model (Maximum sensor error is 1,100 lux). The difference is most likely a result of the specular reflection, which is not considered in the model and was observed to occur at near horizontal blind angles when direct beam sunlight is reflected directly into the space. The modelled and measured transmittance values are displayed in Figure 5-10. The maximum accumulated error in measured values is +/- 0.015.

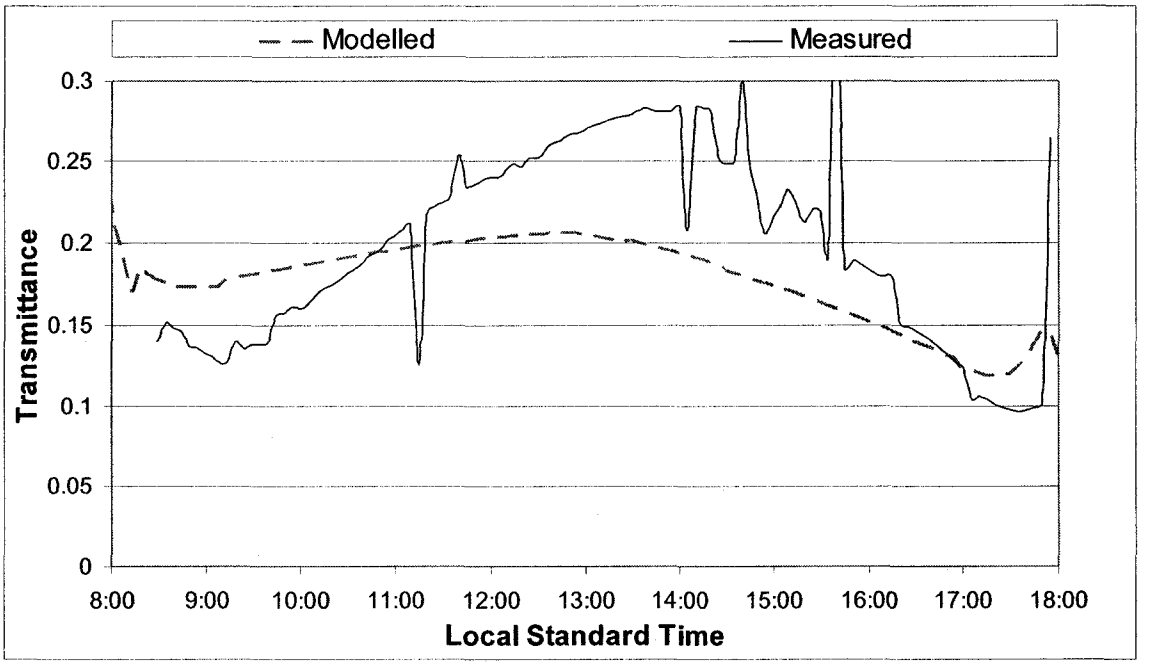

Figure 5-10: *Transmittance, Controlled slat angle, Modelled vs. Measured (March 20, 2007)*

In order to reduce the effect of specular reflection, data was collected for a similar day (March 28) with the blinds controlled to have a minimum slat angle of 10 degrees. Exterior illuminance values for this day were previously shown in Figure 5-2. Measured and modelled values of interior blind illuminance are presented in Figure 5-11. The transmittance values for this day are shown in Figure 5-12.

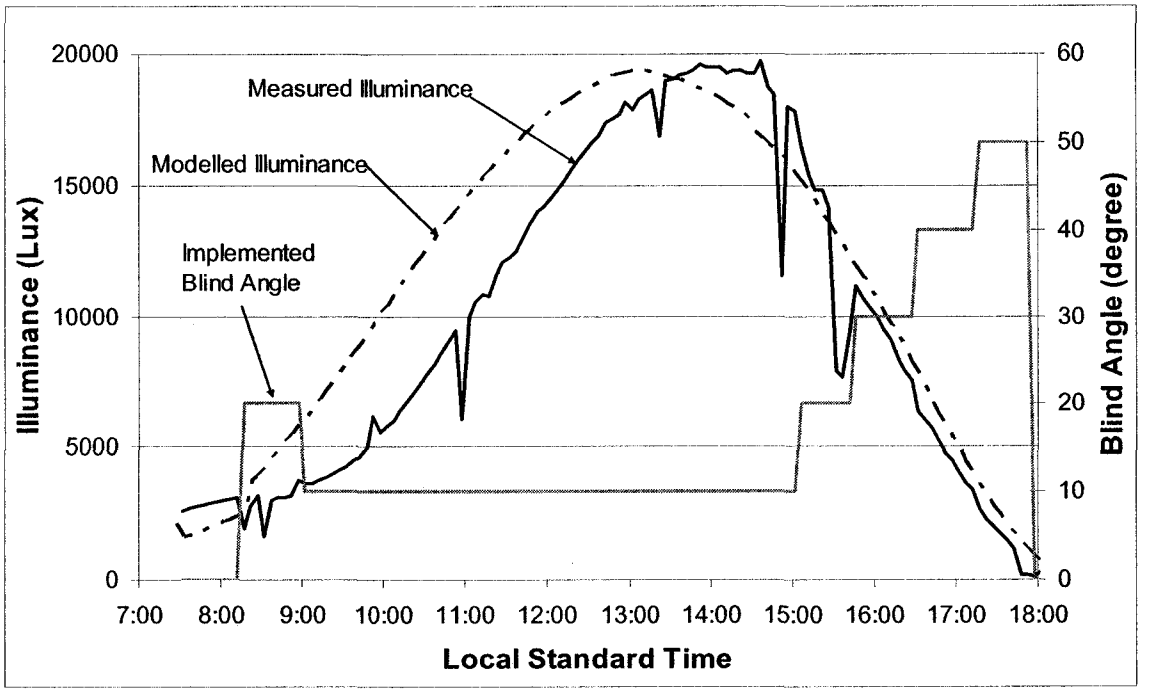

Figure 5-11: *Interior Blind Illuminance, Controlled Slat Angle with 10 degree minimum, Modelled vs. Measured (March 28, 2007)*

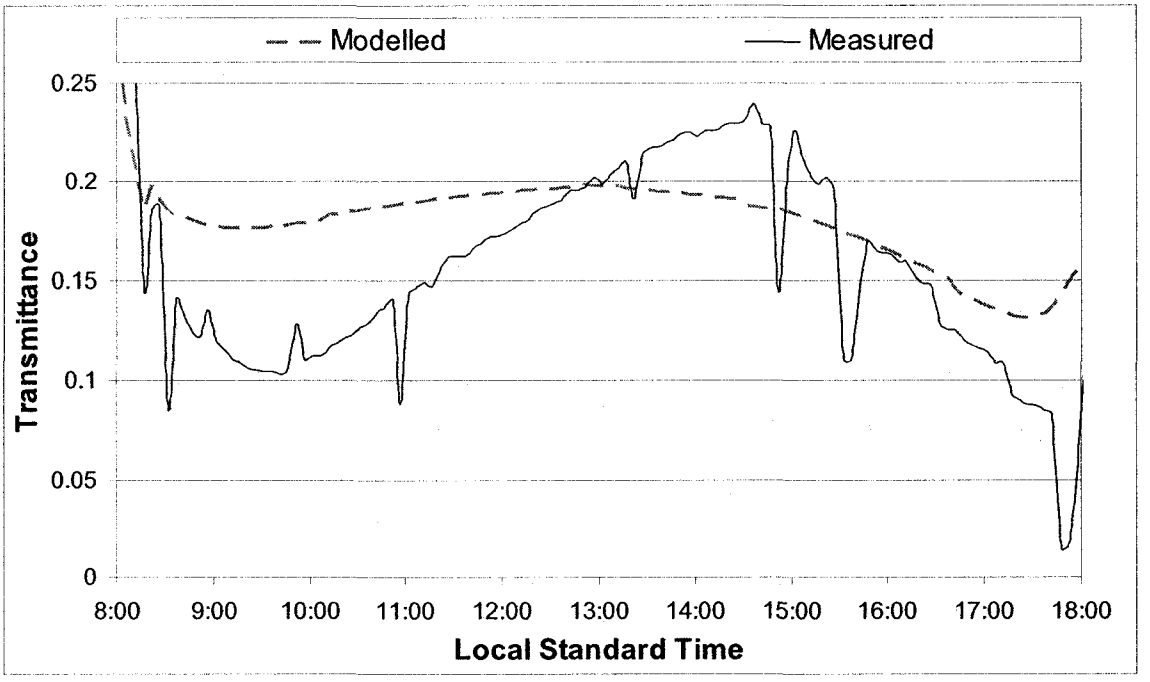

Figure 5-12: *Transmittance, Controlled Slat Angle with 10 degree minimum, Modelled vs. Measured (March 28, 2007)*

The difference between peak modelled and measured transmittance is about 10% on March 20. This is reduced to 6% on March 28. This result shows that the transmitted illuminance from specular reflection may be reduced significantly by a small increase in the minimum blind angle.

The results do show, however, that there is a discrepancy for the modelled results in the early morning. This is expected to be from the above noted specular reflection effect at high azimuth angles. The observed error only occurs in the morning when the high incident angles may result in specularly reflected daylight to the exterior, rather than diffuse reflection into the interior.

5.4.2 Electric Lighting Energy Reduction

The use of a dimmable fluorescent luminaire in conjunction with the controlled blinds can give a generalized idea of the power reduction that can be realized in perimeter zones. It is shown that the luminaire in this zone can be dimmed to its lowest level when the blind illuminance exceeds approximately 3,500 lx. On clear days, this condition was satisfied for most of the day even when the blind angle was maintained at cut-off.

The reduction of the transmitted illuminance when the solar surface azimuth is near 90 degrees, as was seen in Figure 5-9, causes the luminaire to abruptly increase its output. The resulting power consumption curve of the luminaire corresponding to a controlled blind scenario is presented in Figure 5-13, along with measured interior blind illuminance values for March 20, 2007.

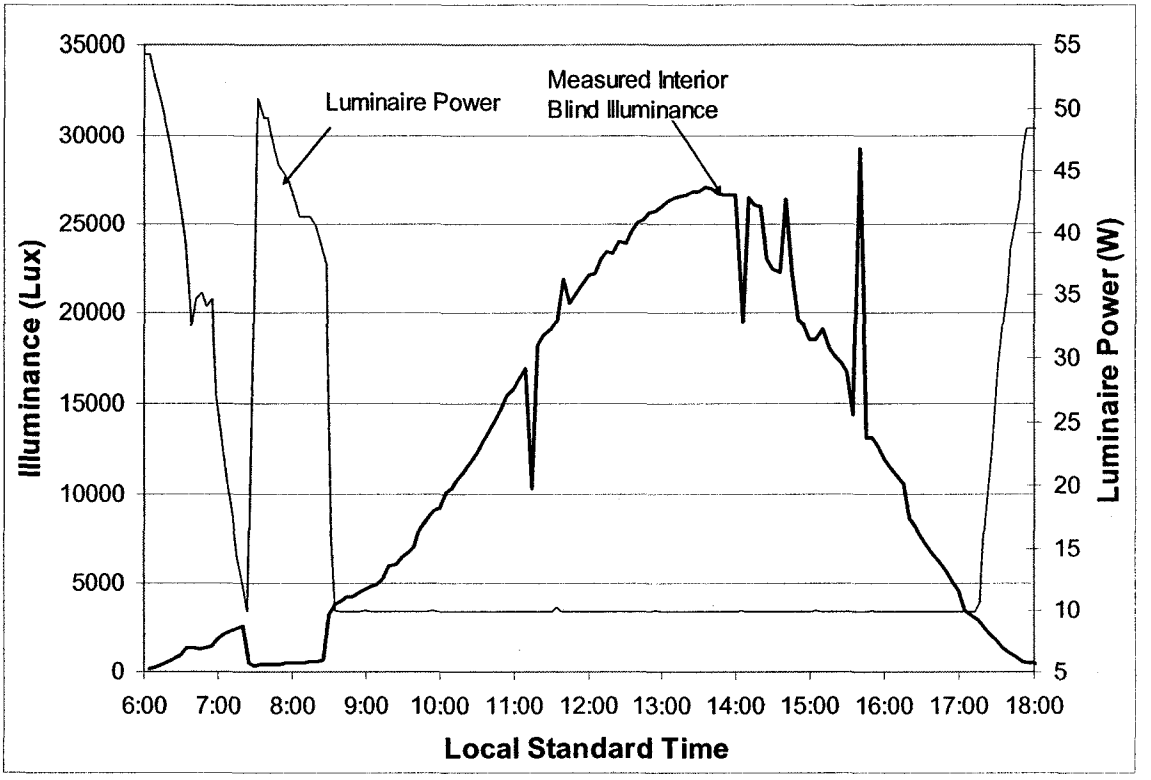

Figure 5-13: *Exterior Illuminance and Dimmed Luminaire Power consumption (March 20, 2007)*

The luminaire used in this study has a non-linear power consumption profile, as was shown in Figure 4-8, which is a function of the digital dimming level. At 100% luminous output, the luminaire consumes approximately 64 watts.

Using the data obtained from March 20, 2007, three cases for light control in this zone, and the corresponding power consumptions are presented in Table 5-2. The base case used is when there is no control, or when the luminaire is at full power from 6:00 am to 6:00 pm. Compared to the base case, the results from the measurements on March 20, 2007 show that a 67% reduction in lighting power consumption during the 12-hour period is possible.

Further energy savings may be realized if the luminaire is switched off, rather than maintaining the output at 1%. In this case, a 77% reduction in power consumption is

possible. This method, however, may not be advisable for electronic dimmable ballasts as the lifespan and power consumption at ballast start-up needs to be considered (To et al., 2002).

Table 5-2: *Effect of control strategies on luminaire power consumption (March 20, 2007)*

Case	Consumption (kJ) (6:00 – 18:00)	Percent reduction
No Control (Base)	2,765	---
Dimming to 1%	923	67%
Turn off at 1%	631	77%

Chapter 6: Discussion

6.1 Applicability of Model-Based Control for Motorized Blinds

It was found from the experimental results in this study that the model developed to predict the transmittance of a fenestration system with an interior mounted venetian blind is sufficient to predict the interior blind illuminance on clear-sky days. This is especially true for high blind angles and during the peak daylight period.

It is proposed that an application could be developed that uses the results of this study to control venetian blinds located on un-shaded areas of the building façade. As presented to this point, the control strategy would work on clear-sky days and for venetian blinds with surfaces that are predominantly diffuse-reflecting in the visual range.

The clear-sky illuminance model presented is also effective at determining the total vertical illuminance on a façade. As a result, when the sky is clear, no exterior sensor would be required for this control as the transmittance model exterior illuminance input variables could be those determined by the clear-sky model. A more complex system would use multiple sensors to measure the direct and diffuse components of illuminance, to be used as inputs. Either way, determination of whether the sky is actually clear or not, and to what extent shading from the blinds is necessary, would have to be undertaken.

6.2 Control for Visual Comfort

Nazzal's (2005) method of calculating the revised discomfort glare index (DGI_N) was used to roughly quantify an upper threshold within the experimental space at Concordia University. It was desired to derive a maximum blind illuminance threshold that would maintain visual comfort for an occupant in a small office space, and that could easily be programmed within a controller. Of course, since the daylight glare prediction models are not very reliable, as mentioned in the literature review, using the DGI_N calculation method is good only for an approximation. Any control system would need to be flexible enough to allow commissioning so that the subjective response of the occupant could be considered in setting a maximum blind illuminance threshold.

The relationship between the blind illuminance and the illuminance of the floor, wall and ceiling was modelled for the experimental zone. A model of a 3-surface enclosed area was used (Murdoch, 2003), as shown Figure 6-1 and detailed in the appendices. Surface 1 of this model represents the fenestration and, as a worst case scenario, the whole surface was considered to be the glazing and venetian blind. Surface 2 is defined as the back wall, and surface 3 the side walls and floor.

A radiosity analysis of the space was carried out, with the initial illuminance of the blind considered to be the transmitted illuminance from the exterior. The final illuminance of the surfaces was calculated by solving the radiosity equations.

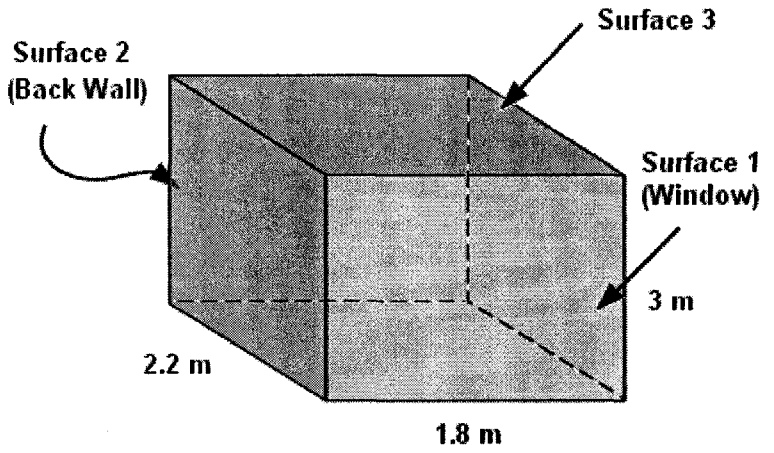

Figure 6-1: *3-Surface Interior Room Model, with Surface 1 as window*

Nazzal's method requires that the window luminance is inputted, as well as the luminance from the surrounding surfaces, at the location of the occupant. This was calculated considering the worst case scenario of an occupant viewing the window directly. The result was that for this office space, the maximum *initial* illuminance of the interior blind surface would need to be below 13,000 lux in order to maintain a *DGI* below 24, which is the threshold for visual comfort. The *final* blind illuminance, due to reflection from the interior surfaces, is calculated to be 15,000 lux, which is the blind illuminance that would cause discomfort.

6.2.1 Modelled Control for Comfort: Heating Season

The model developed for this study was used to calculate the controlled blind angle necessary for maintaining the blind illuminance below a given threshold. The model was run to calculate the required blind angle in order to maintain the blind illuminance below 12,000 lux, just below the worst-case threshold calculated for this space by using the DGI_N. This case of control could be required in the heating season, when maximum solar gains are desired without hindering visual comfort.

Figure 6-2 presents the calculated blind angle, in increments of 10 degrees, required to maintain the blind illuminance below 12,000 lux, along with the cut-off angle, for January 7 and for the Concordia University EV Building façade. The calculated blind illuminance is also presented. Assuming no error in the model, angles up to 60 degrees would be required. It should be noted that for this case, the implemented blind angle would be greater than the calculated cut-off angle only for a short time period.

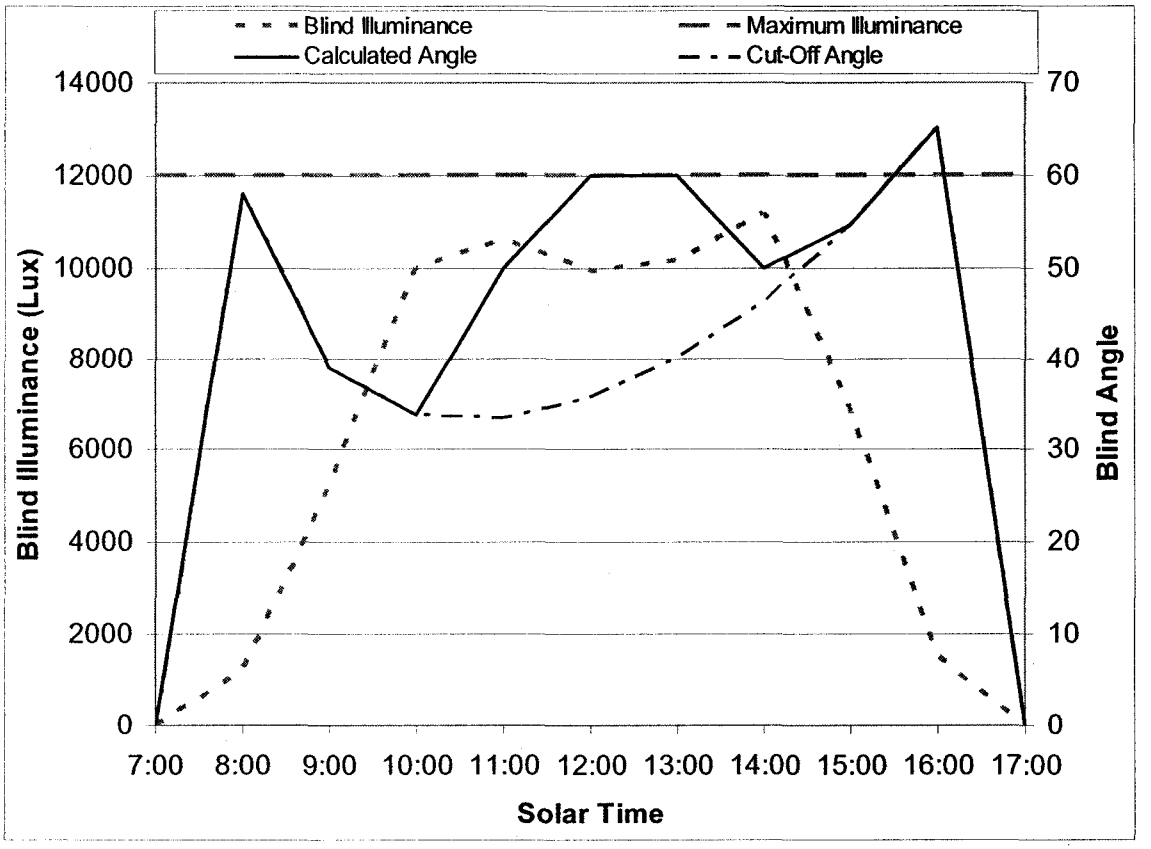

Figure 6-2: *Controlled Blind Angle to maintain transmitted blind illuminance due to transmission from the exterior below 12,000 lux on January 7.*

6.3 Control for Cooling Load Reduction

To demonstrate the model-based control capability of reducing the cooling load, in addition to the cooling load reduction associated with reduced lighting energy consumption, the strategy would be to limit the transmittance to levels such that the requirements for daylighting are met, while reducing unnecessary solar gains. As was seen from the data presenting the transmittance at a fixed blind angle of 70 degrees (Figure 5-6), very high blind angles are required to maintain the peak blind illuminance below 10,000 lux. Thus, it may be considered from the earlier comparison of modelled to experimental results that this model-based control case could be quite accurate.

It was seen in section 5.4.2 that in the studied perimeter zone, a blind illuminance of 3,500 lux was required to fully dim the luminaire. Considering a mid-summer day, July 1, the controlled blind angle model was used to calculate the required angles needed to limit the blind illuminance to 4,000 lux (Figure 6-3). This example demonstrates the control for minimizing the solar gains, while slightly exceeding the daylighting needs.

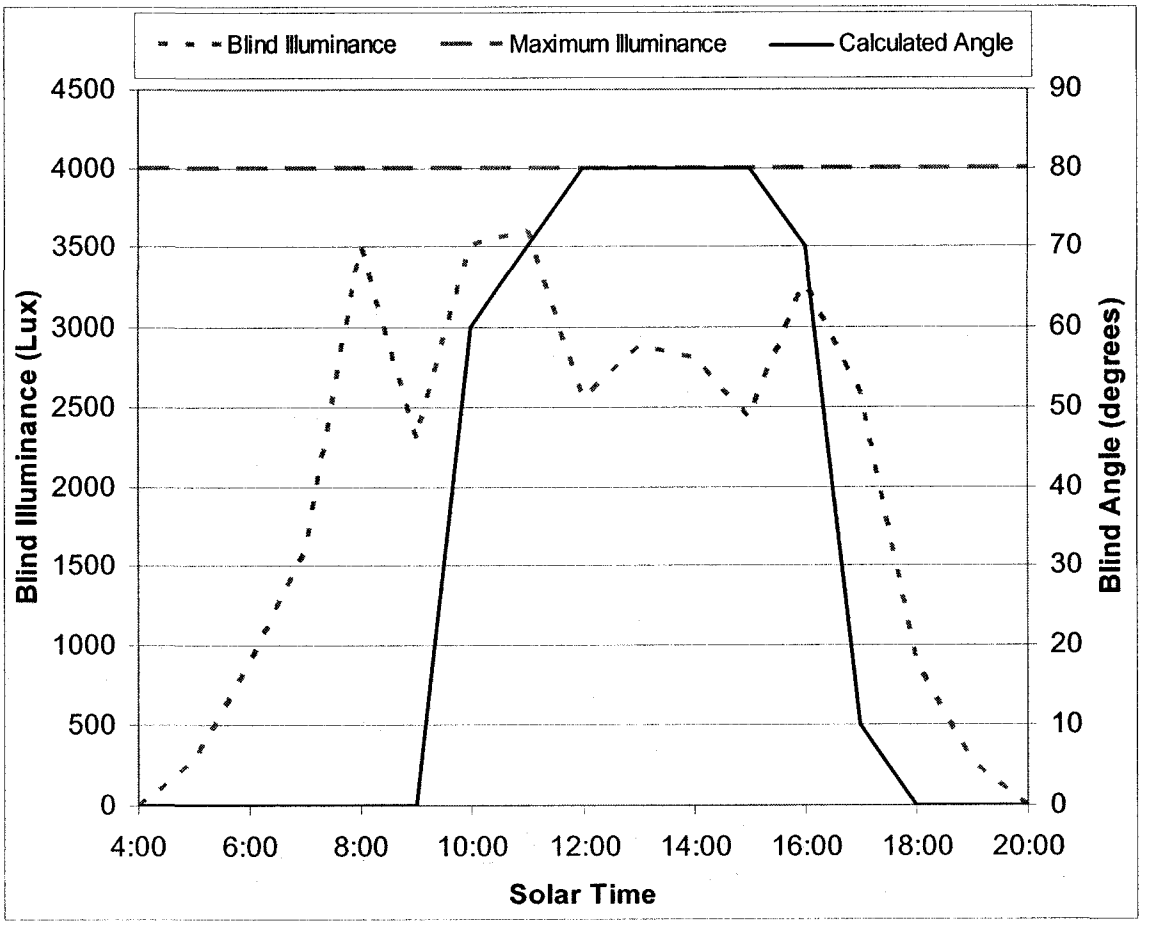

Figure 6-3: *Controlled Blind Angle to maintain blind illuminance below 4,000 lux on July 1.*

Of course, this case does not take into account the exterior view requirements of the occupant, which would be severely reduced for most of the day.

The illuminance distribution on the work-plane was also calculated for this day, using the 3-surface model. Nodes were positioned at 0.5 metre spacing perpendicular from the window, centred in the room, and as displayed in Figure 6-4.

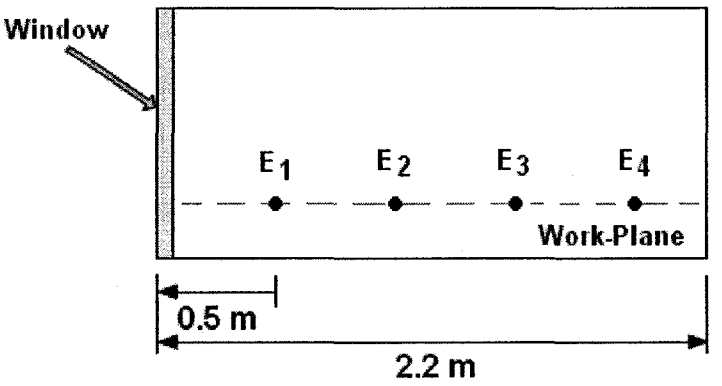

Figure 6-4: *Calculated Work-Plane Illuminance Node Position*

Figure 6-5 displays the calculated work-plane illuminance with respect to time, and Figure 6-6 with respect to the distance from the window.

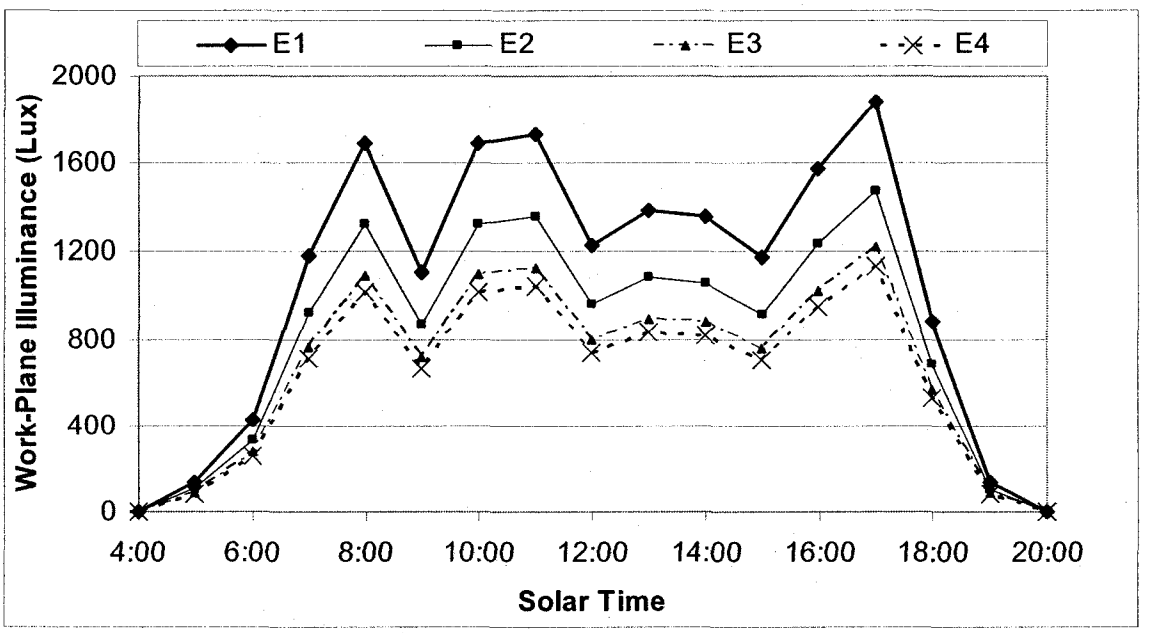

Figure 6-5: *Calculated Work-Plane Illuminance Distribution*

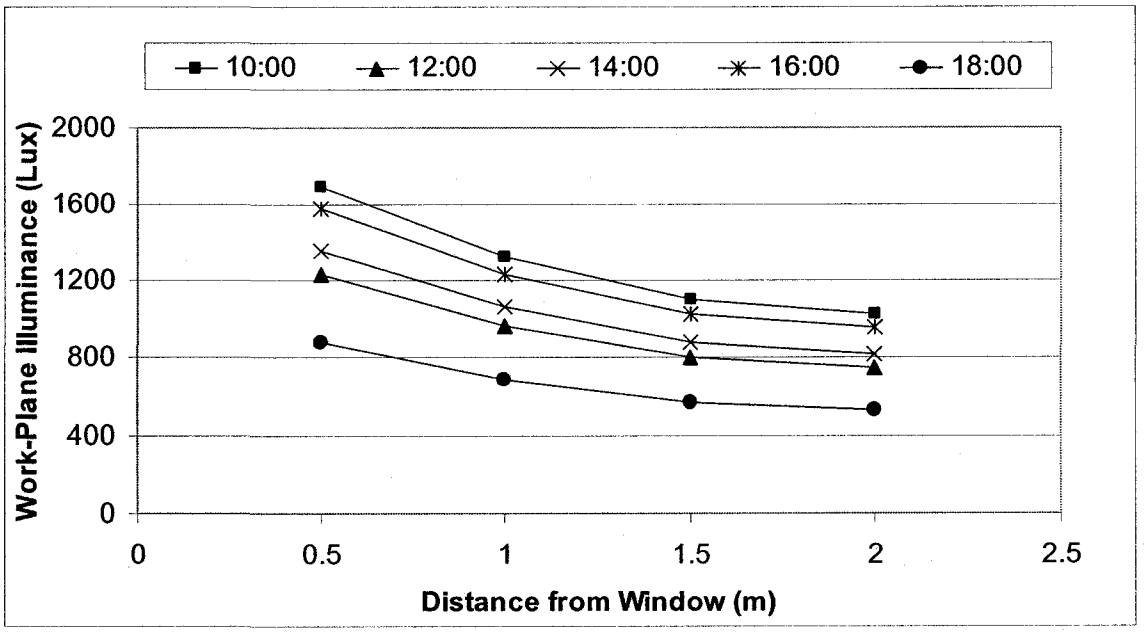

Figure 6-6: *Calculated Work-Plane Illuminance from Window Surface*

As shown in Figure 6-6, the calculated illuminance on the work plane stays above the minimum 400 lux for most of the day.

6.4 Sky Detection

The greatest impediment to the implementation of the model-based control algorithm for venetian blinds is the ability to determine the real-time sky conditions. The direct-beam component of illuminance is predominant, and passing cloud cover can drastically reduce this contribution to the total vertical illuminance. From a visual comfort and energy efficiency standpoint it is desirable to have the blind control respond to changing exterior illuminance levels. This is a challenging task, and has been investigated by very few researchers.

In the case of the model used in this study, direct beam and diffuse illuminance measurements could be used as inputs to successfully determine the blind-angle required to obtain the desired transmission of daylight. However, L. Roche (2000) investigated the open-loop model-based control strategy for an automated roller-blind control system. With regards to the changing sky conditions, Roche states that the use of expensive direct beam sun tracking *pyrheliometers* to determine the components of the exterior illuminance is not financially practical. Instead, he determined whether the sun is visible from the façade by using a single vertical illuminance sensor. To determine whether there was risk of direct sunlight, Roche created an empirical relation for the particular location studied and derived a vertical illuminance threshold as a function of solar altitude and solar surface azimuth. If the measured vertical illuminance was greater than this empirical formulation, the control system concluded that direct beam illuminance was prevalent. A roller blind would then descend to allow direct sun penetration to a maximum of 1 metre from the interior façade.

For the case of venetian blinds, the control is more complex than for a roller blind. It is not a simple matter of opening or closing the blind, and the intensity and direction of the solar flux is very important for determining the transmittance. Furthermore, continuous changes in the blind position would be required to ensure constant interior illuminance levels. This frequent step change in blind position would surely disturb occupants, and possibly a slow movement of the slats would be more ideal.

A single exterior illuminance sensor could also be used to compare the measured illuminance levels to those calculated from ideal sky models in order to determine

whether the sky is clear. If a clear-sky is determined, the modelled components of illuminance could be used to calculate the appropriate blind angle.

From a practical perspective, it is suggested that the control system should determine with a certain statistical accuracy whether the sky is cloudy. If indeed significant cloud cover exists to block direct beam sunlight, it is unlikely that glare would be an issue. In this case, a prudent system would return the blinds to the cut-off angle (as a minimum) in order to ensure that occupants are protected from "sun-spots", or slight breaks in the cloud cover. The statistical determination of cloud-cover would require a continuous record of illuminance measurements: if there is a significant amount of time with cloud cover, one can predict with a certain accuracy that, for example, the next five to ten minutes will have cloud cover. If this is the case, the blinds are returned to the cut-off angle, or more daringly, retracted completely. Any subsequent measurement that indicates that cloud cover is no longer present would return the blinds to the calculated angle for the clear-sky condition that produces the desired interior blind illuminance.

The ability for this system to work depends highly on the maximum comfort threshold for interior illuminance. If the threshold is exceeded only by unobstructed direct sunlight, then the implementation of the system is simplified. If it is possible that obstructed direct beam sunlight could result in an uncomfortable interior blind illuminance, or if the diffuse exterior illuminance alone can cause excessive transmitted daylight, then this would require that the minimum blind angle be greater than horizontal.

6.4.1 CIE Sky Models used to determine "Clear-Sky"

Since the control algorithm will use a continuous calculation of the clear-sky model, as presented in this study, one could utilise a secondary sky model to determine

the vertical illuminance value above which the sky could be determined as "clear". As a comparison, for March 20, the CIE partly-cloudy sky (See section 3.5) is plotted for the EV Building façade, along with the clear-sky model, in Figure 6-7.

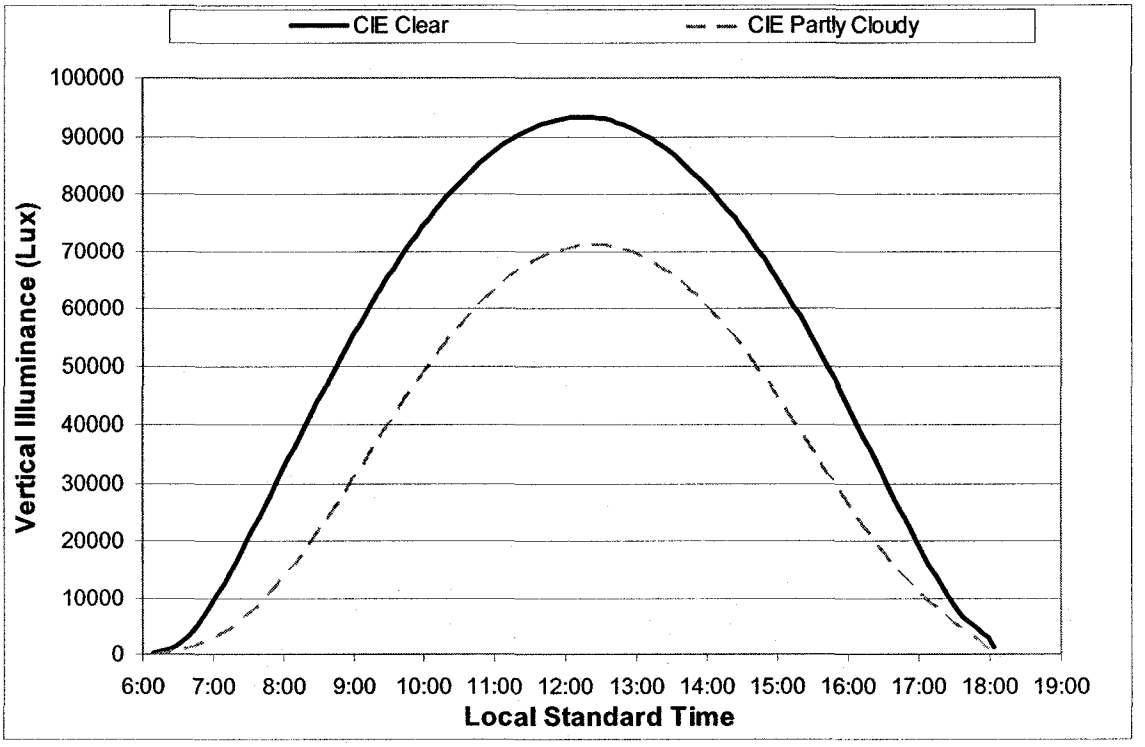

Figure 6-7: *CIE Partly-Cloudy and Clear-Sky vertical illuminance for March 20*

For the "small office" space considered for this study, and as presented in section 6.2, the calculated blind illuminance above which comfort could not be guaranteed was determined to be 13,000 lux. The CIE partly-cloudy sky was inputted into the fenestration transmittance model with the blind slats maintained at horizontal and using March 20 as an example day. The calculated blind illuminance exceeds the upper comfort threshold when the exterior vertical illuminance is 50,000 lux, as seen in Figure 6-8.

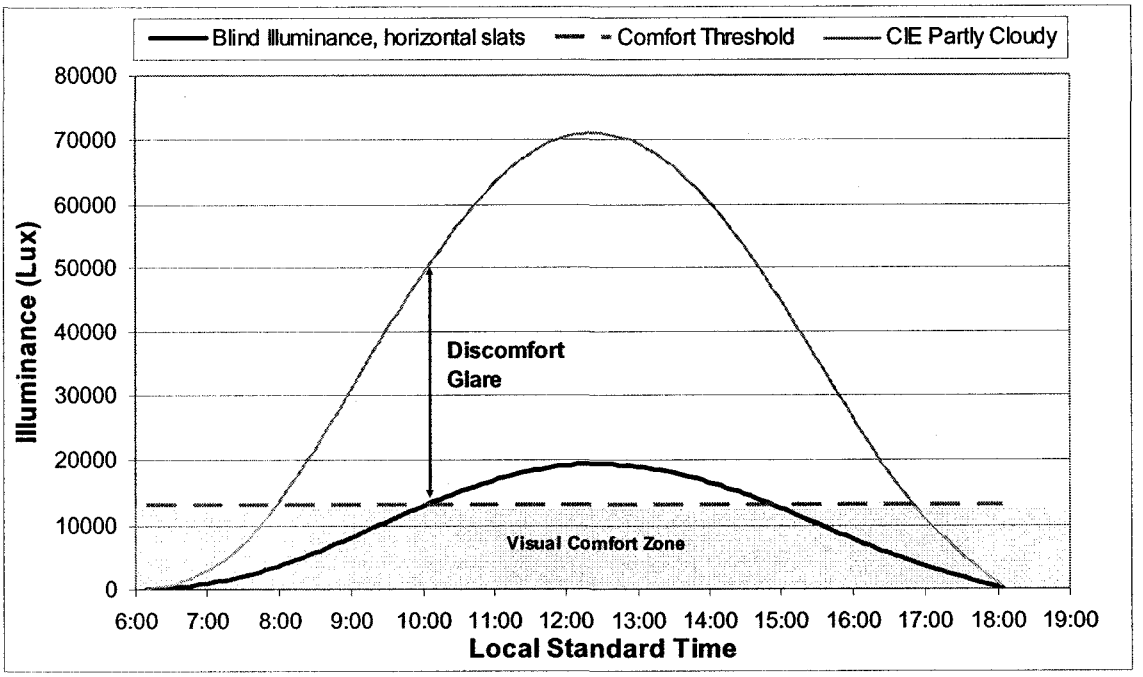

Figure 6-8: *Modelled Interior Blind Illuminance using CIE Overcast sky model as simulation input, for March 20*

The CIE partly-cloudy modelled values could be used as a comparison for determining if the sky is clear. The maximum value would be 50,000 lux for the March 20 case. To be cautious, the blind control would return the slats to the cut-off angle when the measured exterior illuminance descends below the threshold, in the case that passing clouds reveal direct sun.

It is proposed that the clear-sky threshold be the CIE partly-cloudy sky plus 20 percent, to a maximum of 50,000 lux (Figure 6-9). Measured values of exterior global vertical illuminance above this maximum would implement the clear-sky controlled blind angle.

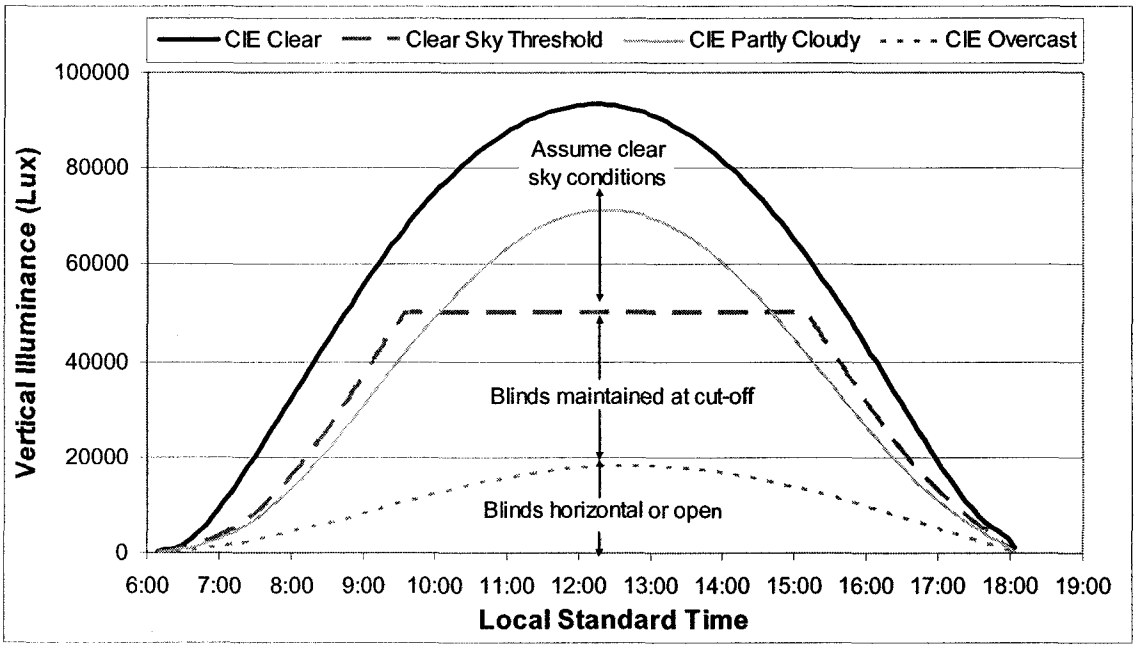

Figure 6-9: *Proposed Exterior Illuminance control threshold, March 20*

As can also be seen in Figure 6-9, there is no risk of discomfort glare for an overcast sky. Measured exterior illuminance below that predicted by the overcast sky could enact horizontal slats, or retract the blinds completely.

6.5 Proposed Control Algorithm

The proposed control algorithm, to be implemented in perimeter zones with exposure to direct sun, is displayed below in Figure 6-10. This open-loop model-based blind control requires as an input either the measured or a modelled illuminance on the exterior façade surface. Venetian blind and glazing properties necessary for the model are also required inputs.

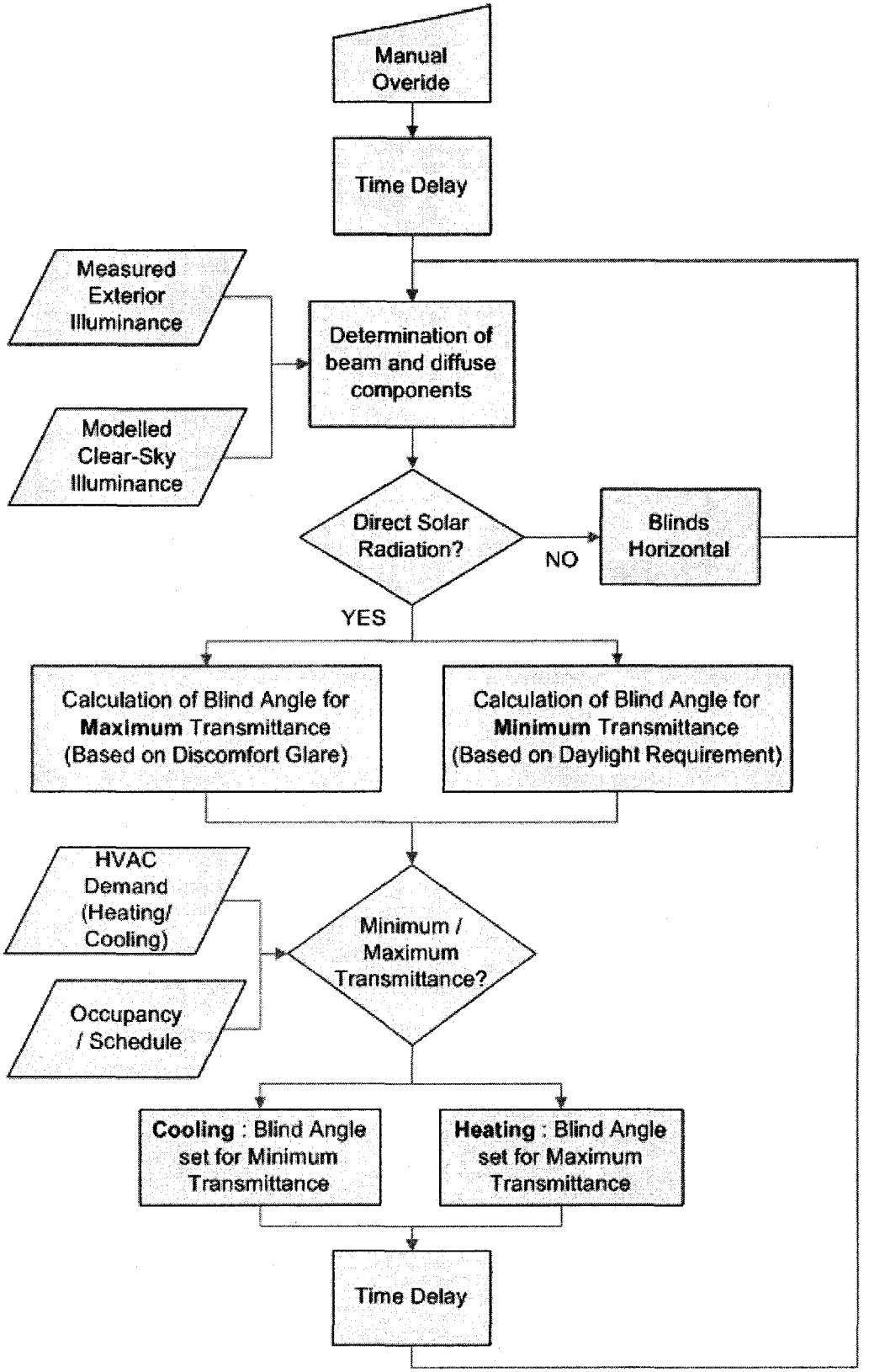

Figure 6-10: *Proposed Control Algorithm*

Chapter 7: Conclusions

A method for controlling venetian blinds using a numerical model developed based on radiosity theory was presented. The goal of this work was to study the potential of a model-based control that transmits the visible portion of solar radiation through the "view" portion of fenestration (Rosenfeld et al., 1977), while considering the visual comfort of occupants, and also the heating and cooling requirements of the building. In order to reduce the requirement of interior sensors, typically necessary for closed-loop control, an open-loop system that uses a single exterior illuminance sensor to determine the state of the sky conditions was explored, and the applicability of the model-based control to transmit a prescribed amount of this daylight was investigated through experimental measurements.

Modelling assumptions were required to simplify the complex optical characteristics of light transmittance through a glazing and venetian blind system. This included a modelling approach whereby only diffuse reflectance of the blind slats was considered, and correction factors were applied to take into account shading due to the window frame and incomplete illuminance of the venetian blind slat, when it exists. It was found that the transmittance of the venetian blind can be modelled with good accuracy (less than 1% absolute error) for high blind angles and peak exterior illuminance levels. Absolute error in transmittance up to 10% was discovered for horizontal blind angles during times of peak illuminance. This is expected to be a result of the specular surface reflectivity of the experimental blind slat used in this study, and

may be reduced when blind slats are used that have lower angular dependent specular reflectivity.

The combination of the CIE clear sky model, along with the experimentally derived ratios of horizontal to vertical illuminance developed by Perez (1990), resulted in an excellent ability to predict the exterior vertical illuminance on clear days. Because of this, it is possible to use a single exterior sensor to determine the "clearness" of the sky and control the blinds accordingly. It is suggested in this study that the blinds be maintained at the direct beam 'cut-off' angle when the exterior vertical illuminance is below a certain threshold, and maintained at the model-based calculated angle when the sky conditions are measured as being clear.

It was also shown, through the numerical model, that the upper value of blind illuminance required to maintain visual comfort, and derived based on the Daylight Glare Index, could be used as a control set-point when transmitted daylight is to be used both for space heating and daylighting. A minimum value of blind illuminance required to reduce perimeter zone lighting could also be employed as the control point when excessive solar heat gains are to be avoided – specifically, when the cooling system of the building is operating, or when load management systems want to shed peak consumption.

In conjunction with the controlled blind experiment where direct beam illuminance was continually blocked, it was found that by using dimmable lighting fixtures with integrated photocells – a product that is currently available on the market – there is the potential to reduce electric lighting in perimeter zones by up to 70%. According to other research, and primarily due to the efficacy of daylight compared to

artificial light sources, the reduction of every three watts of electric lighting energy may correspond to a one watt reduction to the building cooling load (UNEP, 2007).

This study has demonstrated that for the current design trend of buildings with highly glazed perimeter zones, innovative solutions for solar radiation control are viable that allow for the transmittance of human health and productivity enhancing daylight, while reducing the energy burden of increased cooling loads.

7.1 Recommended Future Research

Intelligent building control is becoming increasingly possible and cost effective. It may contribute to significant energy savings and improved comfort for the occupants. Nevertheless, additional work is recommended in the following areas:

1. Supervisory control algorithms need to be developed to integrate lighting-daylighting control with HVAC system control to maximize energy savings.
2. Occupant response has to be considered in implementing control algorithms for blinds.
3. Groups of blinds with partial exposure to sunlight need to be controlled with appropriate control algorithms.
4. Bi-directional transmittance functions, currently being worked on by other researchers (Anderson et al., 2005), may be utilized to develop improved models and control algorithms.

References

Andersen, M., Rubin, M., Powles, R., & Scartezzini, J. L. (2005). Bi-directional transmission properties of venetian blinds: Experimental assessment compared to ray-tracing calculations. *Solar Energy, 78*(2), 187-198.

ASHRAE. (2005). *Handbook of fundamentals*. Atlanta, Georgia: American Society of Heating, Refrigerating, and Air-Conditioning Engineers, Inc.

Athienitis, A. K. (1998). *Building thermal analysis* (2nd ed.) Mathcad electronic book, Mathsoft.

Breitenbach, J., Lart, S., Längle, I., & Rosenfeld, J. L. J. (2001). Optical and thermal performance of glazing with integral venetian blinds. *Energy and Buildings, 33*(5), 433-442.

Bülow-Hübe, H., & Wall, M. (2001). *Solar protection in buildings* No. TABK--01/3060). Lund, Sweden: Department of Construction and Architecture, Lund University.

DiBartolomeo, D. L., Lee, E. S., Rubinstein, F. M., & Selkowitz, S. E. (1996). Developing a dynamic envelope/ lighting control system with field measurements. *Journal of Illuminating Engineering Society, 26*(1), 146-164.

Duffie, J. A., & Beckman, W. A. (2006). *Solar engineering of thermal processes* (3rd ed.). Hoboken, New Jersey: John Wiley & Sons.

Escuyer, S., & Fontoynont, M. (2001). Lighting controls: A field study of office workers' reactions. *Lighting Research and Technology, 33*(2), 77-94.

Fisekis, K., Davies, M., Kolokotroni, M., & Langford, P. (2003). Prediction of discomfort glare from windows. *Lighting Research and Technology, 35*(4), 360-369.

Foster, M., & Oreszczyn, T. (2001). Occupant control of passive systems: The use of venetian blinds. *Building and Environment, 36*(2), 149-155.

French, T. (1941). In Silverberg L. (Ed.), *Venetian blinds*. Manchester 15, England: Thomas French and Sons Limited. from http://www.mae.ncsu.edu/homepages/silverberg/AdaptiveShading/adindex.htm

Galasiu, A. (2004). *Let there be light: The impact of window blinds on daylight-linked dimming and automatic on/off lighting controls* No. NRC-47290) National Research Council of Canada, Institute for Research in Construction.

Gueymard, C. A., Myers, D., & Emery, K. (2002). Proposed reference irradiance spectra for solar energy systems testing. *Solar Energy, 73*(6), 443-467.

Guillemin, A., & Molteni, S. (2002). An energy-efficient controller for shading devices self-adapting to the user wishes. *Building and Environment, 37*(11), 1091-1097.

IES (International Energy Agency). (2001). *'Daylight in buildings', application guide for daylight responsive lighting control.* International Energy Agency, SHC Task 21.

Incropera, F. P., & DeWitt, D. P. (2002). *Introduction to heat transfer* (4th ed.)John Wiley & Sons, New York, NY.

Inoue, T., Kawase, T., Ibamoto, T., Taakusa, S., & Matsuo, Y. (1988). The development of an optimal control system for window shading devices based on investigations in office buildings. *ASHRAE Transactions, 104*, 1034-1049.

IPCC, 2. (2007). *Climate change 2007: Mitigation. contribution of working group III to the fourth assessment report of the intergovernmental panel on climate change.* Cambridge, UK and New York, NY, USA: Cambridge University Press.

Klems, J. H., & Warner, J. L. (1997). Solar heat gain coefficient of complex fenestrations with a venetian blind for differing slat tilt angles. *ASHRAE Transactions, 103*(1)

Kotey, N. A., & Wright, J. L. (2006). Simplified solar optical calculations for windows with venetian blinds. *1st Canadian Solar Buildings Research Network Conference,* Montreal, Canada.

Kreith, F., & Bohn, M. S. (1986). *Principles of heat transfer* (4th ed.). New York, NY: Harper & Row.

Kuhn, T. E. (2006). Solar control: A general evaluation method for facades with venetian blinds or other solar control systems. *Energy and Buildings, 38*(6), 648-660.

Kuhn, T. E., Bühler, C., & Platzer, W. J. (2001). Evaluation of overheating protection with sun-shading systems. *Solar Energy, 69*(Supplement 6), 59-74.

Lee, E. S., DiBatrlomeo, D. L., Vine, E. L., & Selkowitz, S. E. (1998). Integrated performance of an automated venetian blind / electric lighting system in a full-scale private office. *ASHRAE/DOE/BTECC Conference, Thermal Performance of the Exterior Envelopes of Buildings VII,* Clearwater Beach, Florida, USA.

Lee, E. S., & Selkowitz, S. E. (1995). The design and evaluation of integrated envelope and lighting control strategies for commercial buildings. *ASHRAE Transactions, 101*(1), 326-342.

Lee, E. S., Selkowitz, S. E., Hughes, G. D., & Thurm, D. A. (2004). Market transformation opportunities for emerging dynamic facade and dimmable lighting control systems. *ACEEE 2004 Summer Study on Energy Efficiency in Buildings: Breaking Out of the Box,* Asilomar, Pacific Grove, California.

Lee, E. S., DiBartolomeo, D. L., & Selkowitz, S. E. (1998). Thermal and daylighting performance of an automated venetian blind and lighting system in a full-scale private office. *Energy and Buildings, 29*(1), 47-63.

Lee, E. S., & Selkowitz, S. E. (2006). The New York Times headquarters daylighting mock-up: Monitored performance of the daylighting control system. *Energy and Buildings, 38*(7), 914-929.

Lindsay, C. R. T., & Littlefair, P. J. (1993). *Occupant use of venetian blinds in offices* No. PD 233/92)Watford Building Research Establishment.

Littlefair, P. J. (1998). Predicting lighting energy use under daylight linked lighting controls. *Building Research and Information, 26*(4), 208-222.

Love, J. A. (1998). Manual switching patterns observed in private offices. *Lighting Research and Technology, 30*(1), 45-50.

McCluney, R. (1998). Advanced fenestration and daylighting systems. *Daylighting '98: An International Conference on Daylighting Technologies for Energy Efficiency in Buildings,* Ottawa, Canada.

McGuire, M. E. (2005). A system for optimizing interior daylight distribution using reflective venetian blinds with independent blind angle control. (Master of Science in Building Technology, Massachusetts Institute of Technology).

Merriam-webster online dictionary. (2005)., 2008, from www.merriam-webster.com

Ministère des Ressources naturelles et de la Faune (MRNF). (2005). *L'énergie au Québec: Édition 2004,* Gouvernement du Québec.

Murdoch, J. B. (2003). *Illuminating engineering: From Edison's lamp to the LED.* New York, New York: Visions Communication.

Nabil, A., & Mardaljevic, J. (2006). Useful daylight illuminances: A replacement for daylight factors. *Energy and Buildings, 38*(7), 905-913.

Nazzal, A. A. (2001). A new daylight glare evaluation method: Introduction of the monitoring protocol and calculation method. *Energy and Buildings, 33*(3), 257-265.

Nazzal, A. A. (2005). A new evaluation method for daylight discomfort glare. *International Journal of Industrial Ergonomics, 35*(4), 295-306.

Newsham, G. R. (1994). Manual control of window blinds and electric lighting: Implications for comfort and energy consumption. *Indoor Environment, 3*, 135-144.

Office of Energy Efficiency (OEE). (2006). *The state of energy efficiency in Canada, report 2006.* Ottawa, Canada: National Resources Canada.

Osterhaus, W. K. E. (2005). Discomfort glare assessment and prevention for daylight applications in office environments. *Solar Energy, 79*(2), 140-158.

Park, K., & Athienitis, A. K. (2003). Workplane illuminance prediction method for daylighting control systems. *Solar Energy, 75*(4), 277-284.

Pedersen, M. C. (2004, A day in the light. [Electronic version]. *Metropolis Magazine,* Retrieved September, 2007 from www.metropolismag.com

Perez, R., Ineichen, P., Seals, R., Michalsky, J., & Stewart, R. (1990). Modeling daylight availability and irradiance components from direct and global irradiance. *Solar Energy, 44*(5), 271-289.

Pflaum, R. (2001). *DALI manual.* Frankfurt am Main, Germany: DALI AG (Digital Addressable Lighting Interface Activity Group) of ZVEI. Retrieved September, 2007 from www.dali-ag.org

Reinhart, C. F., & Voss, K. (2003). Monitoring manual control of electric lighting and blinds. *Lighting Research and Technology, 35*(3), 243-260.

Reinhart, C. F. (2004). Lightswitch-2002: A model for manual and automated control of electric lighting and blinds. *Solar Energy, 77*(1), 15-28.

Roche, L. (2002). Summertime performance of an automated lighting and blinds control system. *Lighting Research and Technology, 34*(1), 11-25.

Rosenfeld, A. H., & Selkowitz, S. E. (1977). Beam daylighting: An alternative illumination technique. *Energy and Buildings, 1*(1), 43-50.

Rosenfeld, J. L. J., Platzer, W. J., van Dijk, H., & Maccari, A. (2001). Modelling the optical and thermal properties of complex glazing: Overview of recent developments. *Solar Energy, 69*(Supplement 6), 1-13.

Ruck, N. C. (2006). International energy agency's solar heating and cooling task 31, 'Daylighting buildings in the 21st century'. *Energy in Buildings, 38*(7), 718-720.

Selkowitz, S. E. (2001). Integrating advanced facades into high performance buildings. Paper presented at the *7th International Glass Processing Days,* Tampere, Finland.

Selkowitz, S. E., Lee, E. S., & Aschehoug, O. (2003). Perspectives on advanced facades with dynamic glazings and integrated lighting controls. Paper presented at the *CISBAT 2003, Innovation in Building Envelopes and Environmental Systems, International Conferences on Solar Energy in Buildings,* Lausanne, Switzerland.

To, D. W. T., Sing, L. K., Chung, T., & Leung, C. (2002). Potential energy saving for a side-lit room using daylight-linked fluorescent lamp installations. *Lighting Research and Technology, 34*(2), 121-132.

Tzempelikos, A., & Athienitis, A. K. (2007). The impact of shading design and control on building cooling and lighting demand. *Solar Energy, 81*(3), 369-382.

UNEP. (2007). *Buildings and climate change: Status, challenges and opportunities.* United Nations Environment Programme.

van Dijk, D., & Bakker, L. (1998). The characterization of the daylight properties of special glazings and solar shading devices. Paper presented at the *Proceedings of EuroSun 98 Conference,* Portoroz, Slovenia.

van Dijk, D., & Oversloot, H. (2003). WIS, the European tool to calculate thermal and solar properties of windows and window components. Paper presented at the *Eighth International IBPSA Conference,* Eindhoven, The Netherlands.

Vartiainen, E. (2001). Electricity benefits of daylighting and photovoltaics for various solar facade layouts in office buildings. *Energy and Buildings, 33*, 113-120.

Veitch, J. A. (2006). *Lighting for well-being: A revolution in lighting?* No. NRCC-49205). Ottawa, Canada: National Research Council of Canada, Institute for Research in Construction.

Voss, K. (2000). Toward lean buildings - examples and experience from a German demonstration program for energy efficiency and solar energy use in commercial buildings. Paper presented at the *Eurosun,* Copenhagen, Denmark.

Webb, A. R. (2006). Considerations for lighting in the built environment: Non-visual effects of light. *Energy and Buildings, 38*(7), 721-727.

Wienold, J., & Christoffersen, J. (2006). Evaluation methods and development of a new glare prediction model for daylight environments with the use of CCD cameras. *Energy and Buildings, 38*(7), 743-757.

Appendices

Transmittance of a venetian blind and fenestration system.

These calculations show the method where the blind angle is set to the cut-off angle. The slat angle can also be forced to stay as a constant value by simply setting the blind angle to be a certain angle.

Blind Geometry:

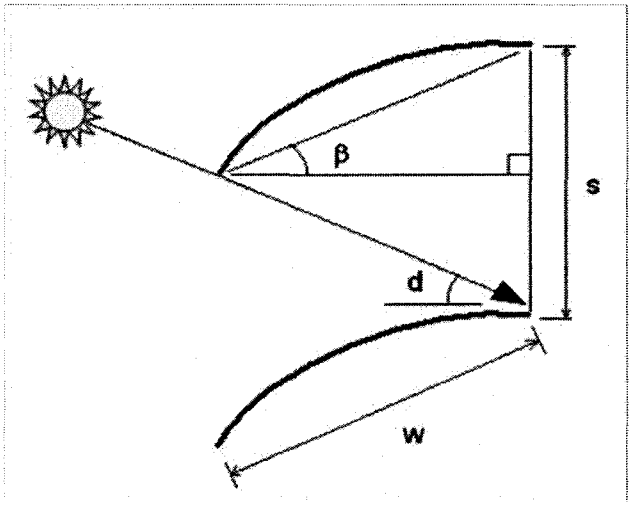

Known:
d, sun profile angle
s, distance b/w slats
w, width of slats

Want to find β, slat angle

Sine Law:

$$\frac{\sin(d + \beta)}{s} = \frac{\sin(90deg - d)}{w}$$

$$\sin(d + \beta) = \cos(d) \cdot \frac{s}{w}$$

$w := 47mm$ $s := 44mm$

The following calculations determine the position of the sun from Duffie and Beckman (2006) and Athienitis (1998). The results are to be used in the sky illuminance models.

SOLAR GEOMETRY:

Location: Montreal

Latitude: $Lat := 45.5deg$

Longitude: $Lon := 74deg$ .. West (+)

$LSM := 75deg$ .. local standard meridian

$\psi := 20deg$ .. surface azimuth

EV16.117 facade: 20° w of s

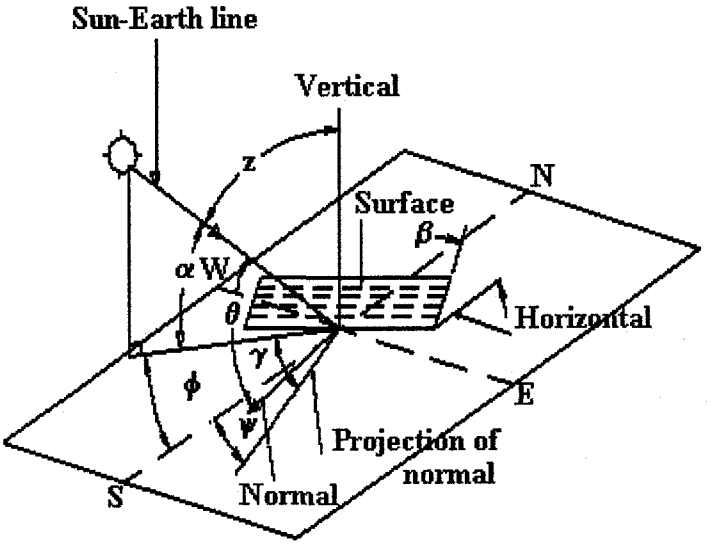

Enter Day Number: $n := 1,2..365$ ... julian day nuber

Local Standard Time: $t := 0,1..23$ ... time, in hours

Declination Angle: $\delta(n) := 23.45deg \cdot \sin\left[360deg \cdot \frac{(284 + n)}{365}\right]$

Equation of Time:

$$ET(n) := \left[9.87 \cdot \sin\left[4 \cdot \pi \cdot \frac{(n - 81)}{364}\right] - 7.53 \cdot \cos\left[2 \cdot \pi \cdot \frac{(n - 81)}{364}\right] - 1.5 \cdot \sin\left[2 \cdot \pi \cdot \frac{(n - 81)}{364}\right]\right] \cdot min$$

Apparent Solar Time: $AST(n,t) := t \cdot hr + ET(n) + \frac{(LSM - Lon) \cdot hr}{15deg}$

Hour Angle: $H(n,t) := (AST(n,t) - 12hr) \cdot 15 \frac{deg}{hr}$

Sunset hour angle: $h_S(n) := (\operatorname{acos}(-\tan(Lat)\cdot\tan(\delta(n))))$ .. altitude is equal to 0 deg

Sunset Time: $t_S(n) := h_S(n)\cdot\frac{hr}{15deg}$ .. from solar noon

Solar Altitude: (note: result is zero for negative values)

$$\alpha(n,t) := 0.5\cdot\operatorname{asin}\left[(\cos(Lat))\cdot\cos(\delta(n))\cdot\cos(H(n,t)) + (\sin(Lat))\cdot\sin(\delta(n))\right] \ldots$$
$$+ 0.5\cdot\left|\operatorname{asin}\left[(\cos(Lat))\cdot\cos(\delta(n))\cdot\cos(H(n,t)) + (\sin(Lat))\cdot\sin(\delta(n))\right]\right|$$

Solar Azimuth:

$$\phi(n,t) := \operatorname{acos}\left(\frac{\sin(\alpha(n,t))\cdot\sin(Lat) - \sin(\delta(n))}{\cos(\alpha(n,t))\cdot\cos(Lat)}\right)\cdot\frac{H(n,t)}{|H(n,t)|}$$

Surface Solar Azimuth:

$$\gamma(n,t) := \phi(n,t) - \psi$$

Surface Plane Angle: $\beta surf := 90deg$ .. vertical surface (facade)

Angle of Incidence:

$$\theta(n,t) := \operatorname{acos}(\cos(\alpha(n,t))\cdot\cos(|\gamma(n,t)|)\cdot\sin(\beta surf) + \sin(\alpha(n,t))\cdot\cos(\beta surf))$$

.. eq: 12.6, Murdoch

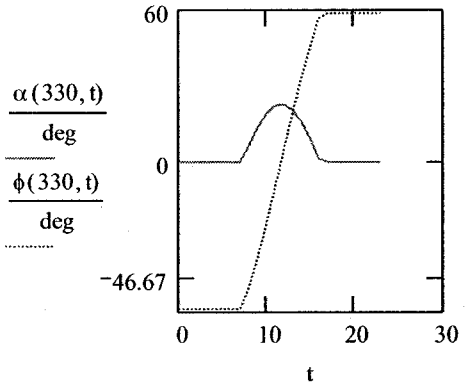

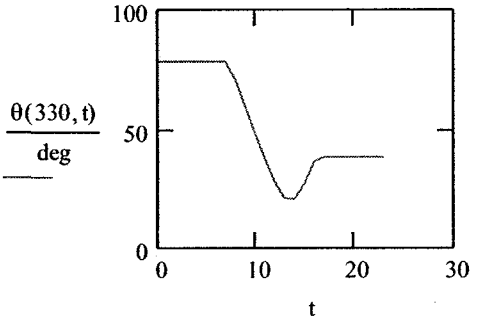

Window Transmittance $n := 79$ .. set day number

From experimental results, the following formula was derived for a double pane, argon filled window in a commercial office.

$\tau_{wd} := 0.62$ .. diffuse transmittance

Beam Transmittance: Two seperate data sets were curve fitted. The results are:

$$\tau_w(n,t) := \left(-0.375\cdot\theta(n,t)^3 + 0.645\cdot\theta(n,t)^2 - 0.423\cdot\theta(n,t) + 0.797\right)\cdot(\theta(n,t) < 90\text{deg})$$

$$\tau_{w2}(n,t) := \left(-0.294\cdot\theta(n,t)^3 + 0.435\cdot\theta(n,t)^2 - 0.258\cdot\theta(n,t) + 0.769\right)\cdot(\theta(n,t) < 90\text{deg})$$

.. dec 29 data

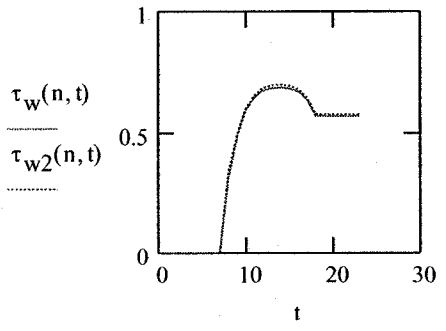

Sky Model (CIE)

In an overcast sky, there is no solar illuminance.

CLEAR SKY will be analysed, as well as the direct sunlight. The component of direct beam solar illuminance is predominant. The diffuse reflected ground component (horizontal) will be additive

Sky Illuminance:

$$E_{hc}(n,t) := 1000\text{lx}\cdot\left[0.8 + 15.5\left(\sin(\alpha(n,t))\right)^{0.5}\right]\cdot(\alpha(n,t) > 0)$$

... sky illuminance, clear sky, horizontal

Horizontal to Vertical Illumiance Ratio

$-0.0175\cdot t^2 + 0.5001\cdot t - 2.3697$ .. calculated for March 20

$$\text{Ratio}(t) := \left(-0.0175 \cdot t^2 + 0.5 \cdot t - 2.3697\right) \cdot (\alpha(n,t) > 0\text{deg})$$

$$E_{vc}(n,t) := \text{Ratio}(t)\, E_{hc}(n,t)$$

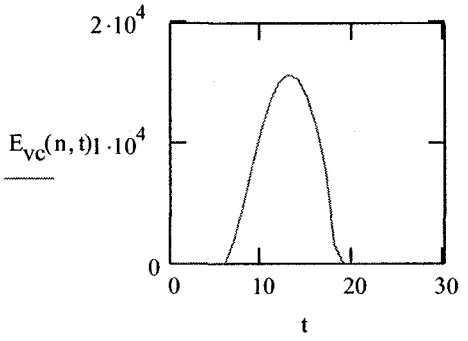

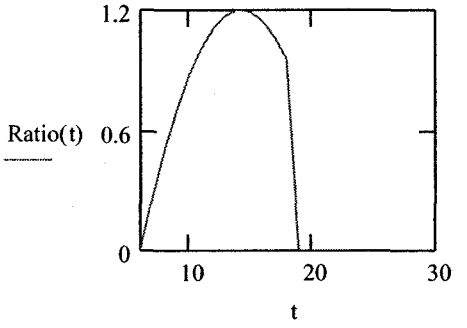

Solar Direct Beam Illuminance

$c := 0.21$ ... clear sky, c = 0.8 for a cloudy day.

$$E_{dn}(n,t) := 127.5 \cdot 10^3 \text{lx} \cdot \left[1 + 0.034 \cdot \cos\left[\frac{360}{365} \cdot (n-2)\right]\right] \cdot e^{\frac{-c}{\sin(\alpha(n,t)) + (\alpha(n,t)=0)}} \cdot (\alpha(n,t) > 0)$$

... singularity if α=0

Angle of Incidence on slat: EXAMPLE!

$\beta\text{slat} := 20\text{deg}$ .. slat angle used as an example

$$\theta\text{slat}(n,t) := \text{acos}\left(\cos(\alpha(n,t)) \cdot \cos(|\gamma(n,t)|) \sin(\beta\text{slat}) + \sin(\alpha(n,t)) \cdot \cos(\beta\text{slat})\right)$$

.. eq: E-Book (Athienitis)

$$E_{sn}(n,t) := E_{dn}(n,t) \cdot \cos(\theta\text{slat}(n,t)) \cdot (\theta\text{slat}(n,t) \le 90\text{deg})$$ ... illuminance normal to slat

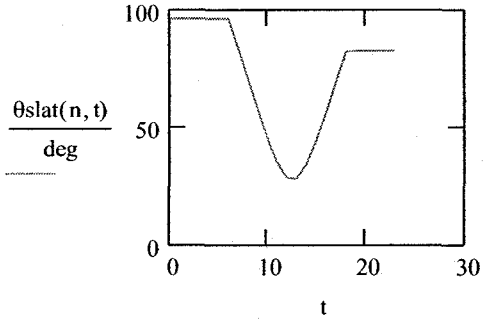

... For the case of fixed blind angle

Ground Illuminance:

$E_g(n,t) := E_{hc}(n,t) + E_{dn}(n,t)\cdot\sin(\alpha(n,t))$ $\rho_g := 0.2$ .. concrete

.. approx. 0.7 for snow

$E_g(n,t) := \text{if}\left[(\gamma(n,t) < -85\text{deg})\cdot(\gamma(n,t) > -95\text{deg}), E_{hc}(n,t), E_{hc}(n,t) + E_{dn}(n,t)\cdot\sin(\alpha(n,t))\right]$

.. Above: correction to account for measured reduction in ground illuminance when the sun is near parallel to building facade surface.

Ground to Vertical Window:

$E_{wg}(n,t) := \frac{\rho_g \cdot E_g(n,t)}{2}$ .. Vertical surface "sees" half of diffuse ground luminance

$E_{total}(n,t) := \text{if}\left(\theta(n,t) < 90\text{deg}, E_{dn}(n,t)\cdot\cos(\theta(n,t)) + E_{vc}(n,t) + E_{wg}(n,t), E_{vc}(n,t) + E_{wg}(n,t)\right)$

$t := 0, .083 .. 23$ ... Time step changed to 5-minute

Vertical Exterior Illuminance on Facade

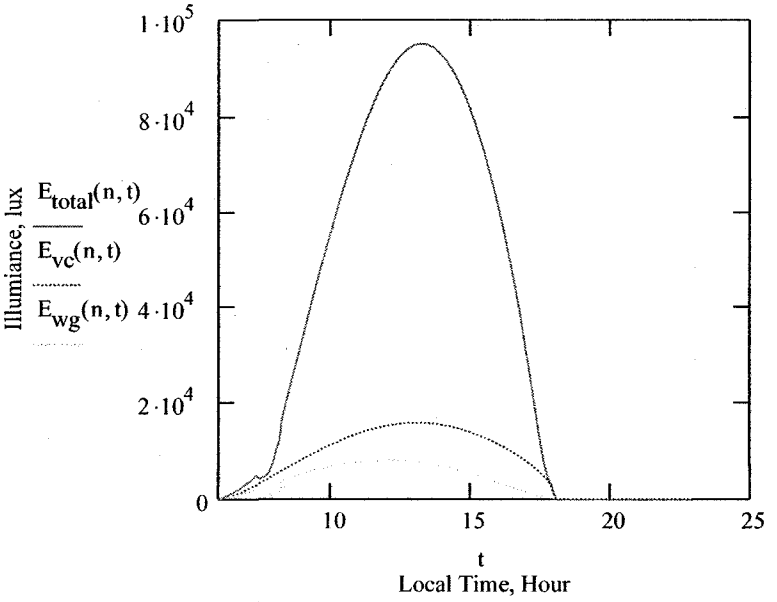

Blind Slat Illuminance

$\rho_{slat} := 0.65$ .. slat reflectance of a light grey slat + 10% (slighly metallic paint)

... Note, this also corresponds to M. Collins' data

Slat angle for glare reduction (Cut-Off):

$$d(n,t) := \operatorname{atan}\left(\frac{\tan(\alpha(n,t))}{\cos(\gamma(n,t))}\right) \quad \text{.. PROFILE ANGLE}$$

$$\beta slat(n,t) := 0.5\left(\operatorname{asin}\left(\cos(d(n,t))\cdot\frac{s}{w}\right) - d(n,t)\right)\cdot\left(|\gamma(n,t)| < 90deg\right)\cdot\left(\alpha(n,t) > 0deg\right) \ldots$$
$$+ 0.5\cdot\left|\left(\operatorname{asin}\left(\cos(d(n,t))\cdot\frac{s}{w}\right) - d(n,t)\right)\cdot\left(|\gamma(n,t)| < 90deg\right)\cdot\left(\alpha(n,t) > 0\cdot deg\right)\right|$$

.. βslat is 0deg if the sun has not risen (α = 0). When the slat angle is calculated to be negative, we keep the slat angle at 0 deg. It is also 0 deg when the surface azimuth angle is greater than 90deg.

Essentially, when d is greater than 37.5 deg, than the blinds angle is calculated to be negative, and in this case the blinds are maintained horizontal.

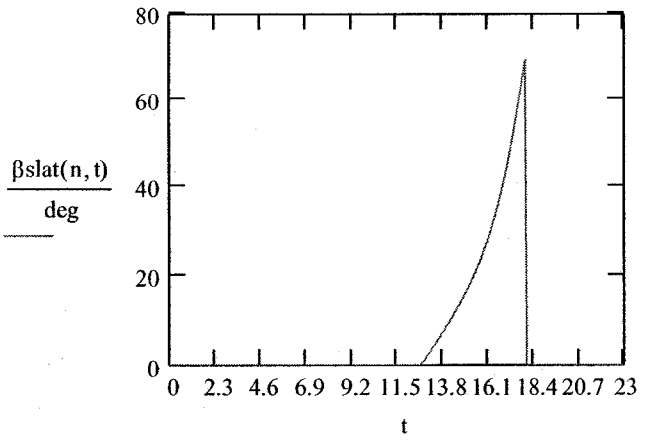

Now that we have calculated the βslat, we can calculate view factors

View Factor Calculations using Hottel's Crossed - String Theory

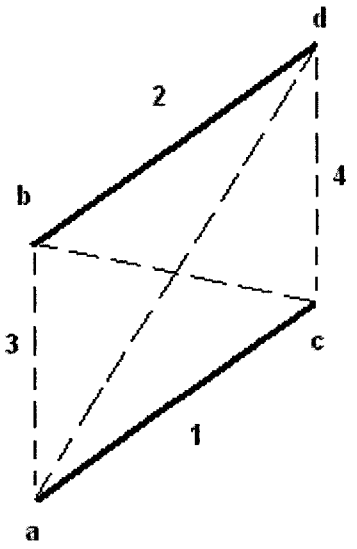

$$F_{1\_2} = \frac{[(ad + cb) - (ab + cd)]}{2 \cdot L1}$$

ab := s ac := w

cd := s bd := w

L1 := w

L3 := s

$cb^2 = s^2 + w^2 - 2 \cdot s \cdot w \cdot \cos(90deg - \beta slat)$ ... from cosine law

$cb(n,t) := \sqrt{s^2 + w^2 - 2 \cdot s \cdot w \cdot \cos(90 \cdot deg - \beta slat(n,t))}$

$ad^2 = (w \cdot \sin(\beta slat) + s)^2 + (w \cdot \cos(\beta slat))^2$

$ad(n,t) := \sqrt{(w \cdot \sin(\beta slat(n,t)) + s)^2 + (w \cdot \cos(\beta slat(n,t)))^2}$

$$F_{1\_2}(n,t) := \frac{[(ad(n,t) + cb(n,t)) - (ab + cd)]}{2 \cdot L1}$$

$F_{2\_1}(n,t) := F_{1\_2}(n,t)$ .. reciprocity

$$F_{3\_4}(n,t) := \frac{[(cb(n,t) + ad(n,t)) - (bd + ac)]}{2 \cdot L3}$$

$F_{4\_3}(n,t) := F_{3\_4}(n,t)$ .. reciprocity

Looking at Triangle abc:

$$F_{1\_3}(n,t) := \frac{ac + ab - cb(n,t)}{2ac}$$ ... From Incorpora, 3-sided triangle

Thus : $F_{1\_4}(n,t) := 1 - F_{1\_3}(n,t) - F_{1\_2}(n,t)$

$$F_{4\_1}(n,t) := \frac{w}{s} \cdot F_{1\_4}(n,t)$$ .. reciprocity

$$F_{4\_2}(n,t) := 1 - F_{4\_1}(n,t) - F_{4\_3}(n,t)$$

$$F_{3\_1}(n,t) := \frac{w}{s} \cdot F_{1\_3}(n,t)$$

$$F_{3\_2}(n,t) := 1 - F_{3\_4}(n,t) - F_{3\_1}(n,t)$$

$$F_{2\_3}(n,t) := F_{3\_2}(n,t) \cdot \frac{s}{w}$$

$$F_{2\_4}(n,t) := 1 - F_{2\_3}(n,t) - F_{2\_1}(n,t)$$

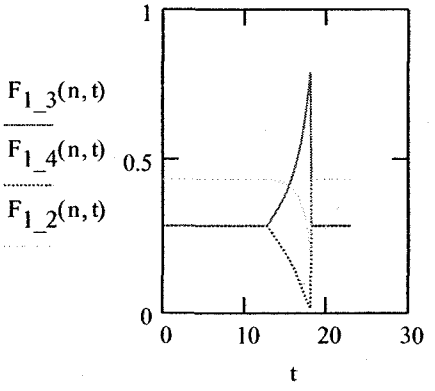

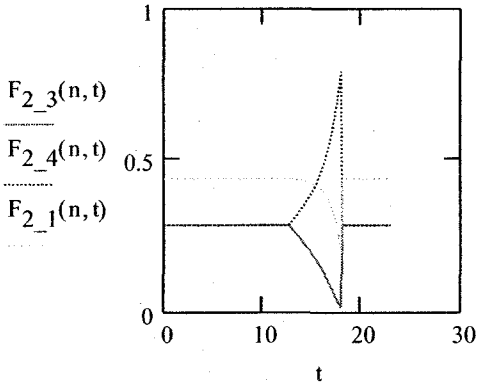

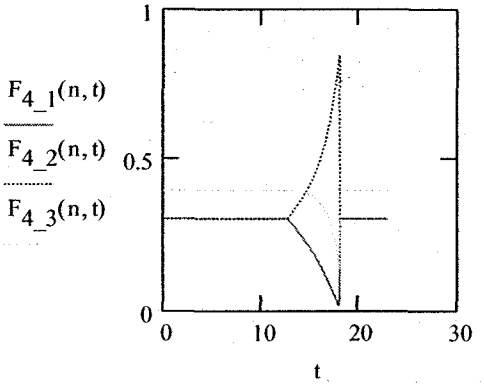

Calculate Slat Illuminance

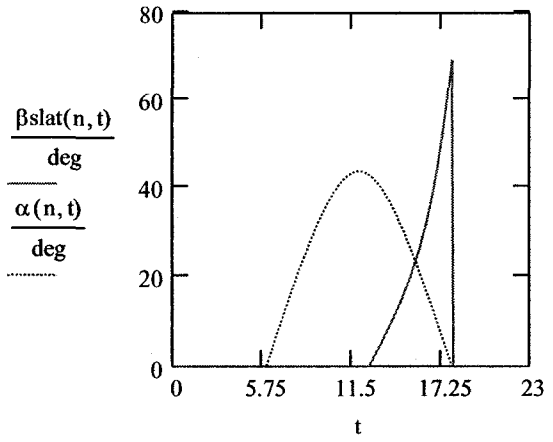

Note: when d>37.5deg, and blinds are horizontal, the complete slat is not illuminated

Re-calculate slat incidence angle for all calculated blind slat angles

$$\theta slat(n,t) := acos\left(cos(\alpha(n,t))\cdot cos(|\gamma(n,t)|)\,sin(\beta slat(n,t)) + sin(\alpha(n,t))\cdot cos(\beta slat(n,t))\right)$$

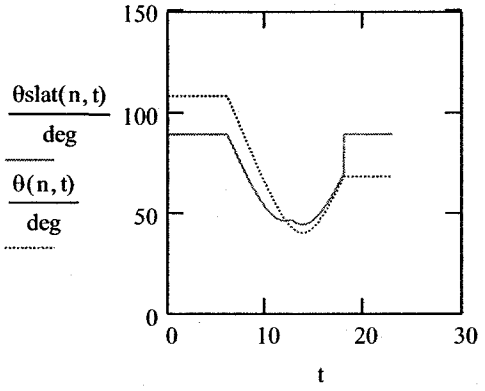

Normal illuminance on the slat

$$E_{sn}(n,t) := E_{dn}(n,t)\cdot cos(\theta slat(n,t))\cdot(\theta slat(n,t) \le 90deg)\cdot[\,|\gamma(n,t)| < (90 - 5.6)deg\,]$$

Note that the term (90-5.6) comes from the frame. That is, solar. surf azi > 84.4 results in full shading of the blind slat.

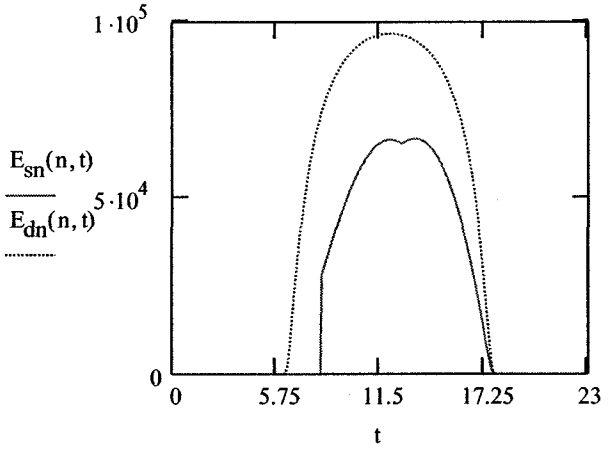

Result of shading from the window frame:

$\chi(n,t) := 90deg + \gamma(n,t)$ ... phase shift of surface azi... 0° is East

$condition1(n,t) := (\chi(n,t) > 85deg) \wedge (\chi(n,t) < 95deg)$ .. No shading

$condition2(n,t) := (\chi(n,t) < 5.6deg) \vee (\chi(n,t) > 174.4deg)$ .. some shading from frame

$$ds(n,t) := if\left(condition1(n,t), 0mm, if\left(condition2(n,t), 1530mm, \frac{150mm}{|\tan(\chi(n,t))|}\right)\right)$$

.. shaded length of blind

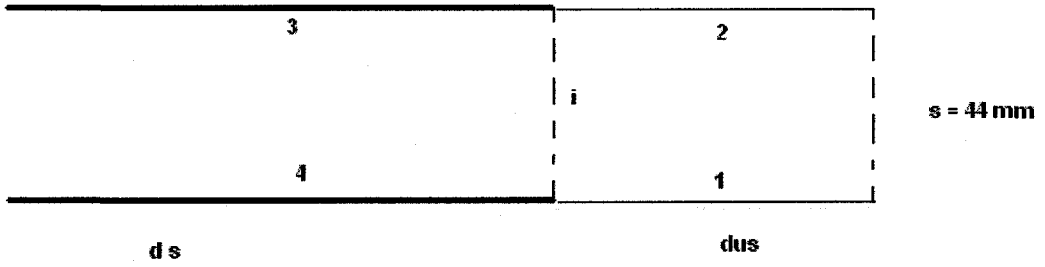

$dus(n,t) := 1530mm - ds(n,t)$ .. un-shaded length

$$Eratio(n,t) := \frac{dus(n,t)}{1530mm}$$ .. un-shaded to full slat length ratio **(Kframe)**

Where Eratio is the percent of unshaded blind to shaded, along the horizontal.

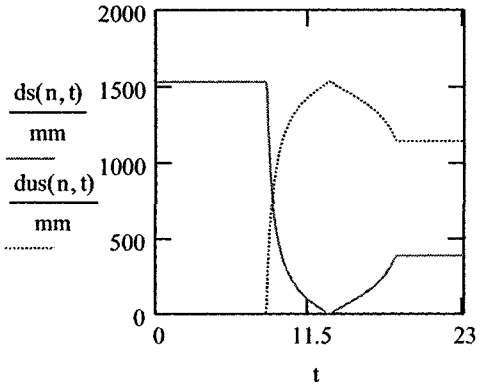

The situation where the blind is horizontal, but the complete slat is not illuminanted:

$$\text{pblind}(n,t) := \text{if}\left[\left(\beta\text{slat}(n,t) = 0\text{deg}\right)\cdot\left(\left|\gamma(n,t)\right| < 90\text{deg}\right)\cdot\left(d(n,t) > 0\text{deg}\right), \frac{s}{w\cdot\tan(d(n,t))}, 1\right] \quad \text{.. Kslat}$$

Note that pblind(n,t) is for when the blind is forced to be horizontal, where in fact it should have been tilted based on the profile angle. This occurs when the blind angle is calculated to be negative.

Also, it only affects the direct illuminance!!

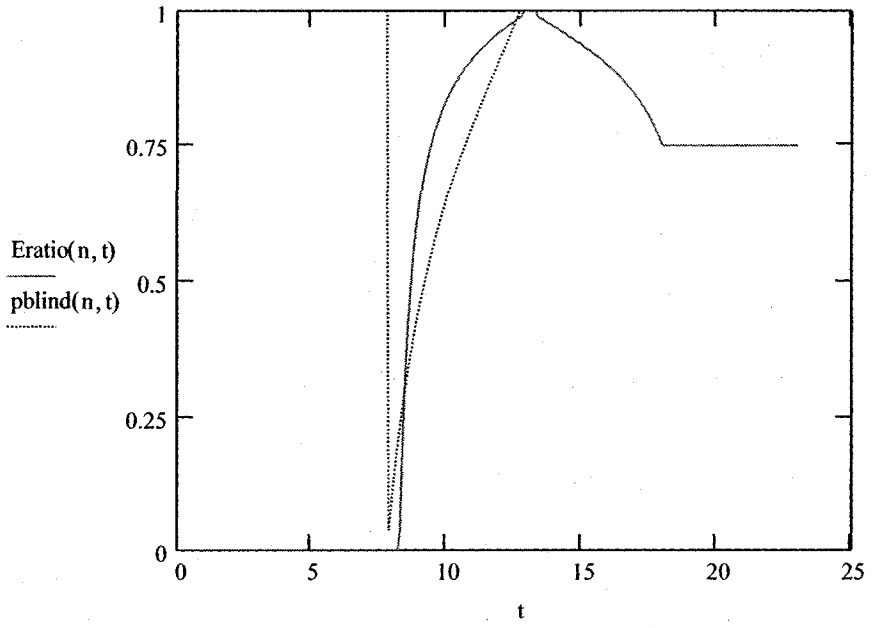

Flux-Transfer Analysis:

Calculate Transmittance through blinds, not considering specular reflection:

Recall: $\rho_{slat}(n,t) := 0.65$

$$E_{sn}(n,t) := E_{dn}(n,t)\cdot\cos(\theta slat(n,t))\cdot(\theta slat(n,t) \le 90deg)\cdot[\,|\gamma(n,t)| < (90 - 5.6)deg\,]$$

$E_{slat}(n,t) := \tau_{w2}(n,t)\cdot E_{sn}(n,t)\cdot Eratio(n,t)\cdot pblind(n,t)$ ... average illuminance of slat due to direct beam sunlight

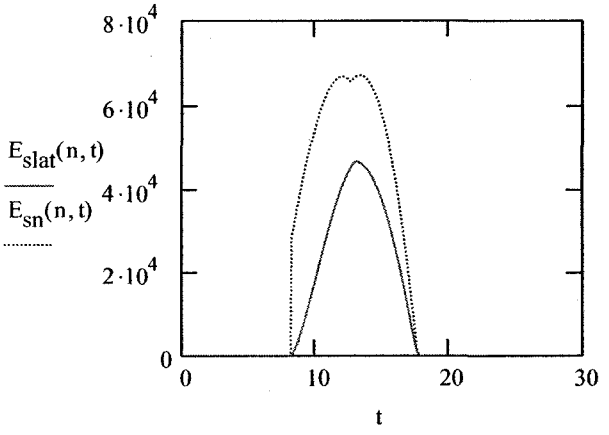

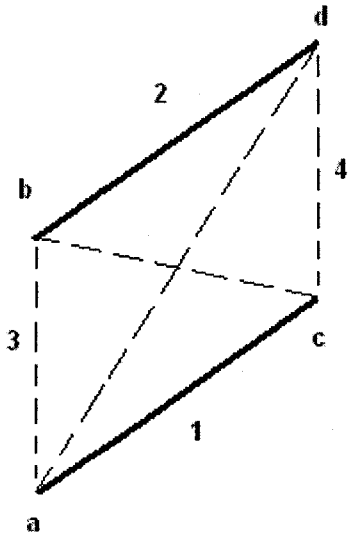

.. Recall surface definition

System of Equations for Radiosity Analysis:

$$M_3(n,t) := \left(E_{vc}(n,t) + E_{wg}(n,t)\right)\cdot\tau_{wd}$$

$$M_1(n,t) = \rho_{slat}(n,t)\cdot\left(M_2(n,t)\cdot F_{1\_2}(n,t) + M_3(n,t)\cdot F_{1\_3}(n,t) + E_{slat}(n,t)\right)$$

$$M_2(n,t) = \rho_{slat}(n,t)\cdot\left(M_3(n,t)\cdot F_{2\_3}(n,t) + M_1(n,t)\cdot F_{2\_1}(n,t)\right)$$

$$M_1(n,t) := \frac{\left[M_3(n,t)\cdot\left[\left(\rho_{slat}(n,t)\right)^2\cdot F_{2\_3}(n,t)\cdot F_{1\_2}(n,t) \ldots + \rho_{slat}(n,t)\cdot F_{1\_3}(n,t)\right] + \rho_{slat}(n,t)\cdot E_{slat}(n,t)\right]}{\left[1 - \left(\rho_{slat}(n,t)\right)^2\cdot F_{1\_2}(n,t)\cdot F_{2\_1}(n,t)\right]}$$

$$M_2(n,t) := \rho_{slat}(n,t)\cdot\left(M_3(n,t)\cdot F_{2\_3}(n,t) + M_1(n,t)\cdot F_{2\_1}(n,t)\right)$$

$$M_4(n,t) := \left(M_2(n,t)\cdot F_{4\_2}(n,t) + M_1(n,t)\cdot F_{4\_1}(n,t) + M_3(n,t)\cdot F_{4\_3}(n,t)\right)$$

... M4 is "blind" illuminance

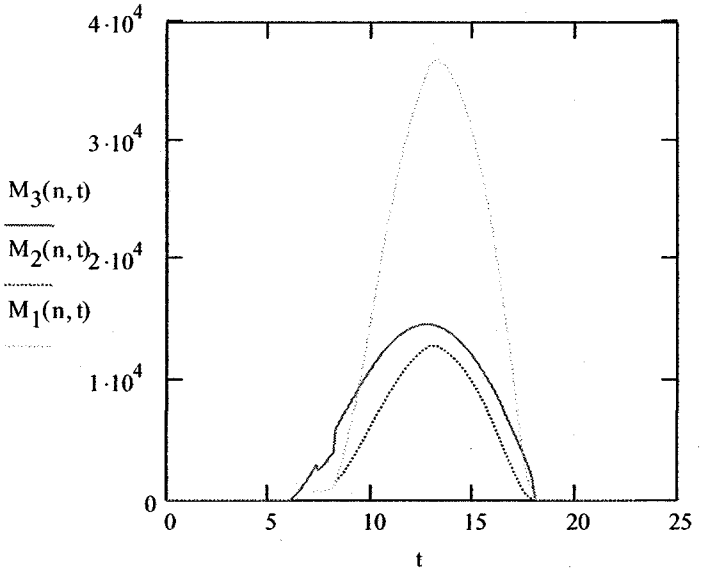

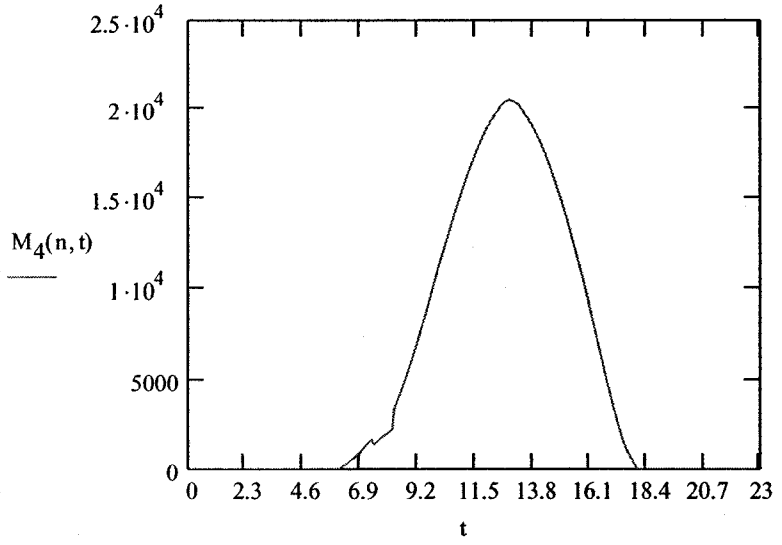

Transmittance Calculation:

$$Trans(n,t) := \frac{M_4(n,t)}{E_{total}(n,t)}$$

Three Surface model of small office space. This uses a flux-transfer analysis (radiosity) within an enclosed room

---

Assume window is complete wall of a 3-surface room (surface 1).

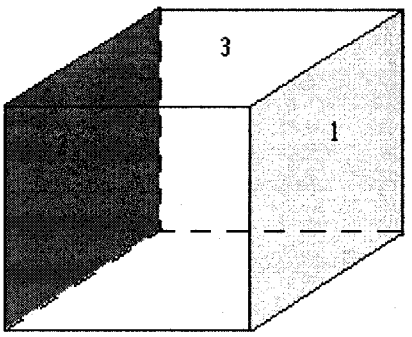

height := 3m

width := 1.8m

.. Entire surface 1 is "window" (ie: floor to ceiling)

length := 2.2m

$\rho_1 := 0.65$ .. blind reflectance

$\rho_c := 0.7$ .. ceiling reflectance, acoustic tile

$\rho_w := 0.75$ .. white paint, wall reflectance $\rho_f := 0.2$ .. floor reflectance

$$\rho_3 := \frac{(\rho_f + 2\cdot\rho_w + \rho_c)}{4}$$ ... weighted average for surface 3

Form Factor Calculations:

$A_3 := 2\cdot width\cdot length + 2\cdot length\cdot height$

$A_1 := width\cdot height$

$A_2 := A_1$

$$s := \frac{width}{height} \qquad t := \frac{length}{height}$$

$$f_{12} := \frac{2}{\pi\cdot s\cdot t}\left[0.5\cdot\ln\left[\frac{(1+s^2)\cdot(1+t^2)}{1+s^2+t^2}\right] + t\cdot\sqrt{1+s^2}\cdot\operatorname{atan}\left(\frac{t}{\sqrt{1+s^2}}\right) \ldots + s\cdot\sqrt{1+t^2}\cdot\operatorname{atan}\left(\frac{s}{\sqrt{1+t^2}}\right) - t\cdot\operatorname{atan}(t) - s\cdot\operatorname{atan}(s)\right]$$

.. form factor
Murdoch, 2003

$f_{12} = 0.109$

$f_{21} := f_{12}$

$f_{12} + f_{13} = 1$ Thus, $f_{13} := 1 - f_{12}$

$f_{23} := f_{13}$

$A_2\cdot f_{23} = A_3\cdot f_{32}$ Thus, $$f_{32} := \frac{A_2\cdot f_{23}}{A_3}$$

$f_{31} := f_{32}$

$f_{33} := 1 - f_{31} - f_{32}$

System of Equations:

$$M_1 = M_{o1} + \rho_3 \cdot M_3 \cdot f_{13} + \rho_w \cdot M_2 \cdot f_{12}$$

$$M_2 = M_{o2} + \rho_1 \cdot M_1 \cdot f_{21} + \rho_3 \cdot M_3 \cdot f_{23}$$

$$M_3 = M_{o3} + \rho_1 \cdot M_1 \cdot f_{31} + \rho_w \cdot M_2 \cdot f_{31} + \rho_3 \cdot M_3 \cdot f_{33} M_{o2} = M_2 - \rho_1 \cdot M_1 \cdot f_{21} - \rho_3 \cdot M_3 \cdot f_{23}$$

$$M_{o1} = M_1 - \rho_3 \cdot M_3 \cdot f_{13} - \rho_w \cdot M_2 \cdot f_{12}$$

$$M_{o3} = M_3 \cdot \left(1 - \rho_3 \cdot f_{33}\right) - \rho_1 \cdot M_1 \cdot f_{31} - \rho_w \cdot M_2 \cdot f_{31}$$

In Matrix Form: $R \cdot M = M_o(n,t)$

$$\begin{pmatrix} 1 & -\rho_w \cdot f_{12} & -\rho_3 \cdot f_{13} \\ -\rho_1 \cdot f_{21} & 1 & -\rho_3 \cdot f_{23} \\ -\rho_1 \cdot f_{31} & -\rho_w \cdot f_{31} & 1 - \rho_3 \cdot f_{33} \end{pmatrix} \cdot \begin{pmatrix} M_1 \\ M_2 \\ M_3 \end{pmatrix} = \begin{pmatrix} M_{o1} \\ M_{o2} \\ M_{o3} \end{pmatrix}$$

$n = 79$ .. day $t := 0, 1 .. 23$ change time step

$$M_o(t) := \begin{pmatrix} M_4(n,t) \\ 0 \\ 0 \end{pmatrix}$$ ... initial surface exitance (illuminance of blinds)

$$R := \begin{pmatrix} 1 & -\rho_w \cdot f_{12} & -\rho_3 \cdot f_{13} \\ -\rho_1 \cdot f_{21} & 1 & -\rho_3 \cdot f_{23} \\ -\rho_1 \cdot f_{31} & -\rho_w \cdot f_{31} & 1 - \rho_3 \cdot f_{33} \end{pmatrix}$$

$M(t) := R^{-1} \cdot M_o(t)$ .. solution

.. So this is the illuminance at each surface. The next step would be to create configuration factors from the planes to multiple point sources on the work plane.

Calculation of Work-Plane Illuminance

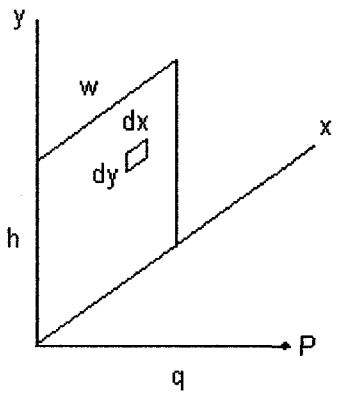

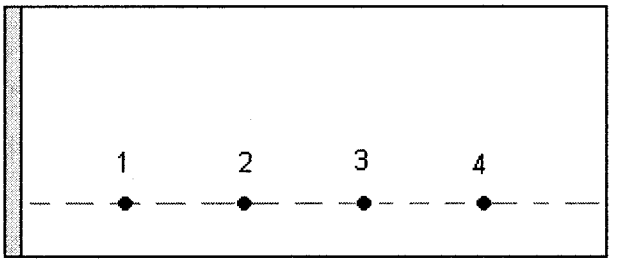

Calculation referenced from Murdoch (2003)

$$E_{ppar} = \frac{L}{2}\left(\frac{h}{\sqrt{h^2+q^2}}\,\text{atan}\left(\frac{w}{\sqrt{h^2+q^2}}\right) + \frac{w}{\sqrt{w^2+q^2}}\cdot\text{atan}\left(\frac{h}{\sqrt{w^2+q^2}}\right)\right)$$

.. point parallel to a plane

$$E_{pperp} = \frac{L}{2}\cdot\left[\text{atan}\left(\frac{w}{q}\right) - \frac{q}{\sqrt{\left(h^2+q^2\right)}}\cdot\text{atan}\left(\frac{w}{\sqrt{h^2+q^2}}\right)\right]$$

.. point perpendicular to plane

Position points 0.8 m off of ground (work plane), in the centre of the room

contribution from surfaces parallel to workplane:

Note: widths are for half of room .. the results is doubled.

Roof (surface 3):
Point 1

$w1 := 0.5m \qquad w2 := length - w1 \qquad h := \frac{width}{2} \qquad q := 2.2m$

$$L3(t) := \frac{M(t)_2}{\pi}$$

$$El_{roof}(t) := L3(t)\left[\left(\frac{h}{\sqrt{h^2+q^2}}\right)\text{atan}\left(\frac{w1}{\sqrt{h^2+q^2}}\right) + \frac{w1}{\sqrt{w1^2+q^2}}\cdot\text{atan}\left(\frac{h}{\sqrt{w1^2+q^2}}\right)\right] \ldots$$
$$+ L3(t)\left[\left(\frac{h}{\sqrt{h^2+q^2}}\right)\text{atan}\left(\frac{w2}{\sqrt{h^2+q^2}}\right) + \frac{w2}{\sqrt{w2^2+q^2}}\cdot\text{atan}\left(\frac{h}{\sqrt{w2^2+q^2}}\right)\right]$$

Point 2:

$w1 := 1m \quad w2 := length - w1$

$$E2_{roof}(t) := L3(t)\left[\left(\frac{h}{\sqrt{h^2+q^2}}\right)\operatorname{atan}\left(\frac{w1}{\sqrt{h^2+q^2}}\right)+\frac{w1}{\sqrt{w1^2+q^2}}\cdot\operatorname{atan}\left(\frac{h}{\sqrt{w1^2+q^2}}\right)\right]\ldots$$
$$+L3(t)\left[\left(\frac{h}{\sqrt{h^2+q^2}}\right)\operatorname{atan}\left(\frac{w2}{\sqrt{h^2+q^2}}\right)+\frac{w2}{\sqrt{w2^2+q^2}}\cdot\operatorname{atan}\left(\frac{h}{\sqrt{w2^2+q^2}}\right)\right]$$

Point 3:

$w1 := 1.5m \quad w2 := length - w1$

$$E3_{roof}(t) := L3(t)\left[\left(\frac{h}{\sqrt{h^2+q^2}}\right)\operatorname{atan}\left(\frac{w1}{\sqrt{h^2+q^2}}\right)+\frac{w1}{\sqrt{w1^2+q^2}}\cdot\operatorname{atan}\left(\frac{h}{\sqrt{w1^2+q^2}}\right)\right]\ldots$$
$$+L3(t)\left[\left(\frac{h}{\sqrt{h^2+q^2}}\right)\operatorname{atan}\left(\frac{w2}{\sqrt{h^2+q^2}}\right)+\frac{w2}{\sqrt{w2^2+q^2}}\cdot\operatorname{atan}\left(\frac{h}{\sqrt{w2^2+q^2}}\right)\right]$$

Point 4:

$w1 := 2m \quad w2 := length - w1$

$$E4_{roof}(t) := L3(t)\left[\left(\frac{h}{\sqrt{h^2+q^2}}\right)\operatorname{atan}\left(\frac{w1}{\sqrt{h^2+q^2}}\right)+\frac{w1}{\sqrt{w1^2+q^2}}\cdot\operatorname{atan}\left(\frac{h}{\sqrt{w1^2+q^2}}\right)\right]\ldots$$
$$+L3(t)\left[\left(\frac{h}{\sqrt{h^2+q^2}}\right)\operatorname{atan}\left(\frac{w2}{\sqrt{h^2+q^2}}\right)+\frac{w2}{\sqrt{w2^2+q^2}}\cdot\operatorname{atan}\left(\frac{h}{\sqrt{w2^2+q^2}}\right)\right]$$

Side Walls (surface 3):

Perpendicular Planes

$h := 2.2m \qquad w1 := 0.5m \qquad w2 := length - w1$

$$E1_{side}(t) := \frac{L3(t)}{2}\cdot\left[\operatorname{atan}\left(\frac{w1}{q}\right)-\frac{q}{\sqrt{\left(h^2+q^2\right)}}\cdot\operatorname{atan}\left(\frac{w1}{\sqrt{h^2+q^2}}\right)\right]\ldots$$
$$+\frac{L3(t)}{2}\cdot\left[\operatorname{atan}\left(\frac{w2}{q}\right)-\frac{q}{\sqrt{\left(h^2+q^2\right)}}\cdot\operatorname{atan}\left(\frac{w2}{\sqrt{h^2+q^2}}\right)\right]$$

$w1 := 1m \qquad w2 := length - w1$

$$E2_{side}(t) := L3(t)\cdot\left[\operatorname{atan}\left(\frac{w1}{q}\right) - \frac{q}{\sqrt{\left(h^2+q^2\right)}}\cdot\operatorname{atan}\left(\frac{w1}{\sqrt{h^2+q^2}}\right)\right] \ldots + L3(t)\cdot\left[\operatorname{atan}\left(\frac{w2}{q}\right) - \frac{q}{\sqrt{\left(h^2+q^2\right)}}\cdot\operatorname{atan}\left(\frac{w2}{\sqrt{h^2+q^2}}\right)\right]$$

$w1 := 1.5m \qquad w2 := length - w1$

$$E3_{side}(t) := L3(t)\cdot\left[\operatorname{atan}\left(\frac{w1}{q}\right) - \frac{q}{\sqrt{\left(h^2+q^2\right)}}\cdot\operatorname{atan}\left(\frac{w1}{\sqrt{h^2+q^2}}\right)\right] \ldots + L3(t)\cdot\left[\operatorname{atan}\left(\frac{w2}{q}\right) - \frac{q}{\sqrt{\left(h^2+q^2\right)}}\cdot\operatorname{atan}\left(\frac{w2}{\sqrt{h^2+q^2}}\right)\right]$$

$w1 := 2m \qquad w2 := length - w1$

$$E4_{side}(t) := L3(t)\cdot\left[\operatorname{atan}\left(\frac{w1}{q}\right) - \frac{q}{\sqrt{\left(h^2+q^2\right)}}\cdot\operatorname{atan}\left(\frac{w1}{\sqrt{h^2+q^2}}\right)\right] \ldots + L3(t)\cdot\left[\operatorname{atan}\left(\frac{w2}{q}\right) - \frac{q}{\sqrt{\left(h^2+q^2\right)}}\cdot\operatorname{atan}\left(\frac{w2}{\sqrt{h^2+q^2}}\right)\right]$$

Window (surface 1)

$$L1(t) := \frac{M(t)_0}{\pi}$$

Perpendicular Planes (note: points are in the middle of the room)

$h := 2.2m \qquad w := \frac{width}{2} \qquad q := 0.5m$

$$Ew1(t) := \frac{2\,L1(t)}{2}\cdot\left[\operatorname{atan}\left(\frac{w}{q}\right) - \frac{q}{\sqrt{\left[h^2+(q)^2\right]}}\cdot\operatorname{atan}\left[\frac{w}{\sqrt{h^2+(q)^2}}\right]\right]$$

$q := 1m$

$$Ew2(t) := \frac{2 L1(t)}{2} \cdot \left[\operatorname{atan}\left(\frac{w}{q}\right) - \frac{q}{\sqrt{\left[h^2 + (q)^2\right]}} \cdot \operatorname{atan}\left[\frac{w}{\sqrt{h^2 + (q)^2}}\right]\right]$$

$q := 1.5m$

$$Ew3(t) := \frac{2 L1(t)}{2} \cdot \left[\operatorname{atan}\left(\frac{w}{q}\right) - \frac{q}{\sqrt{\left[h^2 + (q)^2\right]}} \cdot \operatorname{atan}\left[\frac{w}{\sqrt{h^2 + (q)^2}}\right]\right]$$

$q := 2m$

$$Ew4(t) := \frac{2 L1(t)}{2} \cdot \left[\operatorname{atan}\left(\frac{w}{q}\right) - \frac{q}{\sqrt{\left[h^2 + (q)^2\right]}} \cdot \operatorname{atan}\left[\frac{w}{\sqrt{h^2 + (q)^2}}\right]\right]$$

Back Wall (Surface 2)

$$L2(t) := \frac{M(t)_1}{\pi}$$

Perpendicular Planes (note: points are in the middle of the room)

$h := 2.2m \qquad w := \frac{width}{2} \qquad q := length - 2m$

$$Eb1(t) := \frac{2 L2(t)}{2} \cdot \left[\operatorname{atan}\left(\frac{w}{q}\right) - \frac{q}{\sqrt{\left[h^2 + (q)^2\right]}} \cdot \operatorname{atan}\left[\frac{w}{\sqrt{h^2 + (q)^2}}\right]\right]$$

$q := length - 1.5m$

$$Eb2(t) := \frac{2 L2(t)}{2} \cdot \left[\operatorname{atan}\left(\frac{w}{q}\right) - \frac{q}{\sqrt{\left[h^2 + (q)^2\right]}} \cdot \operatorname{atan}\left[\frac{w}{\sqrt{h^2 + (q)^2}}\right]\right]$$

$q := length - 1m$

$$Eb3(t) := \frac{2 L2(t)}{2} \cdot \left[\operatorname{atan}\left(\frac{w}{q}\right) - \frac{q}{\sqrt{\left[h^2 + (q)^2\right]}} \cdot \operatorname{atan}\left[\frac{w}{\sqrt{h^2 + (q)^2}}\right]\right]$$

$q := length - 0.5m$

$$Eb4(t) := \frac{2\,L2(t)}{2}\cdot\left[\operatorname{atan}\left(\frac{w}{q}\right) - \frac{q}{\sqrt{\left[h^2 + (q)^2\right]}}\cdot\operatorname{atan}\left[\frac{w}{\sqrt{h^2 + (q)^2}}\right]\right]$$

Summations

$$E1(t) := Eb4(t) + Ew1(t) + E1_{side}(t) + E1_{roof}(t)$$

$$E2(t) := Eb3(t) + Ew2(t) + E2_{side}(t) + E2_{roof}(t)$$

$$E3(t) := Eb2(t) + Ew3(t) + E3_{side}(t) + E3_{roof}(t)$$

$$E4(t) := Eb1(t) + Ew4(t) + E4_{side}(t) + E4_{roof}(t)$$

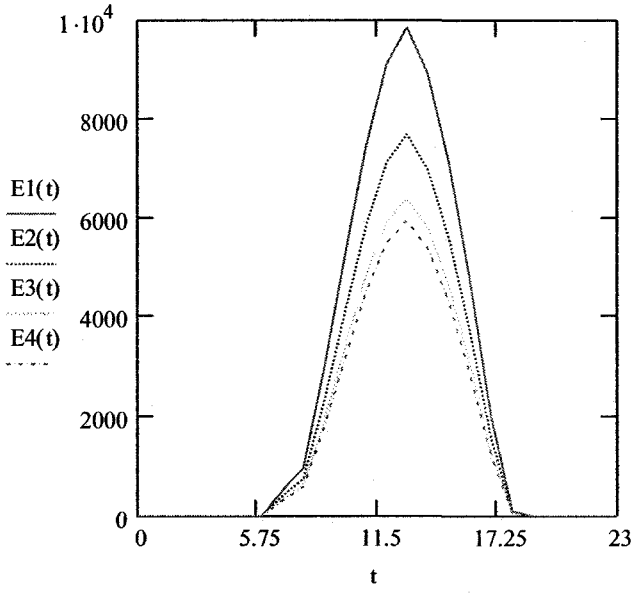

Recall Point Placement:

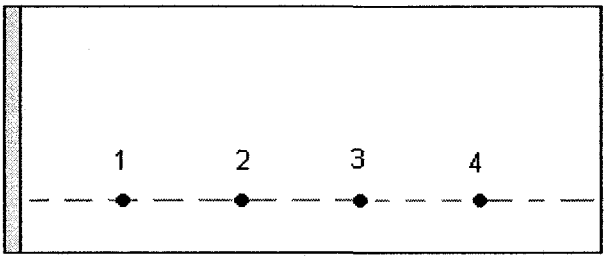

Calculations to determine the blind angle required to maintain a certain blind illuminance

Attempt to solve for M4 = 4000 lux

Recall:

$$\beta slat\_cutoff(n,t) := 0.5\left(\operatorname{asin}\left(\cos(d(n,t))\cdot\frac{s}{w}\right) - d(n,t)\right)\cdot\left(|\gamma(n,t)| < 90deg\right)\cdot\left(\alpha(n,t) > 0deg\right) \ldots$$
$$+ 0.5\cdot\left|\left(\operatorname{asin}\left(\cos(d(n,t))\cdot\frac{s}{w}\right) - d(n,t)\right)\cdot\left(|\gamma(n,t)| < 90deg\right)\cdot\left(\alpha(n,t) > 0\cdot deg\right)\right|$$

Blind surface illuminance re-defined to be a function of blind angle:

$$M_4(n,t,\beta) := \left(M_2(n,t,\beta)\cdot F_{4\_2}(\beta) + M_1(n,t,\beta)\cdot F_{4\_1}(\beta) + M_3(n,t)\cdot F_{4\_3}(\beta)\right)$$

Loop that increases slat angle in steps of 10 degrees until M4 is below the given threshold.

$$A(n,t) := \left|\begin{array}{l} \beta slat \leftarrow 0deg \\ \text{while } M_4(n,t,\beta slat) > 4000lx \\ \quad \beta slat \leftarrow \beta slat + 10deg \\ \beta slat\_cutoff(n,t) \quad \text{if } \beta slat \le \beta slat\_cutoff(n,t) \end{array}\right.$$

Where A(n,t) is the calculated blind angle.

Determination of Discomfort Glare Index

First, the vertical illuminance parallel to the window, at the point where the person is sitting, must be calculated. Similar to the work-plane calculation, but now we are looking at vertical illuminance.

$M_{o1} := 13000lx$ ... Assume Maximum Initial Blind Illuminance

Using the above defined 3-surface model:

$$M_o := \begin{pmatrix} M_{o1} \\ 0 \\ 0 \end{pmatrix} \qquad R := \begin{pmatrix} 1 & -\rho_w \cdot f_{12} & -\rho_3 \cdot f_{13} \\ -\rho_1 \cdot f_{21} & 1 & -\rho_3 \cdot f_{23} \\ -\rho_1 \cdot f_{31} & -\rho_w \cdot f_{31} & 1 - \rho_3 \cdot f_{33} \end{pmatrix}$$

$M := R^{-1} \cdot M_o$ .. surface illuminances

$$M = \begin{pmatrix} 1.557 \times 10^4 \\ 3.397 \times 10^3 \\ 4.284 \times 10^3 \end{pmatrix} lx$$

.. So this is the illuminance at each surface. The next step would be to create configuration factors from the planes to multiple point sources at height of occupant.

Recall:

$$E_{ppar} = \frac{L}{2}\left(\frac{h}{\sqrt{h^2 + q^2}}\,\text{atan}\left(\frac{w}{\sqrt{h^2 + q^2}}\right) + \frac{w}{\sqrt{w^2 + q^2}} \cdot \text{atan}\left(\frac{h}{\sqrt{w^2 + q^2}}\right)\right)$$

.. point parallel to a plane

$$E_{pperp} = \frac{L}{2} \cdot \left[\text{atan}\left(\frac{w}{q}\right) - \frac{q}{\sqrt{\left(h^2 + q^2\right)}} \cdot \text{atan}\left(\frac{w}{\sqrt{h^2 + q^2}}\right)\right]$$

.. point perpendicular to plane

Position points 1.3 m off of ground (work plane + 0.5m), in the centre of the room

Solve for vertical illuminance parallel to facade at these points.

Contribution from vertical surfaces:

Note: widths are for half of room .. the results is doubled.

Window (surface 2):
Point 1

$$w := \frac{width}{2} \qquad h2 := 1.3m \qquad h1 := height - h2$$

$$q := 2.2m - 2m \qquad h1 = 1.7\,length$$

$$L1 := \frac{M_0}{\pi} \qquad M_0 = 1.557 \times 10^4\,lx$$

$$E1_{wind} := L1\left[\left(\frac{h1}{\sqrt{h1^2 + q^2}}\right)\operatorname{atan}\left(\frac{w}{\sqrt{h1^2 + q^2}}\right) + \frac{w}{\sqrt{w^2 + q^2}}\cdot\operatorname{atan}\left(\frac{h1}{\sqrt{w^2 + q^2}}\right)\right] \ldots + L1\left[\left(\frac{h2}{\sqrt{h2^2 + q^2}}\right)\operatorname{atan}\left(\frac{w}{\sqrt{h2^2 + q^2}}\right) + \frac{w}{\sqrt{w^2 + q^2}}\cdot\operatorname{atan}\left(\frac{h2}{\sqrt{w^2 + q^2}}\right)\right]$$

Point 2:

$$q := 2.2m - 1.5m$$

$$E2_{wind} := L1\left[\left(\frac{h1}{\sqrt{h1^2 + q^2}}\right)\operatorname{atan}\left(\frac{w}{\sqrt{h1^2 + q^2}}\right) + \frac{w}{\sqrt{w^2 + q^2}}\cdot\operatorname{atan}\left(\frac{h1}{\sqrt{w^2 + q^2}}\right)\right] \ldots + L1\left[\left(\frac{h2}{\sqrt{h2^2 + q^2}}\right)\operatorname{atan}\left(\frac{w}{\sqrt{h2^2 + q^2}}\right) + \frac{w}{\sqrt{w^2 + q^2}}\cdot\operatorname{atan}\left(\frac{h2}{\sqrt{w^2 + q^2}}\right)\right]$$

Point 3:

$$q := 2.2m - 1m$$

$$E3_{wind} := L1\left[\left(\frac{h1}{\sqrt{h1^2 + q^2}}\right)\operatorname{atan}\left(\frac{w}{\sqrt{h1^2 + q^2}}\right) + \frac{w}{\sqrt{w^2 + q^2}}\cdot\operatorname{atan}\left(\frac{h1}{\sqrt{w^2 + q^2}}\right)\right] \ldots + L1\left[\left(\frac{h2}{\sqrt{h2^2 + q^2}}\right)\operatorname{atan}\left(\frac{w}{\sqrt{h2^2 + q^2}}\right) + \frac{w}{\sqrt{w^2 + q^2}}\cdot\operatorname{atan}\left(\frac{h2}{\sqrt{w^2 + q^2}}\right)\right]$$

Point 4:

$$q := 2.2m - 0.5m$$

$$E4_{wind} := L1\left[\left(\frac{h1}{\sqrt{h1^2 + q^2}}\right)\operatorname{atan}\left(\frac{w}{\sqrt{h1^2 + q^2}}\right) + \frac{w}{\sqrt{w^2 + q^2}}\cdot\operatorname{atan}\left(\frac{h1}{\sqrt{w^2 + q^2}}\right)\right] \ldots$$
$$+ L1\left[\left(\frac{h2}{\sqrt{h2^2 + q^2}}\right)\operatorname{atan}\left(\frac{w}{\sqrt{h2^2 + q^2}}\right) + \frac{w}{\sqrt{w^2 + q^2}}\cdot\operatorname{atan}\left(\frac{h2}{\sqrt{w^2 + q^2}}\right)\right]$$

Side Walls (surface 3):

Perpendicular Planes

$w2 := 1.3m \quad w1 := height - h2 \quad h := 2.2m - 2m \quad q := \frac{width}{2}$

$$L3 := \frac{M_2}{\pi}$$

$$E1_{side} := L3\cdot\left[\operatorname{atan}\left(\frac{w1}{q}\right) - \frac{q}{\sqrt{\left(h^2 + q^2\right)}}\cdot\operatorname{atan}\left(\frac{w1}{\sqrt{h^2 + q^2}}\right)\right] \ldots$$
$$+ L3\cdot\left[\operatorname{atan}\left(\frac{w2}{q}\right) - \frac{q}{\sqrt{\left(h^2 + q^2\right)}}\cdot\operatorname{atan}\left(\frac{w2}{\sqrt{h^2 + q^2}}\right)\right]$$

$h := 2.2m - 1.5m$

$$E2_{side} := L3\cdot\left[\operatorname{atan}\left(\frac{w1}{q}\right) - \frac{q}{\sqrt{\left(h^2 + q^2\right)}}\cdot\operatorname{atan}\left(\frac{w1}{\sqrt{h^2 + q^2}}\right)\right] \ldots$$
$$+ L3\cdot\left[\operatorname{atan}\left(\frac{w2}{q}\right) - \frac{q}{\sqrt{\left(h^2 + q^2\right)}}\cdot\operatorname{atan}\left(\frac{w2}{\sqrt{h^2 + q^2}}\right)\right]$$

$h := 2.2m - 1m$

$$E3_{side} := L3\cdot\left[\operatorname{atan}\left(\frac{w1}{q}\right) - \frac{q}{\sqrt{\left(h^2 + q^2\right)}}\cdot\operatorname{atan}\left(\frac{w1}{\sqrt{h^2 + q^2}}\right)\right] \ldots$$
$$+ L3\cdot\left[\operatorname{atan}\left(\frac{w2}{q}\right) - \frac{q}{\sqrt{\left(h^2 + q^2\right)}}\cdot\operatorname{atan}\left(\frac{w2}{\sqrt{h^2 + q^2}}\right)\right]$$

$h := 2.2m - 0.5m$

$$E4_{side} := L3 \cdot \left[\operatorname{atan}\left(\frac{w1}{q}\right) - \frac{q}{\sqrt{\left(h^2 + q^2\right)}} \cdot \operatorname{atan}\left(\frac{w1}{\sqrt{h^2 + q^2}}\right) \right] \ldots + L3 \cdot \left[\operatorname{atan}\left(\frac{w2}{q}\right) - \frac{q}{\sqrt{\left(h^2 + q^2\right)}} \cdot \operatorname{atan}\left(\frac{w2}{\sqrt{h^2 + q^2}}\right) \right]$$

Floor (surface 3)

$L3 = 1.364 \times 10^3\ lx$

Perpendicular Planes (note: points are in the middle of the room)

$h := 2.2m - 2m$ $\qquad w := \frac{width}{2}$ $\qquad q := 1.3m$

$$E1_{floor} := \frac{2L3}{2} \cdot \left[\operatorname{atan}\left(\frac{w}{q}\right) - \frac{q}{\sqrt{\left[h^2 + (q)^2\right]}} \cdot \operatorname{atan}\left[\frac{w}{\sqrt{h^2 + (q)^2}}\right] \right]$$

$h := 2.2m - 1.5m$

$$E2_{floor} := \frac{2L3}{2} \cdot \left[\operatorname{atan}\left(\frac{w}{q}\right) - \frac{q}{\sqrt{\left[h^2 + (q)^2\right]}} \cdot \operatorname{atan}\left[\frac{w}{\sqrt{h^2 + (q)^2}}\right] \right]$$

$h := 2.2m - 1m$

$$E3_{floor} := \frac{2L3}{2} \cdot \left[\operatorname{atan}\left(\frac{w}{q}\right) - \frac{q}{\sqrt{\left[h^2 + (q)^2\right]}} \cdot \operatorname{atan}\left[\frac{w}{\sqrt{h^2 + (q)^2}}\right] \right]$$

$h := 2.2m - 0.5m$

$$E4_{floor} := \frac{2L3}{2} \cdot \left[\operatorname{atan}\left(\frac{w}{q}\right) - \frac{q}{\sqrt{\left[h^2 + (q)^2\right]}} \cdot \operatorname{atan}\left[\frac{w}{\sqrt{h^2 + (q)^2}}\right] \right]$$

Ceiling (surface 3)

Perpendicular Planes (note: points are in the middle of the room)

$h := 2.2m - 2m \qquad w := \frac{width}{2} \qquad q := height - 1.3m$

$$E1_{ceil} := \frac{2L3}{2} \cdot \left[atan\left(\frac{w}{q}\right) - \frac{q}{\sqrt{\left[h^2 + (q)^2\right]}} \cdot atan\left[\frac{w}{\sqrt{h^2 + (q)^2}}\right]\right]$$

$h := 2.2m - 1.5m$

$$E2_{ceil} := \frac{2L3}{2} \cdot \left[atan\left(\frac{w}{q}\right) - \frac{q}{\sqrt{\left[h^2 + (q)^2\right]}} \cdot atan\left[\frac{w}{\sqrt{h^2 + (q)^2}}\right]\right]$$

$h := 2.2m - 1m$

$$E3_{ceil} := \frac{2L3}{2} \cdot \left[atan\left(\frac{w}{q}\right) - \frac{q}{\sqrt{\left[h^2 + (q)^2\right]}} \cdot atan\left[\frac{w}{\sqrt{h^2 + (q)^2}}\right]\right]$$

$h := 2.2m - 0.5m$

$$E4_{ceil} := \frac{2L3}{2} \cdot \left[atan\left(\frac{w}{q}\right) - \frac{q}{\sqrt{\left[h^2 + (q)^2\right]}} \cdot atan\left[\frac{w}{\sqrt{h^2 + (q)^2}}\right]\right]$$

Summations Vertical illuminances at points across the room (adaption illuminance)

$Ev1 := E1_{wind} + E1_{side} + E1_{floor} + E1_{ceil}$

$Ev2 := E2_{wind} + E2_{side} + E2_{floor} + E2_{ceil}$

$Ev3 := E3_{wind} + E3_{side} + E3_{floor} + E3_{ceil}$

$Ev4 := E4_{wind} + E4_{side} + E4_{floor} + E4_{ceil}$

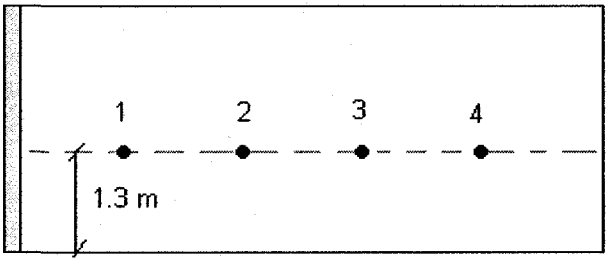

$d1 := 2.2m - 2m$

$d2 := 2.2m - 1.5m$

$d3 := 2.2m - 1m$

$d4 := 2.2m - 0.5m$

$Ev1 = 1.525 \times 10^4 lx$ $d1 = 0.2 m$

$Ev2 = 1.272 \times 10^4 lx$ $d2 = 0.7 m$

$Ev3 = 1.009 \times 10^4 lx$ $d3 = 1.2 m$

$Ev4 = 8.277 \times 10^3 lx$ $d4 = 1.7 m$

Calculation of Daylight Glare Index

This is a calculation of the daylight glare index, from the work of Ali A. Nazzal. It is used for determining what the maximum blind illuminance should be. Nazzal bases his calculation method on that developed by Chauvel, but he makes it more practical for a simple monitoring procedure for a window using photosensors.

This calculation is for a worst-case scenario. I can calculate the blind illuminance, and thus it's luminance (diffuse emitting lamberian surface). I estimate where the user is sitting, which in my office is maximum 2.2 m away, though this is much smaller than normal. So I'll look at 1 to 2 m for this calc.
The adaption luminance is that provided by the total surroundings, and this is compared to the window luminance. The greater the difference between the two values, the more discomfort.

I assume that the adaption luminance is only affected by the window source, so this is a conservative estimate being that other sources are not considered, which would increase the comfort.

Just as a note, the DGI is very sensitive to the Ladaption value

At 1 to 2 m from the window, it would appear that Eblind < 15,000 lux is reasonable for visual comfort. (DGI ~ < 24)

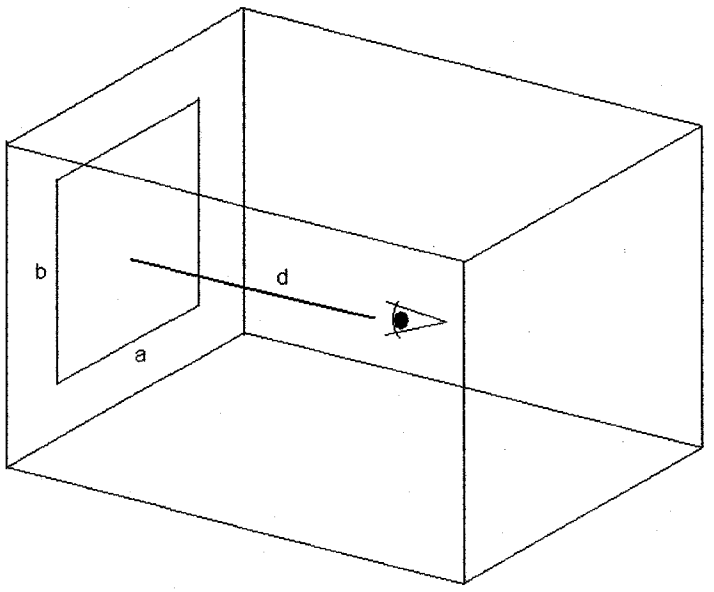

$b := 2.6m$

$a := 1.5m$

Put the person at 1.7m from the window, perpendicular

$d := 1.7m$

$X := \frac{a}{2 \cdot d} \quad Y := \frac{b}{2 \cdot d}$

$X = 0.441$

$Y = 0.765$

$\omega_N := \frac{(a \cdot b \cdot \cos(\operatorname{atan}(X)) \cdot \cos(\operatorname{atan}(Y)))}{d^2}$

$A := \frac{X}{\left(\sqrt{1 + X^2}\right)} \quad B := \frac{Y}{\left(\sqrt{1 + X^2}\right)} \quad C := \frac{Y}{\left(\sqrt{1 + Y^2}\right)} \quad D := \frac{X}{\left(\sqrt{1 + Y^2}\right)}$

$\phi_1 := \frac{(A \cdot \operatorname{atan}(B) + C \cdot \operatorname{atan}(D))}{\pi}$

... Siegel and Howell (1972). Thermal Radiation and Heat Transfer. MacGraw Hill, New York

$\phi_1 = 0.144$

$\Omega_{pNwindow} := 2 \cdot \pi \cdot \phi_1$

$\Omega_{pNwindow} = 0.902$

$L_{window} := \frac{M_0}{\pi \cdot lx} \quad L_{adaption} := \frac{Ev4}{\pi \cdot lx} \quad L_{exterior} := \frac{M_0}{[2 \cdot (\pi - 1)] lx}$

$DGI_N := 8 \cdot \log\left[0.25 \frac{\left(L_{exterior}\right)^2 \cdot \Omega_{pNwindow}}{L_{adaption} + 0.07 \cdot \left(L_{window}^{\ 2} \cdot \omega_N\right)^{0.5}}\right]$

$DGI_N = 24.002$ ... calculated for inital blind illuminance of: $M_{oI} = 1.3 \times 10^4 lx$

DGIN of 24 is "just uncomfortable"

Note that this is assuming the full area has a window.. meaning we can go higher with the blind illuminance.

PEREZ (1990) MODEL

Requires 3 inputs:

1) Dh : the diffuse horizontal irradiance

2) I : the normal incidence direct irradiance

3) Z : the zenith angle, in radians

In order to calculate Z and Dh, n (julian day number) is required.

$k := 1.041$ .. constant

Calculation of Solar Radiation

$I_{sc} := 1353 \frac{watt}{m^2}$ .. solar constant

$I_{on}(n) := I_{sc} \cdot \left(1 + 0.033 \cdot \cos\left(360 \cdot \frac{n}{365} deg\right)\right)$ .. **normal incidence**

$\varepsilon(Dh, I, Z) := \frac{\left[\frac{(Dh + I)}{Dh} + k \cdot Z^3\right]}{\left(1 + k \cdot Z^3\right)}$ ... 2) **Sky Clearness**

$mo(Z) := \frac{1}{\cos(Z) + 0.50572 \cdot (96.07995 - Z)^{-1.6364}}$

Kasten, F., and A. T. Young. 1989. "Revised **optical air mass** tables and approximation formula." Applied Optics 28:4735–4738.

$\Delta(Dh, Z, n) := \frac{Dh \cdot mo(Z)}{I_{on}(n)}$ ... **3) sky brightness**

4. Atmospheric precipitable water content

$W_{atm}(Td) := e^{0.07 \cdot Td - 0.075}$

Where Td (°C) is the three hourly surface dew point temperature

Other Important Variables:

$Ihd(I,Z) := I \cdot \cos(Z)$ Horizontal Direct irradiation

$G(Dh,Z,I) := I \cdot \cos(Z) + Dh$ Global Horizontal Radiation

Discrete sky clearness categories (Overcast -> Clear)

$$bin(Dh,I,Z) := \begin{cases} 1 & \text{if } (\varepsilon(Dh,I,Z) < 1.065) \\ 2 & \text{if } (1.065 \le \varepsilon(Dh,I,Z) < 1.230) \\ 3 & \text{if } (1.230 \le \varepsilon(Dh,I,Z) < 1.5) \\ 4 & \text{if } (1.5 \le \varepsilon(Dh,I,Z) < 1.95) \\ 5 & \text{if } (1.95 \le \varepsilon(Dh,I,Z) < 2.8) \\ 6 & \text{if } (2.8 \le \varepsilon(Dh,I,Z) < 4.5) \\ 7 & \text{if } (4.5 \le \varepsilon(Dh,I,Z) < 6.2) \\ 8 & \text{if } (\varepsilon(Dh,I,Z) \ge 6.2) \end{cases}$$

.. 1 is overcast, 8 is clear

Once we get the bin, we can get our coefficients (a, b and c)

Global Luminous Efficacy

$$a\_gle := \begin{pmatrix} 96.83 \\ 107.54 \\ 98.73 \\ 92.72 \\ 86.73 \\ 88.34 \\ 78.63 \\ 99.65 \end{pmatrix} \quad b\_gle := \begin{pmatrix} -0.47 \\ 0.79 \\ 0.70 \\ 0.56 \\ 0.98 \\ 1.39 \\ 1.47 \\ 1.86 \end{pmatrix} \quad c\_gle := \begin{pmatrix} 11.5 \\ 1.79 \\ 4.4 \\ 8.36 \\ 7.10 \\ 6.06 \\ 4.93 \\ -4.46 \end{pmatrix} \quad d\_gle := \begin{pmatrix} -9.16 \\ -1.19 \\ -6.95 \\ -8.31 \\ -10.94 \\ -7.6 \\ -11.37 \\ -3.15 \end{pmatrix}$$

Direct Luminous Efficacy

$$a\_dle := \begin{pmatrix} 57.2 \\ 98.99 \\ 109.83 \\ 110.34 \\ 106.36 \\ 107.19 \\ 105.75 \\ 101.18 \end{pmatrix} \quad b\_dle := \begin{pmatrix} -4.55 \\ -3.46 \\ -4.9 \\ -5.84 \\ -3.97 \\ -1.25 \\ 0.77 \\ 1.58 \end{pmatrix} \quad c\_dle := \begin{pmatrix} -2.98 \\ -1.21 \\ -1.71 \\ -1.99 \\ -1.75 \\ -1.51 \\ -1.26 \\ -1.10 \end{pmatrix} \quad d\_dle := \begin{pmatrix} 117.12 \\ 12.38 \\ -8.81 \\ -4.56 \\ -6.16 \\ -26.73 \\ -34.44 \\ -8.29 \end{pmatrix}$$

Diffuse Luminous Efficacy

$$a\_difle := \begin{pmatrix} 97.24 \\ 107.22 \\ 104.97 \\ 102.39 \\ 100.71 \\ 106.42 \\ 141.88 \\ 152.23 \end{pmatrix} \quad b\_difle := \begin{pmatrix} -0.46 \\ 1.15 \\ 2.96 \\ 5.59 \\ 5.94 \\ 3.83 \\ 1.90 \\ 0.35 \end{pmatrix} \quad c\_difle := \begin{pmatrix} 12 \\ 0.59 \\ -5.53 \\ -13.95 \\ -22.75 \\ -36.15 \\ -53.24 \\ -45.27 \end{pmatrix} \quad d\_difle := \begin{pmatrix} -8.91 \\ -3.95 \\ -8.77 \\ -13.90 \\ -23.74 \\ -28.83 \\ -14.03 \\ -7.98 \end{pmatrix}$$

Zenith Luminance Prediction

$$a\_zlp := \begin{pmatrix} 40.86 \\ 26.58 \\ 19.34 \\ 13.25 \\ 14.47 \\ 19.76 \\ 28.39 \\ 42.91 \end{pmatrix} \quad c\_zlp := \begin{pmatrix} 26.77 \\ 14.73 \\ 2.28 \\ -1.39 \\ -5.09 \\ -3.88 \\ -9.67 \\ -19.62 \end{pmatrix} \quad c2\_zlp := \begin{pmatrix} -29.59 \\ 58.46 \\ 100 \\ 124.79 \\ 160.09 \\ 154.61 \\ 151.58 \\ 130.8 \end{pmatrix} \quad d\_zlp := \begin{pmatrix} -45.75 \\ -21.25 \\ 0.25 \\ 15.66 \\ 9.13 \\ -19.21 \\ -69.39 \\ -164.08 \end{pmatrix}$$

Model Formulation

1) Diffuse horizontal illuminance

$$dh(Dh,Z,I,n,Td) := if\left[Dh > 0, Dh\cdot\left(\begin{array}{l} a\_difle_{bin(Dh,I,Z)} + b\_difle_{bin(Dh,I,Z)}\cdot W_{atm}(Td) \ldots \\ + c\_difle_{bin(Dh,I,Z)}\cdot\cos(Z) \ldots \\ + d\_difle_{bin(Dh,I,Z)}\cdot\ln(\Delta(Dh,Z,n)) \end{array}\right)\cdot lx\cdot\frac{m^2}{W}, 0lx\right]$$

2) Direct Illuminance

$$id(Dh,I,Z,Td,n) := \max\left[0lx, I\cdot\left[\begin{array}{l} a\_dle_{bin(Dh,I,Z)} + b\_dle_{bin(Dh,I,Z)}\cdot W_{atm}(Td) \ldots \\ + c\_dle_{bin(Dh,I,Z)}\cdot e^{(5.73\cdot Z-5)} \ldots \\ + d\_dle_{bin(Dh,I,Z)}\cdot\Delta(Dh,Z,n) \end{array}\right]\cdot lx\cdot\frac{m^2}{W}\right]$$

3.2 Diffuse Irradiance and Illuminance on tilted surfaces modelling

$$Xc = Xh\cdot\left[\left(1 - F_1\right)\cdot\frac{(1 + \cos(\beta))}{2} + F_1\cdot\frac{a}{b} + F_2\cdot\sin(\beta)\right]$$

.. where Xc and Xh are, respectively, the tilted and horizontal diffuse value of either illuminance or irradiance. β is the considered surface's slope, F.1 and F.2 are coefficients expresssing the degree of circumsolar and horizon/zenith anisotropy respectively; they are functions of the sky condition. The terms "a" and "b" are given below:

$$a(\theta) := \max(0, \cos(\theta)) \text{ and } \qquad b(Z) := \max(0.087, \cos(Z))$$

.. where θ is the incidence angle of the sun on the considered slope

Values of F1 and F2

$F_1 = F_{11} + F_{12}\cdot\Delta + F_{13}\cdot Z$ ... circumsolar brightening coefficient

$F_2 = F_{21} + F_{22}\cdot\Delta + F_{23}\cdot Z$ ... Horizon Brightening Coefficient

Illuminance Coefficients....

$$F11IL := \begin{pmatrix} 0.011 \\ 0.429 \\ 0.809 \\ 1.014 \\ 1.282 \\ 1.426 \\ 1.485 \\ 1.170 \end{pmatrix} \quad F12IL := \begin{pmatrix} 0.570 \\ 0.363 \\ -0.054 \\ -0.252 \\ -0.420 \\ -0.653 \\ -1.214 \\ -0.300 \end{pmatrix} \quad F13IL := \begin{pmatrix} -0.081 \\ -0.307 \\ -0.442 \\ -0.531 \\ -0.689 \\ -0.779 \\ -0.784 \\ -0.615 \end{pmatrix}$$

$$F21IL := \begin{pmatrix} -0.095 \\ 0.050 \\ 0.181 \\ 0.275 \\ 0.380 \\ 0.425 \\ 0.411 \\ 0.518 \end{pmatrix} \quad F22IL := \begin{pmatrix} 0.158 \\ 0.008 \\ -0.169 \\ -0.350 \\ -0.559 \\ -0.785 \\ -0.629 \\ -1.892 \end{pmatrix} \quad F23IL := \begin{pmatrix} -0.018 \\ -0.065 \\ -0.092 \\ -0.096 \\ -0.114 \\ -0.097 \\ -0.082 \\ -0.055 \end{pmatrix}$$

$$F1IL(Dh,I,Z,n) := F11IL_{bin(Dh,I,Z)} + F12IL_{bin(Dh,I,Z)} \cdot \Delta(Dh,Z,n) + F13IL_{bin(Dh,I,Z)} \cdot Z$$

$$F2IL(Dh,I,Z,n) := F21IL_{bin(Dh,I,Z)} + F22IL_{bin(Dh,I,Z)} \cdot \Delta(Dh,Z,n) + F23IL_{bin(Dh,I,Z)} \cdot Z$$

$$dc(Dh,I,Z,Td,n,\beta,\theta) := dh(Dh,Z,I,n,Td) \cdot \left[\begin{array}{l} (1 - F1IL(Dh,I,Z,n)) \cdot \frac{(1+\cos(\beta))}{2} \ldots \\ + F1IL(Dh,I,Z,n) \cdot \frac{a(\theta)}{b(Z)} \ldots \\ + F2IL(Dh,I,Z,n) \cdot \sin(\beta) \end{array} \right]$$

Reference:F:\Thesis Drive\Modelling\hottel_EV_bldg.mcd irradiance compents imported

$Td := 0$ .. dew point temp.

$\psi := 20deg$ $\beta = 90\,deg$ $\theta(t) := \theta(t, \psi, \beta)$ $n := 79$

$Dh(t) := I_{ds\_h}(t)$ ... diffuse horizontal irradiance (From Hottel Model, Duffie and Beckman (2006))

$I(t) := I_b(t, \psi, \beta)$ .. normal incidence direct beam (hottel)

$Z(t) := \phi(t)$ ... zenith angle

$t := 5hr, 6hr .. 18hr$

$Ratio(t) := \frac{dc(Dh(t), I(t), Z(t), Td, n, \beta, \theta(t))}{dh(Dh(t), Z(t), I(t), n, Td)}$ **.. vertical to horizontal ratio**